INFORMATION TO USERS

This manuscript has been reproduced from the microfilm master. UMI films the text directly from the original or copy submitted. Thus, some thesis and dissertation copies are in typewriter face, while others may be from any type of computer printer.

The quality of this reproduction is dependent upon the quality of the copy submitted. Broken or indistinct print, colored or poor quality illustrations and photographs, print bleedthrough, substandard margins, and improper alignment can adversely affect reproduction.

In the unlikely event that the author did not send UMI a complete manuscript and there are missing pages, these will be noted. Also, if unauthorized copyright material had to be removed, a note will indicate the deletion.

Oversize materials (e.g., maps, drawings, charts) are reproduced by sectioning the original, beginning at the upper left-hand corner and continuing from left to right in equal sections with small overlaps. Each original is also photographed in one exposure and is included in reduced form at the back of the book.

Photographs included in the original manuscript have been reproduced xerographically in this copy. Higher quality 6" x 9" black and white photographic prints are available for any photographs or illustrations appearing in this copy for an additional charge. Contact UMI directly to order.

UMI

A Bell & Howell Information Company
300 North Zeeb Road, Ann Arbor MI 48106-1346 USA
313/761-4700 800/521-0600

Downloaded from SHAREOK. Persistent Handle URL: https://hdl.handle.net/11244/5653

NOTE TO USERS

The original manuscript received by UMI contains pages with indistinct and/or slanted print. Pages were microfilmed as received.

This reproduction is the best copy available

UMI

UNIVERSITY OF OKLAHOMA

GRADUATE COLLEGE

CHARACTERIZATION OF PURE AND PHASE-STABILIZED SODIUM PHOSPHATE

A Dissertation

SUBMITTED TO THE GRADUATE FACULTY

in partial fulfillment of the requirements for the

degree of

Doctor of Philosophy

By

RENÉE S. COLE

Norman, Oklahoma

1998

UMI Number: 9839787

UMI Microform 9839787
Copyright 1998, by UMI Company. All rights reserved.

This microform edition is protected against unauthorized copying under Title 17, United States Code.

UMI
300 North Zeeb Road
Ann Arbor, MI 48103

© Copyright by Renée S. Cole 1998

All Rights Reserved

CHARACTERIZATION OF PURE

AND PHASE-STABILIZED SODIUM PHOSPHATE

A DISSERTATION APPROVED FOR THE

DEPARTMENT OF CHEMISTRY AND BIOCHEMISTRY

BY

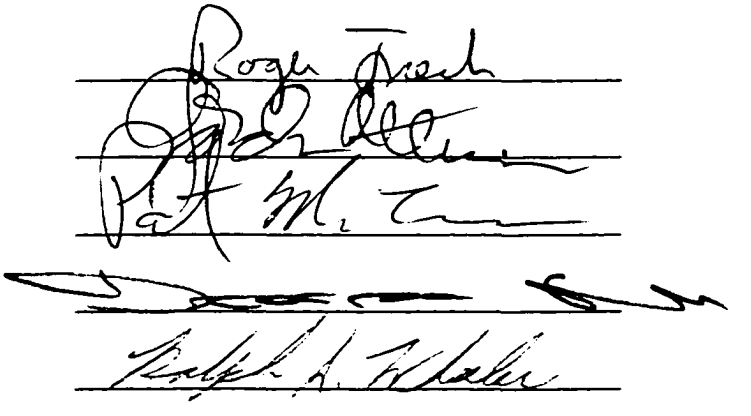

Dedicated to Greg

with all my love

ACKNOWLEDGMENTS

I would first like to thank Dr. Roger Frech, who has been more than just an advisor to me. His role as my mentor has provided me with the encouragement and support I needed but provided enough space to let me grow and develop. I have greatly enjoyed our conversations about science, teaching and life in general.

I would like to thank Drs. Atkinson, McCann, van der Helm and Wheeler for their time, assistance and willingness to serve on my committee. I have greatly appreciated their comments and advice throughout my graduate study. I would like to thank the Department of Chemistry and Biochemistry, the Department of Education, the Graduate College and NSF EPSCoR for the financial assistance they have provided me during my tenure at the University of Oklahoma. I would like to thank Dr. Barry Weaver for the access to the powder x-ray diffractometer in the Department of Geology early in my career at OU. I would especially like to thank Dr. Winton Cornell at the University of Tulsa for allowing me access to the powder x-ray diffractometer in the Department of Engineering and Applied Sciences. Without his assistance, this would still be a work in progress.

I would also like to thank the members of the Frech group, past and present, for their friendship and contributions to my graduate experience. My gratitude and appreciation go to Shawna York, Dr. Sangamithra Chintapalli, Dr. Andrew Mattioda, Dr. Xulong Zhang, Dr. Gamini Dharmasena, Palmer Graves, Sharon Sanderson, Chris

Rhodes, Jeff Ciaccio, Corbin Zea, Dr. Barry Klassen, Dr. Weiwei Huang and Dave Roth.

Last, but certainly not least, I would like to thank my family for their love and support. My parents have always supported and encouraged me in my endeavors, and I value their love and faith in me greatly. My daughter Mackenzie, who brings such joy to my life, is a constant source of love and attention. But most of all, I want to thank my husband Greg, for without his unwavering love and support this would have been infinitely more difficult.

TABLE OF CONTENTS

ACKNOWLEDGMENTS	v
LIST OF TABLES	x
LIST OF FIGURES	xii
ABSTRACT	xvii
CHAPTER 1: INTRODUCTION	
Introduction	I
Polymorphism and Phase Stabilization	3
Fast-ion Conductors	5
Raman Studies of Phase Transitions and Phase Stabilization	9
Overview of Research	11
References	12
CHAPTER 2: EXPERIMENTAL	
Sample Preparation	18
Lithium Sodium Sulfate and Lithium Potassium Sulfate	18
Sodium Phosphate	19
Raman Spectroscopy	20
Infrared Spectroscopy	21
Differential Scanning Calorimetry	24
Powder X-ray Diffraction	24
List of Reagents	24
References	25
CHAPTER 3: $Y_2(SO_4)_3$ SUBSTITUTED $LiNaSO_4$ AND $LiKSO_4$	
Introduction	26
Lithium Sodium Sulfate: Raman Spectra	27
Lithium Potassium Sulfate: Raman Spectra	35
Lithium Potassium Sulfate: DSC and XRD	43
Conclusion	47

References 49
CHAPTER 4: CHARACTERIZATION OF SODIUM PHOSPHATE
Introduction 51
XRD and DSC Results 51
Vibrational Spectroscopy 58
Raman Results 64
References 72
CHAPTER 5: ANION STABILIZED SODIUM PHOSPHATE
Introduction 75
Results 78
Differential Scanning Calorimetry 79
Powder X-ray Diffraction 81
Infrared Spectroscopy 88
Raman Spectroscopy 90
Discussion 95
Conclusion 97
References 98
CHAPTER 6: CATION STABILIZED SODIUM PHOSPHATE
Introduction 101
Results 103
The $Na_{3-2x}Mg_xPO_4$ System 103
Powder X-ray Diffraction 103
Differential Scanning Calorimetry 108
Raman Spectroscopy 110
The $Na_{3-2x}Zn_xPO_4$ System 119
Powder X-ray Diffraction 119
Differential Scanning Calorimetry 122
Raman Spectroscopy 124
Discussion 131

Conclusion 135
References 136
CHAPTER 7: CATION/ANION STABILIZED SODIUM PHOSPHATE
Introduction 137
Results 138
Differential Scanning Calorimetry 138
Powder X-ray Diffraction 140
Raman Spectroscopy 143
Discussion 153
Conclusions 156
References 157
CHAPTER 8: SUMMARY OF CONCLUSIONS
Conclusions 158
Future Studies 161

LIST OF TABLES

Table		Page
3.1.	Frequencies (in cm^{-1}) of the SO_4^{2-} modes in $Y_2(SO_4)_3$-substituted $LiNaSO_4$.	36
3.2.	Frequencies (in cm^{-1}) of the SO_4^{2-} modes in $Y_2(SO_4)_3$-substituted $LiKSO_4$.	44
3.3.	Values of d-spacings (in Å) and relative intensities of pure $LiKSO_4$, 90/10 $LiKSO_4$/ $Y_2(SO_4)_3$, and pure $Y_2(SO_4)_3$.	45
4.1.	Comparison of d-spacings (in Å) of α-Na_3PO_4. The d-spacings of the w-phase are also included.	56
4.2.	Frequencies of the PO_4^{3-} Raman vibrational modes of Na_3PO_4. Values at 24°C are for the α-phase, and values at 360°C are for the γ-phase.	59
4.3.	Frequencies of the PO_4^{3-} infrared vibrational modes of Na_3PO_4.	71
5.1.	Summary of previous studies of $Na_{3-x}S_xP_{1-x}O_4$.	77
5.2.	Powder x-ray diffraction data for Na_3PO_4 phases. Data are reported as d-spacings in Å with relative intensities in parentheses.	84
5.3.	Powder x-ray diffraction data for Na_2SO_4 phases. Data are reported as d-spacings in Å with relative intensities in parentheses.	87

6.1. Powder x-ray diffraction data for $Na_{3-2x}Mg_xPO_4$ for increasing values of x. Data are reported as d-spacings in Å with relative intensities in parentheses. 106

6.2. Powder x-ray diffraction data for $Na_{3-2x}Zn_xPO_4$ for increasing values of x. Data are reported as d-spacings in Å with relative intensities in parentheses. 121

7.1. Powder x-ray diffraction data for $Na_{3-3x}Zn_xS_xP_{1-x}O_4$ for increasing values of x. Data are reported as d-spacings in Å with relative intensities in parentheses. 142

LIST OF FIGURES

Figure	Page
2.1. High Temperature Raman Cell	22
2.2. Sample Holder for Capillary Tubes	23
3.1. Raman spectra of $LiNaSO_4$ substituted with Y^{3+} in the SO_4^{2-} ν_1 region with increasing concentration of $Y_2(SO_4)_3$.	28
3.2. Raman spectra of $LiNaSO_4$ substituted with Y^{3+} in the SO_4^{2-} ν_3 region with increasing concentration of $Y_2(SO_4)_3$.	29
3.3. Raman spectra of $LiNaSO_4$ substituted with Y^{3+} in the SO_4^{2-} ν_4 region with increasing concentration of $Y_2(SO_4)_3$.	31
3.4. Raman spectra of $LiNaSO_4$ substituted with Y^{3+} in the SO_4^{2-} ν_2 region with increasing concentration of $Y_2(SO_4)_3$.	32
3.5. Temperature-dependent Raman spectra of $LiNaSO_4$ in the SO_4^{2-} ν_3 and ν_1 regions. The spectrum at 600°C corresponds to the high-temperature phase.	34
3.6. Raman spectra of $LiKSO_4$ substituted with Y^{3+} in the SO_4^{2-} ν_1 region with increasing concentration of $Y_2(SO_4)_3$.	37
3.7. Raman spectra of $LiKSO_4$ substituted with Y^{3+} in the SO_4^{2-} ν_3 region with increasing concentration of $Y_2(SO_4)_3$.	38
3.8. Raman spectra of $LiKSO_4$ substituted with Y^{3+} in the SO_4^{2-}	40

ν_4 region with increasing concentration of $Y_2(SO_4)_3$.

3.9. Raman spectra of $LiKSO_4$ substituted with Y^{3+} in the SO_4^{2-} ν_2 region with increasing concentration of $Y_2(SO_4)_3$. 41

3.10. Temperature-dependent Raman spectra of $LiKSO_4$ in the SO_4^{2-} ν_1, ν_2 and ν_4 regions. The spectra at 500°C correspond to the high-temperature phase. 42

4.1. DSC thermogram of anhydrous Na_3PO_4. 53

4.2. XRD pattern of α-Na_3PO_4. Some peaks are labeled in terms of d-spacings in Å. 55

4.3. Temperature-dependent Raman spectra of Na_3PO_4 in the PO_4^{3-} ν_2 and ν_4 spectral regions. The spectrum at 360°C corresponds to the γ-phase. 65

4.4. Temperature-dependent Raman spectra of Na_3PO_4 in the PO_4^{3-} ν_1 spectral region. The spectrum at 360°C corresponds to the γ-phase. 67

4.5. Temperature-dependent Raman spectra of Na_3PO_4 in the PO_4^{3-} ν_3 spectral region. The spectrum at 360°C corresponds to the γ-phase. 68

4.6. Infrared spectrum of α-Na_3PO_4. 70

5.1. DSC thermograms of $Na_{3-x}S_xP_{1-x}O_4$ for increasing values of x. 80

5.2. XRD patterns of $Na_{3-x}S_xP_{1-x}O_4$ for increasing values of x. 82

5.3. Infrared spectra of $Na_{3-x}S_xP_{1-x}O_4$ for increasing values of x. 89

5.4. Raman spectra of $Na_{3-x}S_xP_{1-x}O_4$ in the ν_2 and ν_4 spectral regions for increasing values of x. 91

5.5. Raman spectra of $Na_{3-x}S_xP_{1-x}O_4$ in the ν_1 and ν_3 spectral regions for increasing values of x. 92

6.1. XRD patterns of $Na_{3-2x}Mg_xPO_4$ for increasing values of x. 105

6.2. DSC thermograms of $Na_{3-2x}Mg_xPO_4$ for increasing values of x. 109

6.3. Raman spectra of $Na_{3-2x}Mg_xPO_4$ in the ν_2 and ν_4 spectral regions for increasing values of x. 112

6.4. Raman spectra of $Na_{3-2x}Mg_xPO_4$ in the ν_1 spectral region for increasing values of x. 114

6.5. Raman spectra of $Na_{3-2x}Mg_xPO_4$ in the ν_3 spectral region for increasing values of x. 115

6.6. Raman spectra of $Na_{3-2x}Mg_xPO_4$ in the ν_3 spectral region for increasing values of x. 116

6.7. Raman spectra of $Na_{2.84}Mg_{0.08}PO_4$ in the ν_1 and ν_3 spectral regions. 118

6.8. XRD patterns of $Na_{3-2x}Zn_xPO_4$ for increasing values of x. 120

6.9. DSC thermograms of $Na_{3-2x}Zn_xPO_4$ for increasing values of x. 123

6.10. Raman spectra of $Na_{3-2x}Zn_xPO_4$ in the ν_1 spectral region for increasing values of x. 125

6.11. Raman spectra of $Na_{3-2x}Zn_xPO_4$ in the ν_2 and ν_4 spectral regions for increasing values of x. 126

6.12. Raman spectra of $Na_{3-2x}Zn_xPO_4$ in the ν_2 and ν_4 spectral regions for increasing values of x. 127

6.13. Raman spectra of $Na_{3-2x}Zn_xPO_4$ in the ν_3 spectral region for increasing values of x. 129

6.14. Raman spectra of $Na_{3-2x}Zn_xPO_4$ in the ν_3 spectral region for increasing values of x. 130

6.15. Raman spectra of $Na_{3-2x}Mg_xPO_4$ in the low frequency region for increasing values of x. 133

6.16. Raman spectra of $Na_{3-2x}Zn_xPO_4$ in the low frequency region for increasing values of x. 134

7.1. DSC thermograms of $Na_{3-3x}Zn_xS_xP_{1-x}O_4$ for increasing values of x. 139

7.2. XRD patterns of $Na_{3-3x}Zn_xS_xP_{1-x}O_4$ for increasing values of x. 141

7.3. Raman spectra of $Na_{3-3x}Zn_xS_xP_{1-x}O_4$ in the ν_2 and ν_4 spectral regions for increasing values of x. 144

7.4. Raman spectra of $Na_{3-3x}Zn_xS_xP_{1-x}O_4$ in the ν_2 and ν_4 spectral regions for increasing values of x. 145

7.5. Raman spectra of $Na_{3-3x}Zn_xS_xP_{1-x}O_4$ in the ν_1 spectral region for increasing values of x. 148

7.6. Raman spectra of $Na_{3-3x}Zn_xS_xP_{1-x}O_4$ in the ν_1 spectral region for increasing values of x. 149

7.7. Raman spectra of $Na_{3-3x}Zn_xS_xP_{1-x}O_4$ in the ν_3 spectral region 150

for increasing values of x.

7.8. Raman spectra of $Na_{3-3x}Zn_xS_xP_{1-x}O_4$ in the ν_3 spectral region 151

for increasing values of x.

8.1. The solid solution limits of different dopants vary dramatically. 159

ABSTRACT

The stabilization of polymorphic compounds has been of interest for some time. Previous studies have shown it is possible to stabilize the high-temperature, fast-ion-conducting phase of sodium phosphate (Na_3PO_4), but these systems have not been thoroughly characterized. Therefore, a systematic study was conducted of pure Na_3PO_4 and solid solutions of Na_3PO_4 doped with $Mg_3(PO_4)_2$, $Zn_3(PO_4)_2$, Na_2SO_4 and $ZnSO_4$. The techniques used in this study were Raman and infrared spectroscopies, differential scanning calorimetry, and powder x-ray diffraction.

Na_3PO_4 has two solid phases: the tetragonal α phase, stable to 320°C, and the cubic γ phase, stable from 320°C to the melt at 1500°C. Initially, a factor group analysis of the expected modes and their symmetry-based assignments was performed for these two phases. A temperature-dependent Raman study was then performed for the pure compound. The bands change from sharp multiplets to broad bands with increasing temperature. The broad bands and collapsed band structure seen in γ-Na_3PO_4 are indicative of the high disorder present.

γ- Na_3PO_4 is stabilized in all four dopant systems. The percentage of dopant necessary for complete stabilization is different for anion, cation, and combined dopants. The two cation dopant systems, $Na_3PO_4/Mg_3(PO_4)_2$ and $Na_3PO_4/Zn_3(PO_4)_2$, exhibit similar behavior although the Raman spectra indicate that Zn^{2+} has a stronger interaction than Mg^{2+} with the PO_4^{3-} ion. The Raman spectra in the $Na_3PO_4/ZnSO_4$ system exhibit characteristic bands seen in both the $Zn_3(PO_4)_2$- and Na_2SO_4-doped

systems. A remarkable characteristic of γ-Na_3PO_4 is the amount of aliovalent substitution that can be accommodated in the lattice before phase separation or compound formation occurs: 11% $Mg_3(PO_4)_2$ or $Zn_3(PO_4)_2$, more than 30% $ZnSO_4$, and over 60% Na_2SO_4.

This work illustrates the necessity of using a variety of techniques when characterizing these systems, which undergo complex structural changes that cannot be completely characterized using a single technique. The XRD results indicate a complete transition from α- to γ-Na_3PO_4 with no intermediate structures present. The DSC thermograms show the presence of a perturbed α- or γ-phase, but generally agree with the phases identified by the XRD patterns. Vibrational spectroscopy provides a richer description of the local structural changes occurring.

CHAPTER 1

INTRODUCTION

Research in the area of solid state ionic materials is a multidisciplinary effort involving chemists, chemical engineers, physicists, metallurgists, materials scientists and electrical engineers. This field covers a wide variety of topics including, but not limited to, the relationship between structures and ionic transport, the physics and chemistry of defects, the measurement of ionic transport, the thermodynamics of ionic materials, and the study of ion exchange phenomena.[1, 2] The phenomenon of ionic conduction in solids has been known since the mid-nineteenth century[3], but it has only been in the last 35 years that solid ionic conductors have been widely studied. Solid electrolytes have been used in applied technologies for nearly 100 years beginning with the development of the Nernst glower, which uses stabilized zirconia as a broad spectrum light source.[2, 4]

Much of the interest in solid state ionic conductors has been generated because of their potential applications in solid state batteries, fuel cells and sensors. Some advantages of solid state batteries are that they are free from leakage and they have long shelf lives. The disadvantages of these systems, compared to batteries utilizing liquid electrolytes, are poor interfacial contact, slow mass diffusion, and the formation of highly resistive reaction products that impede the cell reaction.[2, 5] There has also been a great deal of effort devoted to the development of high temperature fuel cells based on oxide ion conducting solid electrolytes. One of the primary advantages of

these systems is that the solid electrolyte can serve as both an ionic conductive layer and as a gas separator.[2, 6] The area of chemical sensors is probably where most of the commercial development of solid electrolytes has been focused. The application of these sensors varies from hazard alarms for home use to control units for automated production lines.[2] The most common application of oxygen sensors is in the measurement of the composition of the exhaust gases from internal combustion engines. These sensors allow for both the control of air pollution and better fuel economy.[2, 4, 7] Some less well-known applications of solid electrolytes are in the determination of thermodynamic data in solid and metal alloy systems, in coulometers and timers, and in electrochromic devices and analogue memory devices.[1, 2, 4, 6, 8, 9]

A solid electrolyte can be characterized as having a high ionic conductivity and a low activation energy. Of course, "high" ionic conductivity is a relative term and should be compared to conductivity values observed in most ionic solids, which is of the order of 10^{-12} to 10^{-6} $\Omega^{-1}cm^{-1}$.[10] Materials that are considered superionic conductors or fast-ion conductors, which is the preferred term, generally have conductivities in the vicinity of 10^{-2} to 1 $\Omega^{-1}cm^{-1}$ and activation energies less than 0.5 eV/ion at the operating temperature.[11, 12] Many of these fast-ion conductors are polymorphic and exhibit high ionic conductivity only after passing through a phase transition into a high-temperature phase. In fact, some of the early applications of solid electrolytes made use of the change in conductivity accompanying the phase transition. One example is the use of silver mercury iodide, which undergoes a phase

transition at 50°C, in a fire detector in the late 1930's.[4] In general, however, it is more important to stabilize the high conductivity phase to room temperature or at least depress the transition temperature to a range that is more suitable for commercial applications.

Polymorphism and Phase Stabilization

Webster's Ninth New Collegiate Dictionary[13] defines polymorphism as "the quality or state of being able to assume different forms: as ... **b:** the property of crystallizing in two or more forms with distinct structure." The historical development of polymorphic concepts as they relate to crystal structures is discussed by Buerger and Bloom in their 1937 article on crystal polymorphism.[14] The existence of polymorphism has been known since around 1798, but the concept was not accepted until about 1823. The first comprehensive study on the nature of polymorphism was reported in 1839 in an investigation of KNO_3. It was quickly determined that polymorphic substances were ubiquitous and polymorphism could be considered an inherent property of the solid state. The thermodynamically stable form at a given temperature and pressure would be the structure with the lowest configuration energy that could accommodate the necessary thermal motions.[14]

It is generally known that only one phase of a chemical species can be thermodynamically stable over a certain range of temperatures and pressures. Within this region all other phases should undergo a phase transition to the stable phase over time. However, there are many examples of substances that remain indefinitely in a

phase that is far from its region of thermodynamic stability. Two well-known examples of this are diamonds (carbon) and pearls (the aragonite form of calcium carbonate), neither of which are the thermodynamically stable phase at room temperature and pressure. Early studies attributed the genesis of "unstable" polymorphic forms to two major factors: (1) the composition of the groups of atoms present prior to the development of the solid phase, and (2) the possible crystal structures into which these groups could aggregate.[15] The majority of the stabilized phases have been attributed to the presence of dissolved impurities in the solid solution. In many cases it seems reasonable that the structure that can most easily accommodate the presence of the impurities will be favored. Buerger stated this quite clearly, writing in 1936 that "The direction of the migration of a transformation point with impurity content is in harmony with Le Chatalier's Rule put in the following specific form: If an impurity is to be housed, then the modification best adapted to housing it will tend to form."[16] This was echoed by Bredig[17] who distinguished between two stabilization mechanisms. The first mechanism is that the high-temperature phase is made thermodynamically stable relative to the solid solution in the low-temperature form. The second mechanism states that stabilization may be a kinetic effect in which the rate of transformation has been slowed to the point where it can be stopped completely upon rapid cooling of the material. One of the first systematic studies on the effect of "foreign" atoms on the stability of polymorphic forms was reported by Bloom and Buerger.[18] They found that the addition of "foreign atoms" could stabilize the high-temperature valentite form of Sb_2O_3 from 573°C down

to room temperature. However, it is not possible to predict which structure will form with the addition of impurities for any polymorphic system.

Fast-ion Conductors

Since the early 1960's, when high conductivity solid ionic conductors began to be extensively studied, investigators have been adding dopant ions to these materials in an attempt to increase their ionic conductivity, stabilize the fast-ion conducting phase, or both. It is known that some type of disorder in the structure is necessary for good ionic conductivity, but the nature of this disorder is quite different for different electrolytes.[11, 19] Some theoretical studies have related the phase transition into the fast-ion conducting state to the influence of defects in the structure.[20, 21] Some of the most widely studied systems are AgI, zirconia, beta aluminas and Nasicon materials.

Tubandt and coworkers discovered in the early 1900's that the solid state conductivity of silver iodide (AgI) jumps to a value almost equal to that observed in the molten salt when it transforms from the β- to the α-phase at 149°C.[22, 23] The conductivity of α-AgI is more than 10 $\Omega^{-1}cm^{-1}$, while that of the low-temperature β-AgI is only around 10^{-5} $\Omega^{-1}cm^{-1}$.[24] It was suggested that the interaction of interstitial cation defects combined with the resulting strain field was primarily responsible for the phase transition to the cation disordered α-phase.[20] Attempts to stabilize this phase to room temperature focused on the addition of dopant cations or anions, but were generally unsuccessful.[10, 25] Bradley and Greene[26, 27] discovered the related

compound of $RbAg_4I_5$, which also exhibits very high ionic conductivity, in an attempt to stabilize α-AgI. Although both compounds show very high ionic conductivity, their structures are not analogous.[28] $Rb_4Cu_{16}I_7Cl_{13}$ is one of the most highly conducting solid electrolytes developed, with a conductivity of 0.3 $\Omega^{-1}cm^{-1}$ at room temperature. This is almost comparable to the conductivity of sulfuric acid solutions.[2] Recently, the α-phase of AgI has been quenched in a silver borate glass matrix with the quenched material displaying an ionic conductivity of about 10^{-1} $\Omega^{-1}cm^{-1}$.[24] Although these systems have primarily been characterized using x-ray diffraction and conductivity measurements, the nature of the phase transition has also been investigated using Raman spectroscopy.[29-32]

Zirconia (ZrO_2), especially stabilized zirconia, is one of the most commonly used oxide ion conductors. ZrO_2 is monoclinic at room temperature and tetragonal at temperatures above 1500°C. Both of these crystal forms are distorted fluorite-type structures. The addition of 10-20 mole percent of CaO causes a cubic fluorite-type solid solution to form which is stable to the melting point.[2] One question that occurs repeatedly in these systems concerns the extent of ordering in stabilized zirconia. Extensive structural studies suggest that the calcia-stabilized zirconia crystals can be described in terms of a cubic matrix within which are microdomains of both $CaZr_4O_9$ and intragranular precipitates of monoclinic ZrO_2. Although the presence of microdomains can be detected, the diffraction patterns suggest that the two features arise from a coherent single crystal which is primarily of the fluorite structure type.[33]

Although stabilized zirconia was one of the first solid electrolytes commercialized, new zirconia solid solutions are still being developed and characterized.[34, 35]

Sodium beta-aluminas are probably the most famous sodium ion conductors. They have primarily been used in sodium/sulfur batteries. Although the "ideal" composition is $Na_2O{\cdot}11Al_2O_3$, this has never been observed. The compounds are always nonstoichiometric as prepared, and the compositions are frequently represented by $Na_{1+x}Al_{11}O_{17+x/2}$.[2, 34, 36–46] Most of these materials have conductivities of about 10^{-6} at room temperature and 10^{-1} $\Omega^{-1}cm^{-1}$ at 300-400°C.[1] Much of the early work on identifying beta-aluminas as fast-ion conductors was done by Kummer and coworkers.[41, 45] This work was quickly followed by additional measurements on the ionic transport and diffusion in these materials.[44, 47] There are two modifications of sodium beta alumina, β-alumina and β″-alumina, both of which have well-characterized structures. The use of the symbols β and β″ generally indicates a specific phase while the spelled out word "beta" refers to the class of compounds having related structures. Both structures form wide ranges of solid solutions, but since β″-alumina exhibits higher ionic conductivities than β-alumina, it is the preferred structure. The β″-aluminas have been shown to have an exceptional ability to undergo ion exchange reactions in which Na^+ ions are replaced by other monovalent, divalent and trivalent cations.[40] β″-alumina can be stabilized to room temperature by the addition of monovalent and divalent dopant ions. The most commonly used dopant ions for stabilizing the β″ structure are Li^+ and Mg^{2+}.[38–40, 46, 48]

Nasicon, which stands for Na Super Ionic Conductors, has the formula $Na_{1+x}Zr_2P_{3-x}Si_xO_{12}$ and was first discovered by Goodenough and coworkers in 1976.[49,50] The best conductivities of around 5 $\Omega^{-1}cm^{-1}$ are achieved at a composition of x=0.2. These materials were quickly viewed as possible substitutes for β- and β"-aluminas in Na/S batteries and other electrochemical cells.[49, 51] The Nasicon structure can accept a large number of substituent ions, leading to the development of many compounds with related structures.[36, 51-56] These materials are often referred to as Nasicon-type or NZP-type compounds. These materials also undergo a variety of phase transitions in which the magnitude of the thermal effects and changes in ionic conductivity are largely dependent on the degree of static disorder, particularly orientational disorder, present in the structure. It has been suggested that the phase transitions are due to the ordering of the Si/P structure.[57, 58] The exact nature of the ionic conductivity in relation to ionic diffusion mechanisms and crystal structure is not yet well understood, so there are still efforts being made to understand the fundamental properties of the Nasicon system.[59]

The need for both a fundamental understanding of fast-ion conductors like β-alumina and Nasicon and for the discovery and characterization of new materials led to the investigation of other sodium ion conductors. Sodium phosphate (Na_3PO_4), with its high sodium concentration and high temperature, fast-ion conducting phase, offered the opportunity to study sodium ion conductivity in a compound containing discrete anions rather than an extended anionic network as is found in Nasicon and β-alumina.[60] The high decomposition point and cubic symmetry of the high

temperature phase also made it amenable to applications in solid state devices. γ-Na_3PO_4 is a versatile host structure and forms a series of solid solutions with substitutions possible in both the sodium and phosphorous sites. The γ-phase can be stabilized to room temperature by doping with divalent, trivalent, tetravalent and hexavalent ions.[60-73] The pure compound has only modest conductivities, $\sigma=10^{-4}$ at 350°C, but the conductivity increases in the solid solutions due to the formation of sodium ion vacancies.[63] The doped γ-Na_3PO_4 solid solutions have promise as sodium ion conducting solid electrolytes with conductivities on the order of 10^{-2} $\Omega^{-1}cm^{-1}$.[64,69,70]

Raman Studies of Phase Transitions and Phase Stabilization

The phases and structure present in these compounds and solid solutions are generally characterized using x-ray diffraction and thermal analysis. However, these techniques are not always sensitive to local structural changes occurring in the materials. The characterization of these materials using vibrational spectroscopy provides another avenue to determine more of the local structure in the crystals. This is particularly true for orientationally disordered crystals since diffraction techniques yield only the average structure, while Raman spectroscopy probes the normal modes of vibrations which are sensitive to the disorder and orientation of ions in the crystal.

Raman spectroscopy has been used to characterize the phase transitions in fast-ion conducting compounds[29-32, 74-83], but in general this work has not been extended to the characterization of the doped or phase-stabilized compounds. One of the first reports on the use of Raman spectroscopy to investigate the mechanism of

phase stabilization was by Scott and coworkers.[79] In their study, the mechanism for the stabilization of the ferroelectric phase III in KNO_3 was investigated. The results of their vibrational spectroscopic study indicate that surface electric fields dominate over stress and strain present in the thin films. Raman spectroscopy has also been used to study perturbations in the superconductor $YBa_2Cu_3O_{7-x}$ caused by impurities in the Cu sites.[84] This has been done by examining the effect of impurities on the vibrations of the CuO_4 vibrational groups.

The most extensive study using Raman spectroscopy to characterize the phase stabilization of fast-ion conductors was conducted in this laboratory in an investigation of the effect of dopant ions on the phase transitions in Na_2SO_4 and related compounds.[85-89, 92] These studies demonstrate the advantages of using Raman spectroscopy as an additional technique to characterize solid solutions. In this case the stabilization of phase III at very low dopant concentrations could be determined using Raman spectroscopy but not using XRD studies. This was likely due to the fact that both phase V and phase III of Na_2SO_4 have orthorhombic structures that are difficult to distinguish using diffraction techniques. However, these phases can be clearly distinguished using Raman spectroscopy.[85, 86, 90, 91] It was also possible to observe the changes in the local environment of the SO_4^{2-} ions as the host lattice was perturbed by the presence of aliovalent cations in systems that were not phase stabilized.[87, 92]

Overview of Research

The work presented here is an extensive study of the characterization of pure Na_3PO_4 and γ-Na_3PO_4 phase stabilized by aliovalent ion substitution as well as some dopant studies on $LiNaSO_4$ and $LiKSO_4$. These investigations contribute to a general understanding of the mechanism of phase stabilization and the ability to prepare stabilized phases with desirable properties. The systematic investigation of the structure and dynamics of the stabilized phase, particularly in respect to the nature of the orientational disorder present, is necessary to further our understanding of the fundamental processes that lead to phase stabilization.

Raman spectroscopy, powder x-ray diffraction and differential scanning calorimetry were used to characterize the samples. A detailed description of the experimental methods used in this study is provided in Chapter 2. The results of the effects of $Y_2(SO_4)_3$ substitution in $LiNaSO_4$ and $LiKSO_4$ are reported in Chapter 3. Phase stabilization was not observed in these systems, but the formation of new compounds or phases was determined. A detailed vibrational analysis and the temperature-dependent Raman spectra of pure Na_3PO_4 are presented in Chapter 4. The effects of aliovalent anion (specifically SO_4^{2-}) doping on Na_3PO_4 are presented in Chapter 5. Phase stabilization is observed in this system over a wide range of solid solution compositions. The phase stabilization and structural changes observed for aliovalent cation doping of Na_3PO_4 with Zn^{2+} or Mg^{2+} are discussed in Chapter 6. The effects of doping Na_3PO_4 simultaneously with both cations and anions are presented

in Chapter 7. The results of the three different types of dopant studies are then summarized and future studies proposed.

References

1. Takahashi, T. in *Superionic Solids and Solid Electrolytes: Recent Trends* (eds. Laskar, A.L. & Chandra, S.) 1-41 (Academic Press, Inc., Boston, 1989).

2. Kudo, T. & Fueki, K. *Solid State Ionics* (Kodansha, Tokyo, 1990).

3. Takahashi, T. in *High Conductivity Solid Ionic Conductors: Recent Trends and Applications* (ed. Takahashi, T.) 1-16 (World Scientific, Singapore, 1989).

4. Huggins, R.A. in *High Conductivity Solid Ionic Conductors: Recent Trends in Applications* (ed. Takahashi, T.) 664-679 (World Scientific, Singapore, 1989).

5. Linford, R.G. in *High Conductivity Solid Ionic Conductors: Recent Trends and Applications* (ed. Takahashi, T.) 564-594 (World Scientific, Singapore, 1989).

6. Shuk, P., Wiemhofer, H.-D., Guth, U., Gopel, W. & Greenblatt, M. *Solid State Ionics* **89**, 179-196 (1996).

7. Etsell, T.H. & Flengas, S.N. *Chem. Rev.* **70**, 339-376 (1970).

8. Kiukkola, K. & Wagner, C. *J. Electrochem. Soc.* **104**, 308-316 (1957).

9. Kiukkola, K. & Wagner, C. *J. Electrochem. Soc.* **104**, 379-387 (1957).

10. Owens, B.B. & Argue, G.R. *J. Electrochem. Soc.* **117**, 898-900 (1970).

11. van Gool, W. in *Solid Electrolytes: General Principles, Characterization, Materials, Applications* (eds. Hagenmuller, P. & van Gool, W.) 9-26 (Academic Press, New York, 1978).

12. Robertson, A.D., West, A.R. & Ritchie, A.G. *Solid State Ionics* **104**, 1-11 (1997).

13. *Webster's Ninth New Collegiate Dictionary* (Merriam-Webster Inc., Springfield, Massachusetts, 1987).

14. Buerger, M.J. & Bloom, M.C. *Z. Krist.* **96**, 182-200 (1937).

15. Bloom, M.C. *Amer. Mineral.* **24**, 281-292 (1939).

16. Buerger, M.J. *Proc. Nat. Acad. Sci.* **22**, 685-689 (1936).

17. Bredig, M.A. *J. Phys. Chem.* **46**, 747-764 (1942).

18. Bloom, M.C. & Buerger, M.J. *Z. Krist.* **96**, 365-375 (1937).

19. Huggins, R.A. in *Solid Electrolytes: General Principles, Characterization, Materials, Applications* (eds. Hagenmuller, P. & van Gool, W.) 27-44 (Academic Press, New York, 1978).

20. Rice, M.J., Strassler, S. & Toombs, G.A. *Phys. Rev. Lett.* **32**, 596-599 (1974).

21. Pardee, W.J. & Mahan, G.D. *J. Solid State Chem.* **15**, 310-324 (1975).

22. Tubandt, C. & Lorenz, E. *Z. Phys. Chem.* **87**, 513-542 (1914).

23. Tubandt, V.C. & Reinhold, H. *Z. Elektrochem.* **29**, 313-317 (1923).

24. Tatsumisago, M., Shinkuma, Y. & Minami, T. *Nature* **354**, 217-218 (1991).

25. Owens, B.B. & Argue, G.R. *Science* **157**, 308-310 (1967).

26. Bradley, J.N. & Greene, P.D. *Trans. Faraday Soc.* **62**, 2069-2075 (1966).

27. Bradley, J.N. & Greene, P.D. *Trans. Faraday Soc.* **63**, 424-430 (1967).

28. Geller, S. *Science* **157**, 310-312 (1967).

29. Hanson, R.C., Fjeldly, T.A. & Hochheimer, H.D. *Phys. Status Solidi B* **70**, 567-576 (1975).

30. Burns, G., Dacol, F.H. & Shafer, M.W. *Solid State Commun.* **19**, 291-295 (1976).

31. Burns, G., Dacol, F.H. & Shafer, M.W. *Solid State Commun.* **19**, 287-290 (1976).

32. Gallagher, D. & Klein, M.V. *J. Phys. C* **9**, L687-L692 (1976).

33. Hudson, B. & Moseley, P.T. *J. Solid State Chem.* **19**, 383-389 (1976).

34. Chiba, R., *et al. Solid State Ionics* **104**, 259-266 (1997).

35. Moreau, S., Gervais, M. & Douy, A. *Solid State Ionics* **101-103**, 625-631 (1997).

36. Alamo, J. *Solid State Ionics* **63-65**, 547-561 (1993).

37. Boilot, J.P., Collin, G., Colomban, P. & Comes, R. *Phys. Rev. B* **22**, 5912-5923 (1980).

38. Duncan, G.K. & West, A.R. *Solid State Ionics* **9/10**, 259-264 (1983).

39. Duncan, G.K. & West, A.R. *Solid State Ionics* **28-30**, 338-343 (1988).

40. Farrington, G.C., Dunn, B. & Thomas, J.O. in *High Conductivity Solid Ionic Conductors: Recent Trends and Applications* (ed. Takahashi, T.) 327-365 (World Scientific, Singapore, 1989).

41. Radzilowski, R.H., Yao, Y.F. & Kummer, J.T. *J. Appl. Phys.* **40**, 4716-4725 (1969).

42. Roth, W.L. *J. Solid State Chem.* **4**, 60-75 (1972).

43. Seevers, R., DeNuzzio, J., Farrington, G.C. & Dunn, B. *J. Solid State Chem.* **50**, 146-152 (1983).

44. Whittingham, M.S. & Huggins, R.A. *J. Chem. Phys.* **54**, 414-416 (1971).

45. Yao, Y.-F.Y. & Kummer, J.T. *J. Inorg. Nucl. Chem.* **29**, 2453-2475 (1967).

46. Zu-Xiang, L. in *High Conductivity Solid Ionic Conductors: Recent Trends and Applications* (ed. Takahashi, T.) 223-241 (World Scientific, Singapore, 1989).

47. Allen, S.J., Jr. & Remeika, J.P. *Phys. Rev. Lett.* **33**, 1478-1481 (1974).

48. West, A.R. *J. Mat. Chem.* **3**, 433-440 (1993).

49. Goodenough, J.B., Hong, H.Y.-P. & Kafalas, J.A. *Mat. Res. Bull.* **11**, 203-210 (1976).

50. Hong, H.Y.-P. *Mat. Res. Bull.* **11**, 173-182 (1976).

51. Yde-Anderson, S., Lundsgaard, J.S., Moller, L. & Engall, J. *Solid State Ionics* **14**, 73-79 (1984).

52. Roy, R., Vance, E.R. & Alamo, J. *Mat. Res. Bull.* **17**, 585-589 (1982).

53. Ishii, T. *Solid State Ionics* **78**, 333-338 (1995).

54. Rangan, K.K. & Gopalakrishnan, J. *Inorg. Chem.* **34**, 1969-1972 (1995).

55. Miyajima, M., Saito, Y., Matsuoka, M. & Yamamoto, Y. *Solid State Ionics* **84**, 61-64 (1996).

56. Verissimo, C., *et al. Solid State Ionics* **100**, 127-134 (1997).

57. Collin, G. & Boilot, J.P. in *Superionic Solids and Solid Electrolytes* (eds. Laskar, A.L. & Chandra, S.) 227-264 (Academic Press, Inc., Boston, 1989).

58. Kreuer, K.-D., Kohler, H. & Maier, J. in *High Conductivity Solid Ionic Conductors: Recent Trends and Applications* (ed. Takahashi, T.) 242-279 (World Scientific, Singapore, 1989).

59. Ivanov-Schitz, A.K. & Bykov, A.B. *Solid State Ionics* **100**, 153-155 (1997).

60. Hooper, A., McGeehin, P., Harrison, K.T. & Tofield, B.C. *J. Solid State Chem.* **24**, 265-275 (1978).

61. Dollase, W.A., Merwin, L.H. & Sebald, A. *J. Solid State Chem.* **83**, 140-149 (1989).

62. Irvine, J.T.S. & West, A.R. *J. Solid State Chem.* **69**, 126-134 (1987).

63. Irvine, J.T.S. & West, A.R. *Mat. Res. Bull.* **22**, 1047-1054 (1987).

64. Irvine, J.T.S. & West, A.R. *Solid State Ionics* **28-30**, 214-219 (1988).

65. Irvine, J.T.S. & West, A.R. *Solid State Ionics* **37**, 73-78 (1989).

66. Irvine, J.T.S. & West, A.R. *J. Solid State Chem.* **74**, 385-392 (1988).

67. Kolsi, A.-W. *Rev. Chim. Miner.* **13**, 416-421 (1976).

68. Kolsi, A.-W., Erb, A. & Freundlich, W. *Comptes Rendus Acad Sc Paris, Serie C* **282**, 575-577 (1976).

69. Milne, S.J. & West, A.R. *Mat. Res. Bull.* **19**, 705-710 (1984).

70. Milne, S.J. & West, A.R. *J. Solid State Chem.* **57**, 166-177 (1985).

71. Newsam, J.M., Cheetham, A.K. & Tofield, B.C. *Solid State Ionics* **1**, 395-410 (1980).

72. Palazzi, M. & Rémy, F. *Bull. Soc. Chim. Fr.* **8**, 2795-2798 (1971).

73. Wiench, V.D.M. & Jansen, M. *Z. Anorg. Allg. Chem.* **486**, 57-60 (1982).

74. Cazzanelli, E. & Frech, R. *J. Chem. Phys.* **81**, 4729-4736 (1984).

75. Cazzanelli, E. & Frech, R. *J. Chem. Phys.* **84**, 626-630 (1986).

76. Choi, B.-K. & Lockwood, D.J. *Solid State Commun.* **76**, 863-866 (1990).

77. Cody, C.A., DiCarlo, L. & Darlington, R.K. *J. Inorg. Nucl. Chem.* **43**, 398 (1981).

78. Montero, S. *Spectrochim. Acta* **32A**, 843-849 (1976).

79. Scott, J.F., Zhang, M.-s., Godfrey, R.B., Aranja, C. & McMillan, L. *Phys. Rev.B* **35**, 4044-4051 (1987).

80. Shand, M., Hanson, R.C., Derrington, C.E. & O'Keefe, M. *Solid State Commun.* **18**, 769-772 (1976).

81. Teeters, D. & Frech, R. *J. Chem. Phys.* **76**, 799-804 (1982).

82. Wang, C.H. & Wright, R.B. *J. Chem. Phys.* **58**, 1411-1419 (1973).

83. Zhang, M.-s., Katiyar, R.S. & Scott, J.F. *Ferroelectrics* **74**, 309-316 (1987).

84. Sengupta, L.C., Roughani, B., Aubel, J., Sundaram, S. & Joiner, W.C.H. *Physica C* **165**, 125-130 (1990).

85. Dharmasena, G. & Frech, R. *Solid State Ionics* **53-56**, 1274-1277 (1992).

86. Dharmasena, G. & Frech, R. *J. Chem. Phys.* **99**, 8929-8935 (1993).

87. Frech, R.E., Cole, R. & Dharmasena, G. *J. Solid State Chem.* **105**, 151-160 (1993).

88. Dharmasena, G., Schlindwein, W.S., Frech, R. & Linford, R.G. *J. Chem. Phys.* **101**, 9232-9235 (1994).

89. Frech, R. & Dharmasena, G. *Solid State Ionics* **70/71**, 191-195 (1994).

90. Choi, B.-K. & Lockwood, D.J. *Solid State Commun.* **72**, 133-137 (1989).

91. Choi, B.-K., Labbé, H.J. & Lockwood, D.J. *Solid State Commun.* **74**, 109-113 (1990).

92. Dharmasena, G. in *Ph.D. Dissertation* (University of Oklahoma, Norman, OK, 1994).

CHAPTER 2

EXPERIMENTAL

This chapter describes the experimental techniques and equipment used for sample preparation and data collection. These data will be presented in the forthcoming chapters, where any additional modifications will be noted.

Sample Preparation

Lithium Sodium Sulfate and Lithium Potassium Sulfate

Single crystals of lithium sodium sulfate ($LiNaSO_4$) and lithium potassium sulfate ($LiKSO_4$) were grown by slow evaporation from aqueous solutions containing equimolar proportions of the appropriate sulfate salts. $LiNaSO_4$ was grown in an aqueous solution at 70°C to which sulfuric acid had been added to obtain a pH of 2. $LiKSO_4$ was grown in solution at 40°C. The single crystals were ground and examined as the host compound for comparison in the preparation of substituted polycrystalline samples, which were used in the Raman studies described in chapter III.

Polycrystalline samples of $LiNaSO_4$ and $LiKSO_4$ doped with $Y_2(SO_4)_3$ were prepared by intimately mixing appropriate amounts of the host salt with $Y_2(SO_4)_3$ using a mortar and pestle, then transferring them to a platinum crucible. The mixtures were melted at 950°C for six hours, lowering the temperature to 700°C for three hours, before cooling to room temperature over a period of six hours. The resulting

polycrystalline masses were ground to a fine powder with a mortar and pestle. The exact purity and grade of each compound are given at the end of this chapter.

Sodium Phosphate

Polycrystalline samples of pure α-Na_3PO_4 were prepared using two different routes: Na_2HPO_4 + Na_2CO_3 and $(NH_4)_2HPO_4$ + Na_2CO_3. Both reactions gave identical final products. The samples were prepared by combining appropriate amounts of the indicated compounds, grinding them together with an agate mortar and pestle, then transferring the mixture to an alumina crucible. The samples were placed in a Lindberg tube furnace, heated at 250°C for three hours, moved to a Thermolyne 46100 high temperature muffle furnace, heated to 650°C for one hour, then 800°C for two hours before slowly cooling to room temperature. The samples were reground and returned to the furnace where they were heated to 650°C for one hour, 800°C for two hours, and 1000°C for 48 hours before being cooled to room temperature.

The doped samples were prepared by combining the component compounds (shown below) in the proper ratios to obtain the desired molar ratios of Na_3PO_4/dopant.

Na^+ Source	PO_4^{3-} Source	Dopant Source	Dopant Ion(s)
Na_2CO_3	$(NH_4)_2HPO_4$	$ZnSO_4$	Zn^{2+} + SO_4^{2-}
Na_2CO_3	$(NH_4)_2HPO_4$	ZnO	Zn^{2+}

$Na_2CO_3 + (NH_4)_2HPO_4 + MgO$	Mg^{2+}
$Na_2CO_3 + (NH_4)H_2PO_4 + MgO$	Mg^{2+}
$Na_2CO_3 + (NH_4)H_2PO_4 + Na_2SO_4$	SO_4^{2-}

The $ZnSO_4 \cdot 7H_2O$ was dehydrated to the anhydrous salt before being used in sample preparation. The samples prepared using ZnO and MgO essentially resulted in dopants of $Zn_3(PO_4)_2$ and $Mg_3(PO_4)_2$, respectively. In the literature both $(NH_4)_2HPO_4$[1] and $(NH_4)H_2PO_4$[2] are used in these reactions. MgO doped samples were prepared using each one, and there was no difference in the resulting products. Therefore, the more readily obtained $(NH_4)_2HPO_4$ was used for a majority of the syntheses. The preparation of the samples containing ZnO, MgO, and $ZnSO_4$ followed the same procedure as that outlined above for the pure Na_3PO_4. The Na_2SO_4-doped samples were not reground in the middle of the heat treatment, but were heated at 1000°C for 48 hours after the first heat treatment at 250, 650, and 800°C. One trial run was made in which the Na_2SO_4-doped samples were also cooled and reground in the middle, but there was no difference in the resulting product. The exact purity and grade of each compound used are given at the end of this chapter.

Raman Spectroscopy

The majority of the Raman spectra were recorded on an I.S.A. Jobin-Yvon T64000 spectrometer in the triple subtractive mode. The scan time was set at sixteen seconds with ten accumulations. The 514.5 nm line of an argon-ion laser was used for excitation at 300 mW output power. With the exception of the temperature-

dependent data, all spectra were measured using the microprobe platform with a backscattering geometry. Samples were prepared by pressing powdered samples between two glass slides. The top slide was then removed and the sample was placed under the 80x objective lens on an Olympus microscope stage. This focused the laser beam to an approximately two micron area on the sample.

Temperature dependent spectra were measured using a high temperature cell placed in the macro chamber. The cell (shown in Figure 2.1) is a modification of a design by Quist.[3, 4] A sample holder appropriate for use with powdered samples in glass capillary tubes is shown in Figure 2.2. The sample holder was custom designed and made by the OU Physics Machine Shop. The temperatures for this cell were calibrated to within 3°C. The macro chamber was also set up in a backscattering configuration.

The $LiNaSO_4$ and $LiKSO_4$ spectra were recorded at a 3 cm^{-1} spectral slitwidth on a system based on a 0.85 m Czerny-Turner double monochromator. A right angle configuration was used for data collection.

Infrared Spectroscopy

Infrared spectra were recorded on a Bruker IFS66V system. Measurements were made in the absorbance mode with a resolution of 2 cm^{-1} and an accumulation of 64 scans. All samples were prepared as KBr pellets with a 13 mm diameter.

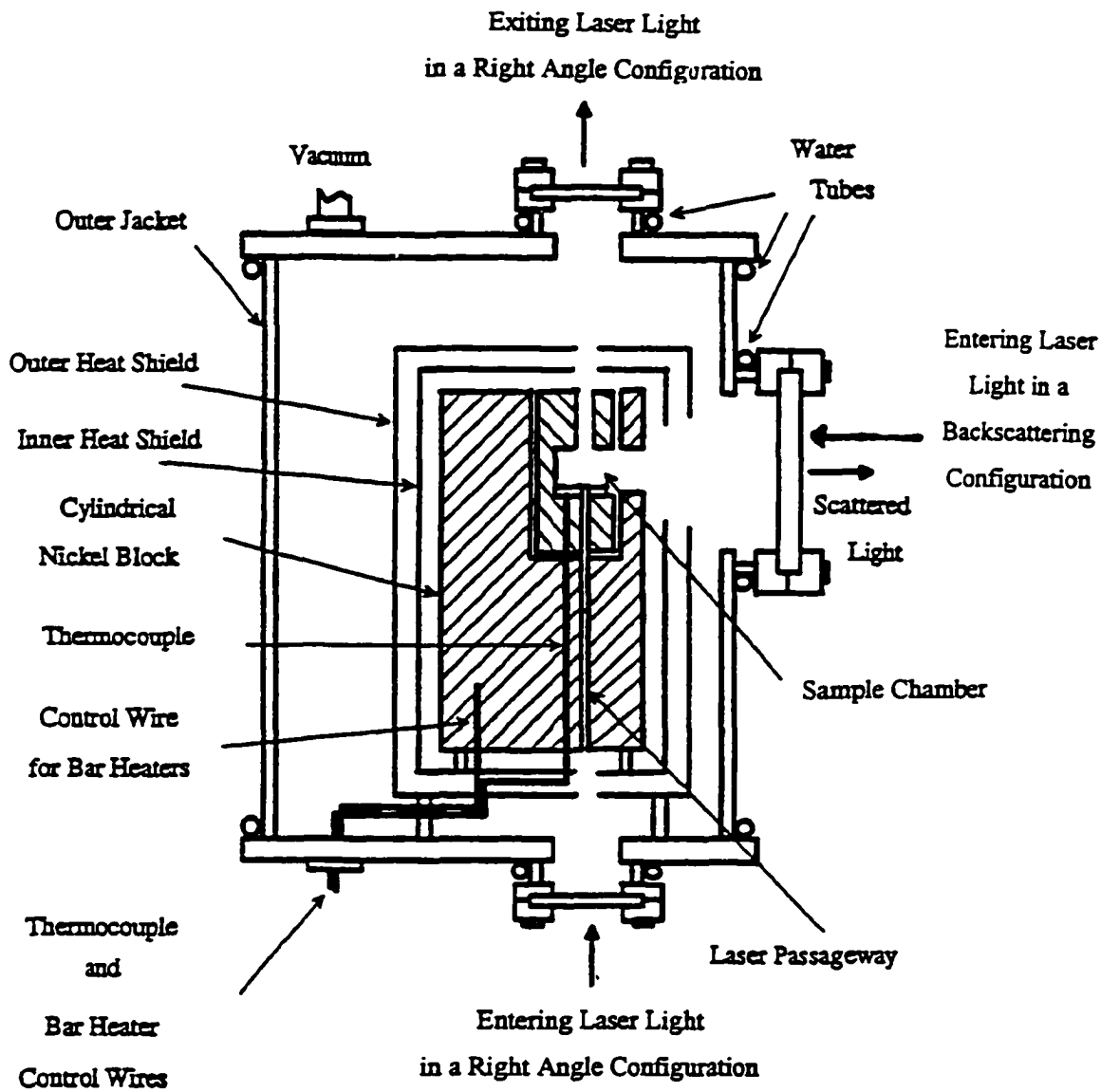

Figure 2.1. High Temperature Raman Cell

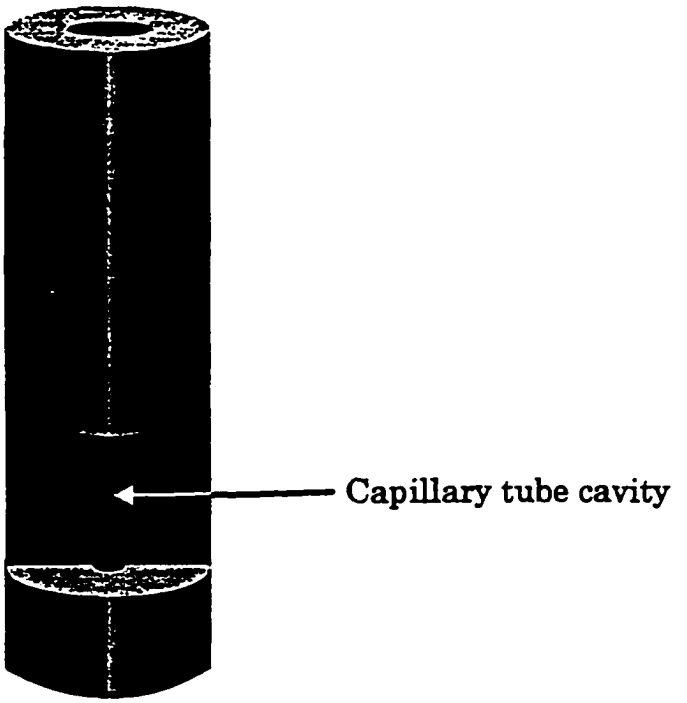

Figure 2.2. Sample Holder for Capillary Tubes

Differential Scanning Calorimetry

The differential scanning calorimetry (DSC) thermograms were recorded on a liquid nitrogen cooled Mettler-Toledo DSC820. Samples were ground powders placed in 40 μL aluminum pans. Thermograms were recorded from 50°C to 400°C and from 400°C to 150°C with heating rates of +10°C/min and -10°C/min, respectively.

Powder X-ray Diffraction

Powder x-ray diffraction (XRD) patterns were recorded on a Phillips-Norelco diffractometer with a fixed divergence slit of 1-degree, a fixed antiscatter slit of 1-degree, and a receiving slit of 0.15 mm. Cu K-α radiation (1.54178 Å) was used with the tube operated at 25 kV and 30 mA. The diffractometer was linked to a computer with OMNI® automation for data collection. Data were collected in the step-scanned, 2-theta mode from 10 to 70 degrees with 0.05 degrees per step and a measuring time of one second per step. Data (counts per second and 2-theta values) were reduced and analyzed using Auto-XRay software. Samples were prepared as smear mounts on glass slides.

List of Reagents

$Li_2SO_4 \cdot H_2O$	Reagent Grade	Aldrich
Na_2SO_4	Reagent Grade	Mallinckrodt
K_2SO_4	Reagent Grade	Aldrich
$Y_2(SO_4) \cdot 8H_2O$	99.9% purity	Alfa

Na_2HPO_4	Reagent Grade	Mallinckrodt
Na_2CO_3	Reagent Grade	Mallinckrodt
$(NH_4)_2HPO_4$	99% purity	Aldrich
$NH_4H_2PO_4$	98+% purity	Aldrich
$ZnSO_4 7H_2O$	99.5% purity	Fluka
ZnO	99.9% purity	Aldrich
MgO	99.9% purity	Aldrich

References

1. Milne, S.J. & West, A.R. *J. Solid State Chem.* **57**, 166-177 (1985).

2. Irvine, J.T.S. & West, A.R. *J. Solid State Chem.* **69**, 126-134 (1987).

3. Quist, A.S. *Appl. Spectrosc.* **25**, 82-84 (1971).

4. Made by Department of Physics Machine Shop, University of Oklahoma.

CHAPTER 3

$Y_2(SO_4)_3$-SUBSTITUTED $LiNaSO_4$ AND $LiKSO_4$

Introduction

The phase stabilization of sodium sulfate by aliovalent cation substitution has been well studied[1-15] so the search for additional systems in which phase stabilization occurs initially focused on other sulfate salts. Because lithium sodium sulfate ($LiNaSO_4$) and lithium potassium sulfate ($LiKSO_4$) are both polymorphic, the effect of aliovalent cation substitution in these compounds was also examined.

$LiNaSO_4$ crystallizes in the P31c (C_{3v}^4) space group with six molecular units in the hexagonal cell.[16] At 518°C this compound undergoes a phase transition into a body-centered cubic phase[17] which has high ionic conductivity.[18] $LiKSO_4$ forms a bimolecular unit cell in the $P6_3$ space group.[19] A transition into an orthorhombic phase occurs at 436°C[20] although no phase of this compound is reported to exhibit unusually high ionic conductivity.

The effect of aliovalent substitution on these compounds has been studied by preparing $LiNaSO_4$ and $LiKSO_4$ with yttrium sulfate, $Y_2(SO_4)_3$, as a substituent over a concentration range of three to fifteen mole percent. The resulting compounds were then investigated using Raman spectroscopy. The $LiKSO_4$ system was also examined using differential scanning calorimetry (DSC) and powder x-ray diffraction (XRD).

Lithium Sodium Sulfate: Raman Spectra

Pure $LiNaSO_4$ has three bands in the ν_1 spectral region at 973, 1000 and 1027 cm^{-1}.[21] These bands are observed in all compositions, as seen in Figure 3.1, although the relative intensity changes. As the percent of $Y_2(SO_4)_3$ increases the intensity of the band at 1027 cm^{-1} decreases until it is barely perceptible. The band at 1000 cm^{-1} increases in intensity relative to the other two bands to become the dominant peak in the 85/15 composition. The band at 973 cm^{-1} decreases in intensity as the percentage of yttrium in the lattice increases. In the 93/7 composition, a new feature at 1013 cm^{-1} appears. This can be assigned to the ν_1 mode of $Y_2(SO_4)_3$ through comparison with the spectrum of pure $Y_2(SO_4)_3$. However, an additional band appears at 1036 cm^{-1} in the 90/10 composition and increases in relative intensity in the 85/15 composition. This band does not correspond to any known mode in either the host or dopant compound and seems to signal the appearance of a new compound or phase.

The ν_3 region of pure $LiNaSO_4$ (shown in Figure 3.2) consists of four bands at 1070, 1124, 1139 and 1174 cm^{-1}. These bands remain detectable throughout the entire series of substituted compositions, although the intensity decreases significantly. At 93/7 $LiNaSO_4$/ $Y_2(SO_4)_3$ additional features not belonging to the host compound can be easily seen. Bands at 1122, 1145 and 1184 cm^{-1} can be attributed to $Y_2(SO_4)_3$. However, the four new components observed at 1092, 1151, 1195 and 1241 cm^{-1} do not belong to either $LiNaSO_4$ or $Y_2(SO_4)_3$.

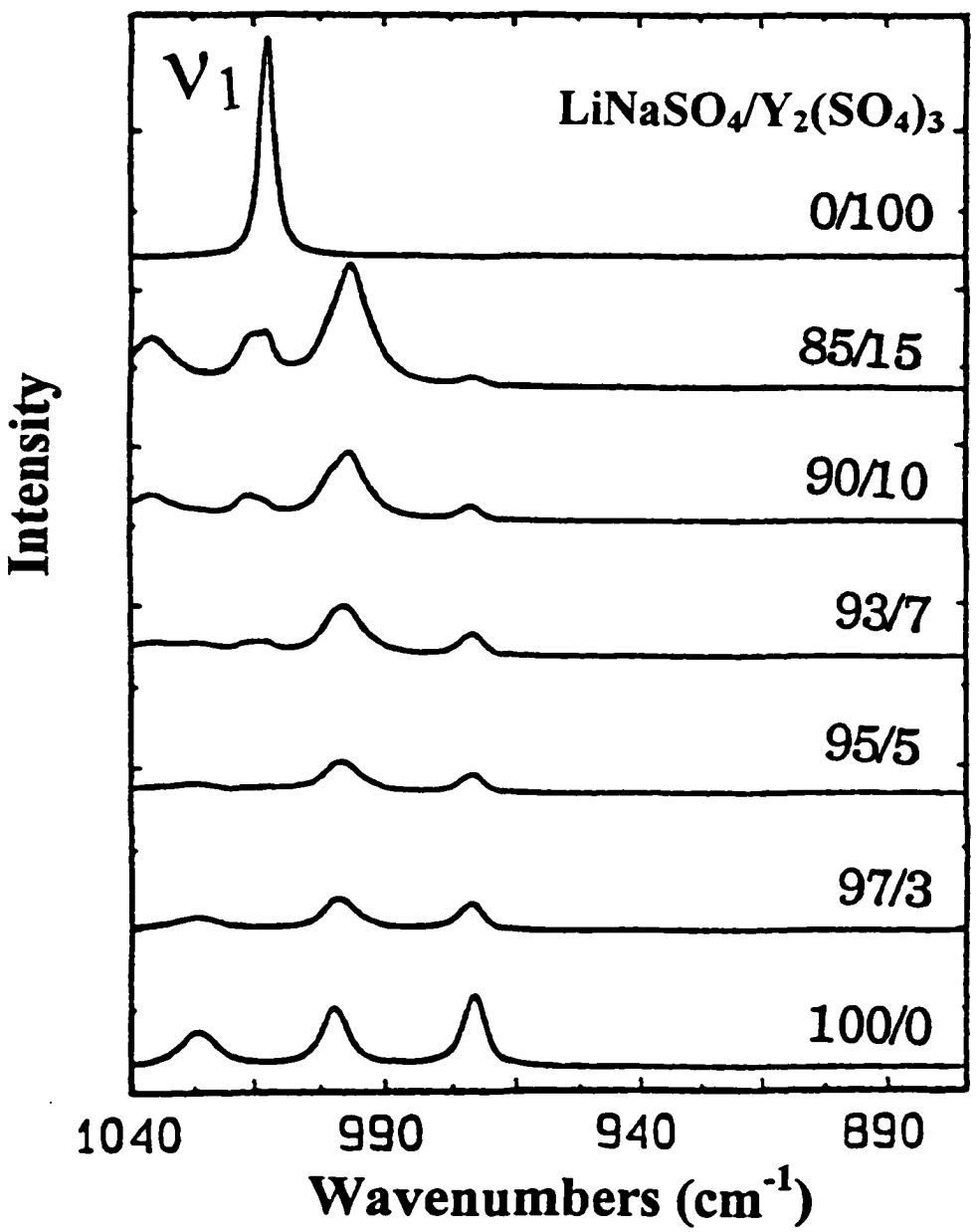

Figure 3.1. Raman spectra of $LiNaSO_4$ substituted with Y^{3+} in the SO_4^{2-} ν_1 region with increasing concentration of $Y_2(SO_4)_3$.

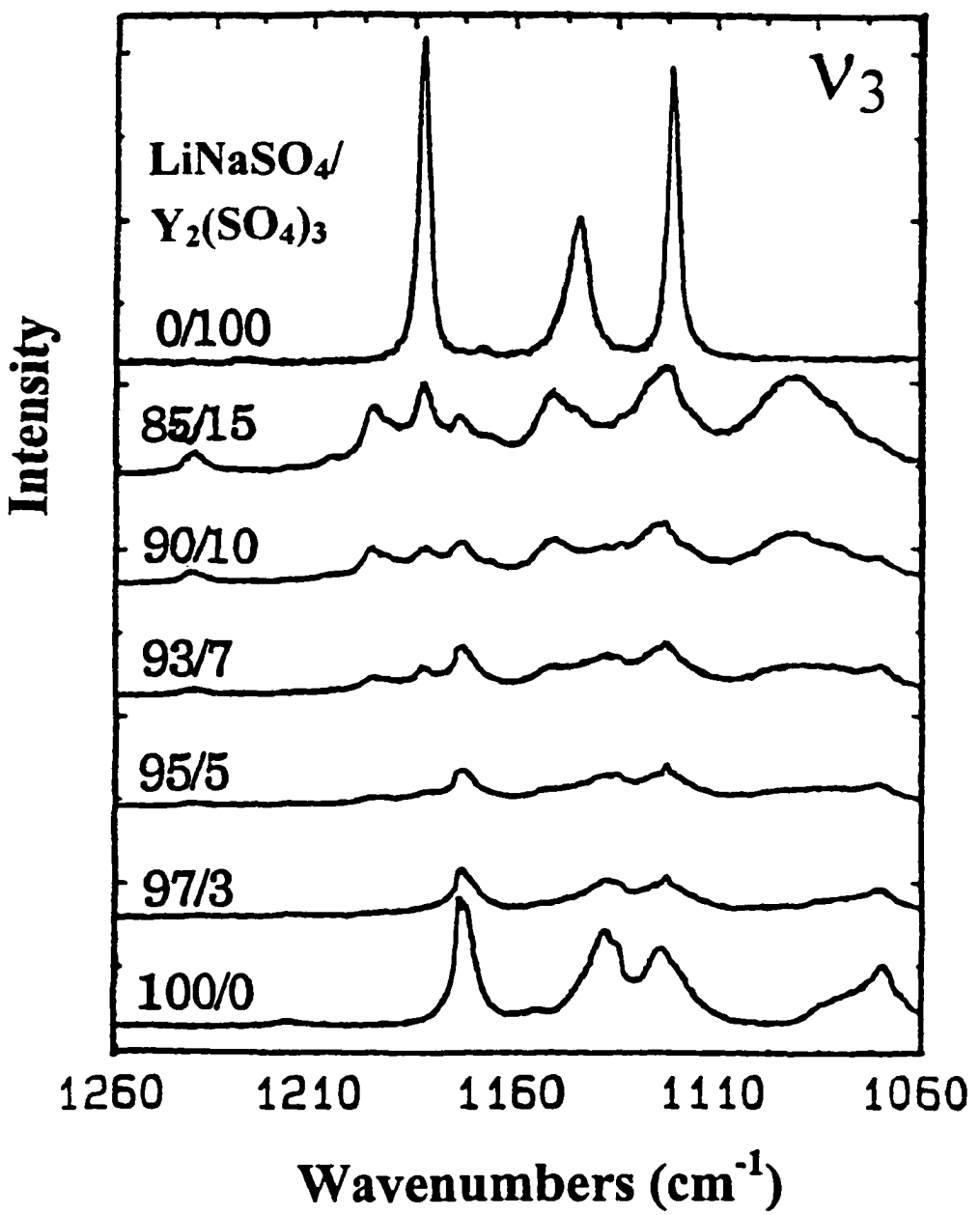

Figure 3.2. Raman spectra of $LiNaSO_4$ substituted with Y^{3+} in the SO_4^{2-} ν_3 region with increasing concentration of $Y_2(SO_4)_3$.

The ν_4 region (see Figure 3.3) shows similar behavior. The pure $LiNaSO_4$ bands at 625, 646 and 661 cm^{-1} are observed in all doped samples, and the two $Y_2(SO_4)_3$ bands at 609 and 654 cm^{-1} can be seen growing in intensity in the more highly doped compositions. A band at 676 cm^{-1} can be seen growing in with only three mole percent $Y_2(SO_4)_3$ and is very strong in the 85/15 composition. The appearance of additional unassigned bands can be seen at 599, 638, 650 and 676 cm^{-1} in the 93/7 composition and increase in intensity with increasing yttrium concentration. There is also an increase in intensity in the low frequency wing of the 625 cm^{-1} band.

The ν_2 region shown in Figure 3.4 is somewhat complicated because of the near coincidence of the $LiNaSO_4$ band at 482 cm^{-1} and the $Y_2(SO_4)_3$ band at 484 cm^{-1}. Since these are the most intense peaks for each compound, this makes it more difficult to detect the initial appearance of the phase separation of $Y_2(SO_4)_3$. However, the ν_2 mode in $LiNaSO_4$ is a broad band with a well-defined shoulder at 475 cm^{-1}. As the percentage of $Y_2(SO_4)_3$ increases, this band narrows and more closely resembles the band shape seen in pure $Y_2(SO_4)_3$. There are two additional $Y_2(SO_4)_3$ components at 452 and 504 cm^{-1} that are observed to grow with increasing concentration as well. This region also shows the appearance of previously unknown bands at 417 and 441 cm^{-1}. The band at 406 cm^{-1} in pure $LiNaSO_4$ has been previously identified through lithium isotopic substitution studies as a lithium mode,

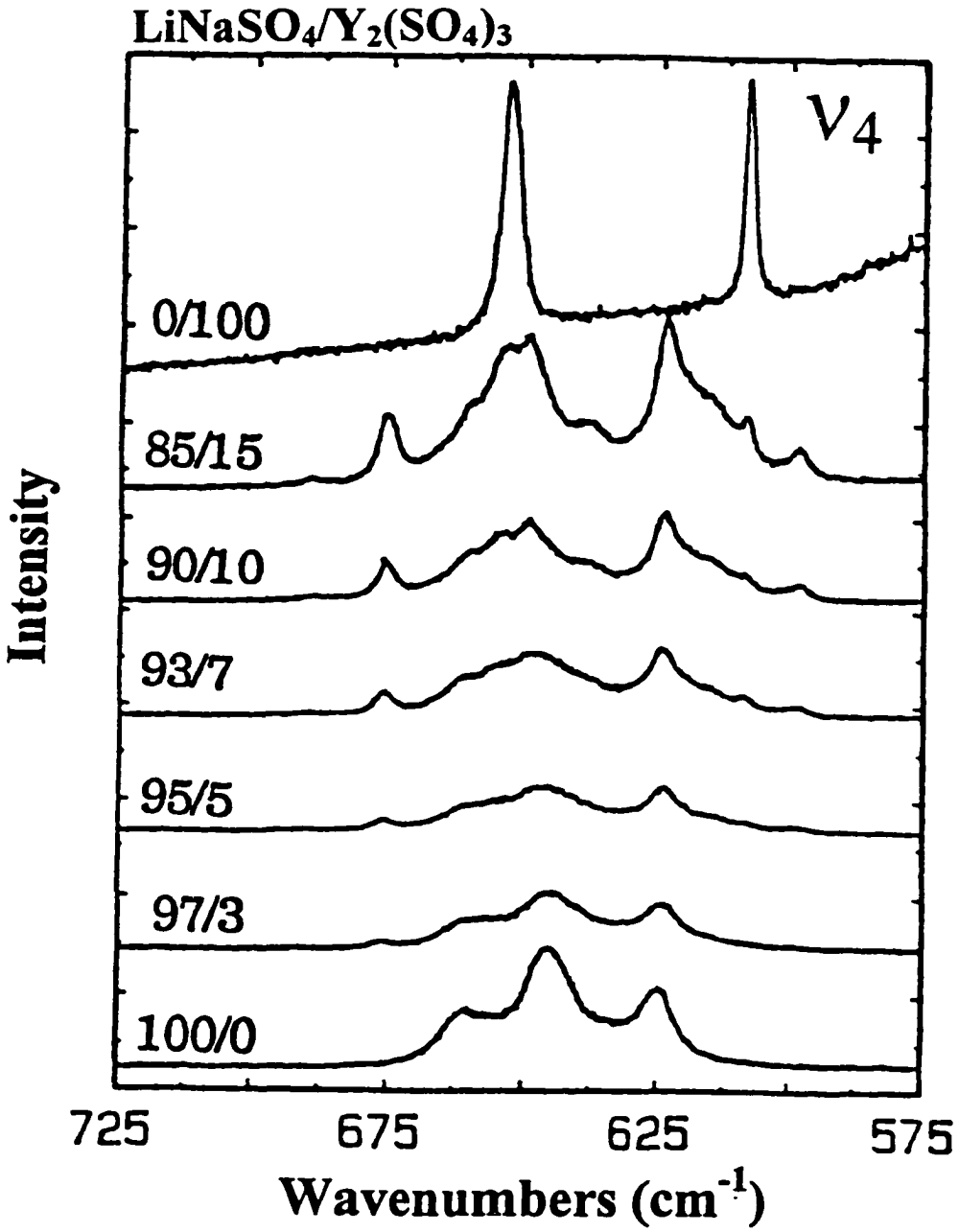

Figure 3.3. Raman spectra of $LiNaSO_4$ substituted with Y^{3+} in the SO_4^{2-} ν_4 region with increasing concentration of $Y_2(SO_4)_3$.

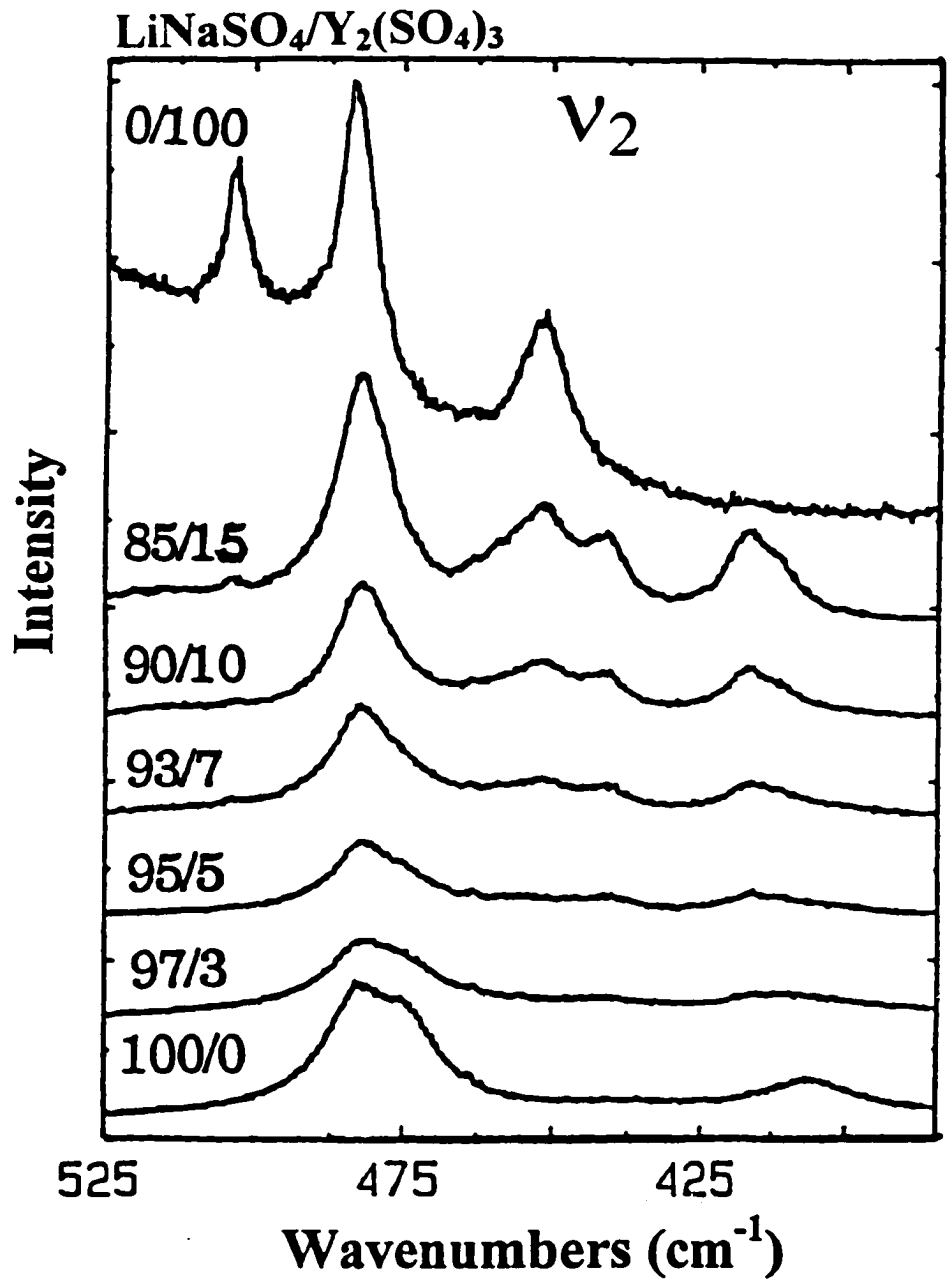

Figure 3.4. Raman spectra of $LiNaSO_4$ substituted with Y^{3+} in the SO_4^{2-} ν_2 region with increasing concentration of $Y_2(SO_4)_3$.

and the band at 417 cm^{-1} in the more highly doped samples may be an analogous feature.

In each spectral region the data provide a consistent picture. Between three and five mole percent $Y_2(SO_4)_3$ the appearance of new bands is observed, some of which can be attributed to $Y_2(SO_4)_3$ and some of which signal the appearance of a new phase or compound. The question is whether the new bands can be assigned to the stabilized high temperature phase of $LiNaSO_4$. This can be checked by examining the Raman spectrum of pure $LiNaSO_4$ above the phase transition temperature. The temperature dependence of the ν_1 and ν_3 spectral regions is shown in Figure 3.5. The bands in the high temperature cubic phase clearly do not correspond to the new bands seen in the doped compounds in these regions. In the 600°C spectrum there is a single ν_1 band at 991 cm^{-1} and a very weak, broad band centered at roughly 1110 cm^{-1} in the ν_3 region. Therefore, partial phase stabilization cannot explain the new bands at 1036, 1092, 1151, 1195 and 1241 cm^{-1}.

The temperature dependence of the ν_1 vibrational multiplet is quite interesting. The highest frequency component quickly collapses while the middle component becomes the more intense of the two remaining components and remains as the only band observable in the high temperature phase. This behavior was previously noted in a single crystal study.[22] What is particularly interesting is that this temperature-dependent behavior is similar to the behavior which is observed with increasing concentration of $Y_2(SO_4)_3$ as seen in Figure 3.1.

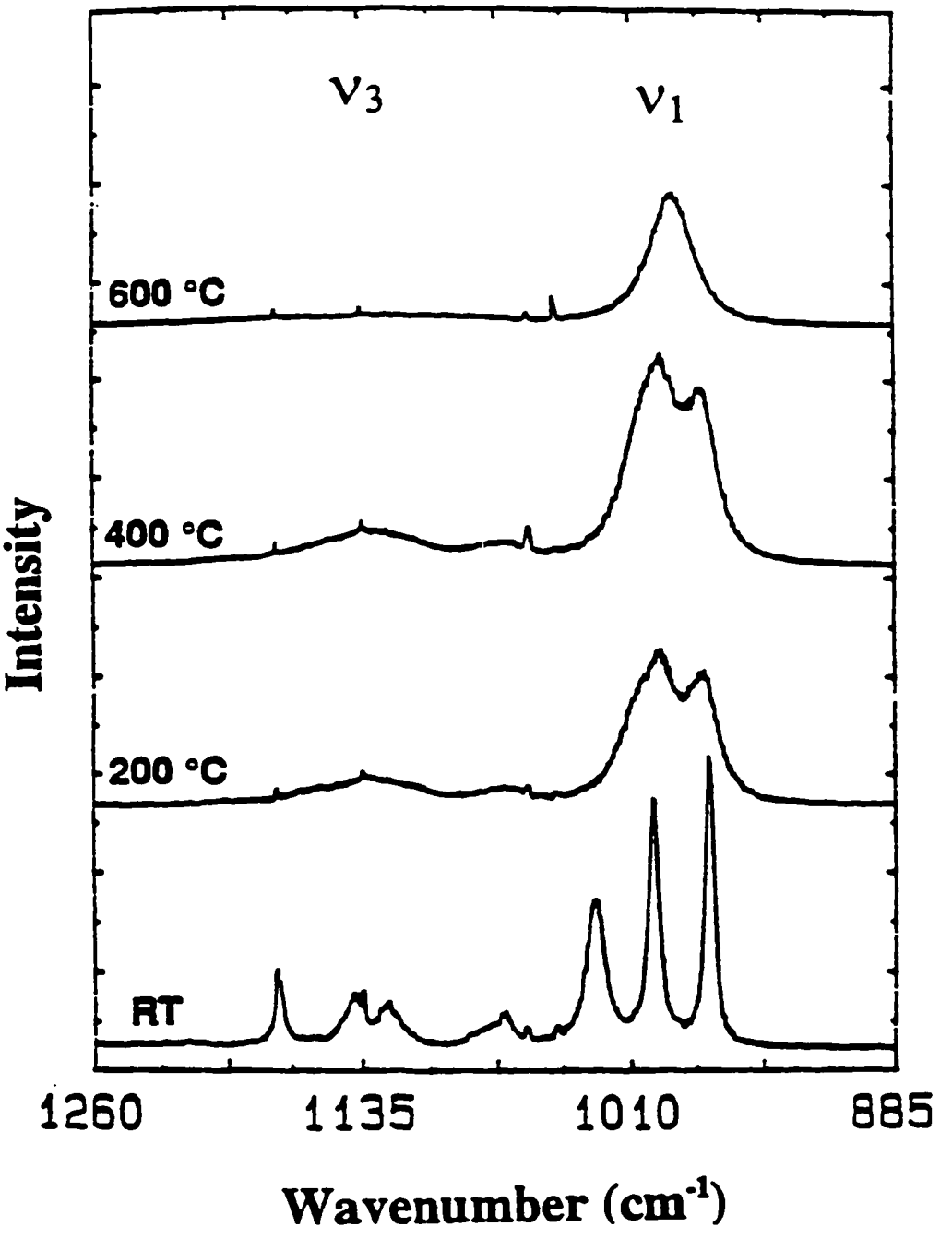

Figure 3.5. Temperature-dependent Raman spectra of $LiNaSO_4$ in the SO_4^{2-} ν_3 and ν_1 regions. The spectrum at 600°C corresponds to the high-temperature phase.

In the high temperature cubic phase there is only one band at 629 cm^{-1} observed in the ν_4 region and one band at 456 cm^{-1} in the ν_2 region. These spectra are not shown although the frequencies are summarized in Table 3.1. Neither of these bands appears to coincide with any of the corresponding features in the substituted compounds, even allowing for a decrease in frequency in the high temperature spectrum due to thermal effects.

Lithium Potassium Sulfate: Raman Spectra

It is an interesting coincidence that both $LiKSO_4$ and $Y_2(SO_4)_3$ have a single band in the ν_1 spectral region at 1013 cm^{-1}. Therefore, it is significant to note the growth of bands at 990 and 1026 cm^{-1} beginning in the 95/5 composition and increasing in intensity with successive $Y_2(SO_4)_3$ doping. The spectra are shown in Figure 3.6.

In the ν_3 spectral region (shown in Figure 3.7) we also see the coincidence of a Na_2SO_4 band with an $Y_2(SO_4)_3$ band at 1122 cm^{-1}. However, in this case there are other bands in both the host and dopant compounds that can be used to distinguish phases. The Na_2SO_4 host bands at 1121 and 1201 cm^{-1} are easily seen at all dopant concentrations. At compositions of 90/10 and above, the three $Y_2(SO_4)_3$ bands at 1122, 1145 and 1184 cm^{-1} can be observed. However, new features at 1153, 1198 and 1232 cm^{-1} appear between three and five mole percent and increase in intensity with increasing dopant concentration.

Table 3-1. Frequencies (in cm^{-1}) of the SO_4^{2-} modes in $Y_2(SO_4)_3$-substituted $LiNaSO_4$.

Spectral Region	$LiNaSO_4$ (α phase)	$LiNaSO_4$	New Compound	$Y_2(SO_4)_3$
ν_1	991	1027 1000 973	1036	1013
ν_2	456	482	441	484 452 501
ν_3	1110	1174 1139 1124 1070	1241 1195 1151 1092	1184 1145 1122
ν_4	629	661 646 625	676 650 638 599	654 609

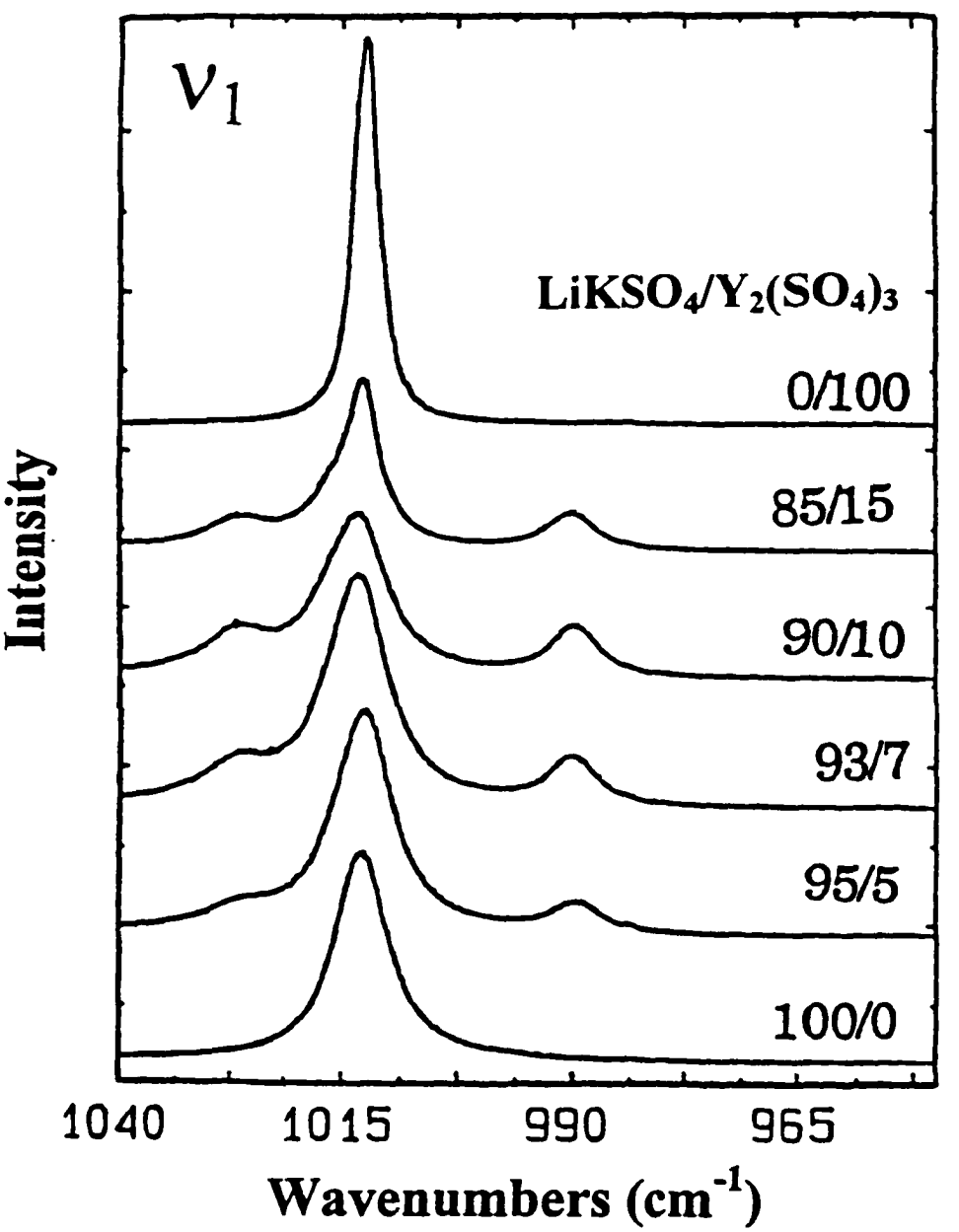

Figure 3.6. Raman spectra of $LiKSO_4$ substituted with Y^{3+} in the SO_4^{2-} ν_1 region with increasing concentration of $Y_2(SO_4)_3$.

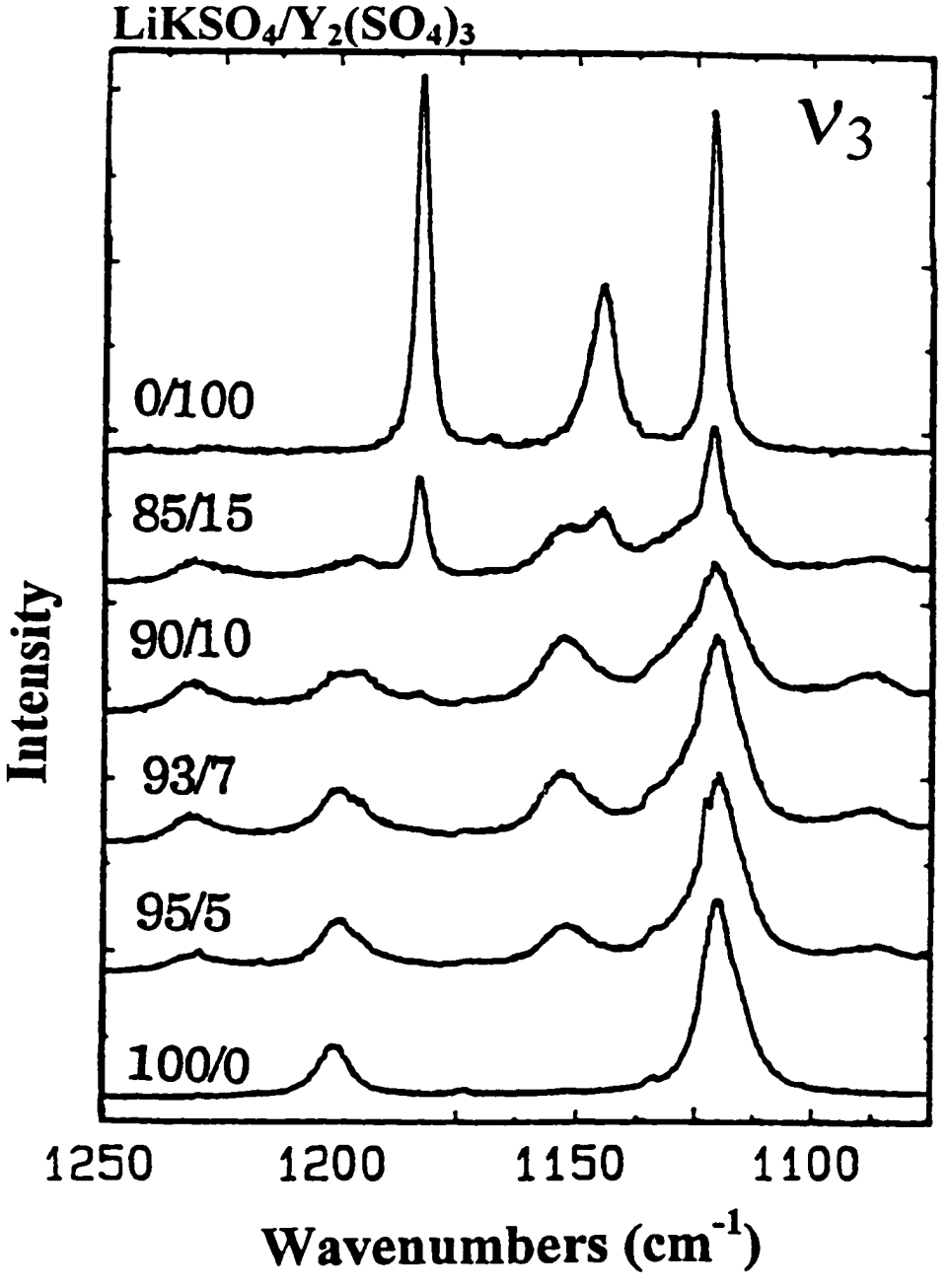

Figure 3.7. Raman spectra of $LiKSO_4$ substituted with Y^{3+} in the SO_4^{2-} ν_3 region with increasing concentration of $Y_2(SO_4)_3$.

The ν_4 spectral region is shown in Figure 3.8. The two bands of the guest $Y_2(SO_4)_3$ at 609 and 654 cm^{-1} appear at 3% $Y_2(SO_4)_3$ and grow with increasing concentration. The two $LiKSO_4$ bands at 625 and 636 cm^{-1} merge into a broad, structured with what appears to be an additional band at 630 cm^{-1}. A distinct new band at 675 cm^{-1} can be observed beginning in the three percent sample and increases in intensity with $Y_2(SO_4)_3$ concentration.

Spectra of the ν_2 region are shown in Figure 3.9. The host $LiKSO_4$ bands at 405, 445 and 465 cm^{-1} and the dopant $Y_2(SO_4)_3$ bands at 452, 484, and 504 cm^{-1} can be identified in all doped samples. The appearance of new bands at 424, 438 and 495 cm^{-1} can also be easily seen.

Again it is important to address the question of whether the new bands originate in the stabilization of the high temperature phase of $LiKSO_4$. Figure 3.10 compares the spectrum of the room temperature hexagonal phase with that of the high temperature orthorhombic phase in the ν_1, ν_2 and ν_4 regions. There is a single ν_1 band at 995 cm^{-1} in the 500°C spectrum which cannot be attributed to the band at 990 cm^{-1} in the substituted compound, since the thermal shift of the band center frequency would tend to place the band at a higher frequency at room temperature. Further, there is no trace of a second component around 1026 cm^{-1} in the high temperature phase. There is only a single band at 628 cm^{-1} in the ν_4 spectral region at 500°C which clearly does not correspond to the new band at 675 cm^{-1} in the substituted phase. Similarly, the ν_2 spectral region shows a single band at 457 cm^{-1}, which does

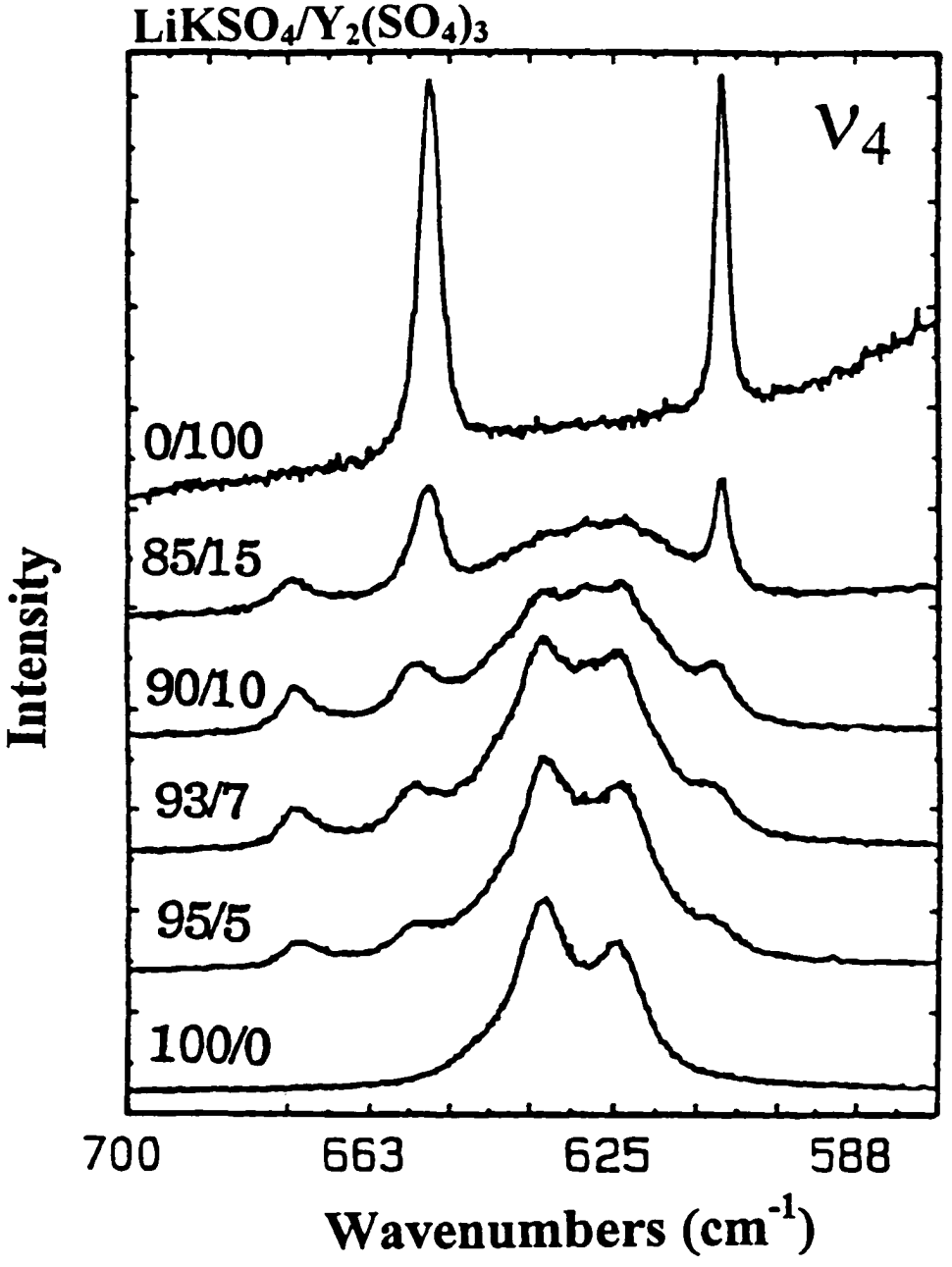

Figure 3.8. Raman spectra of $LiKSO_4$ substituted with Y^{3+} in the SO_4^{2-} ν_4 region with increasing concentration of $Y_2(SO_4)_3$.

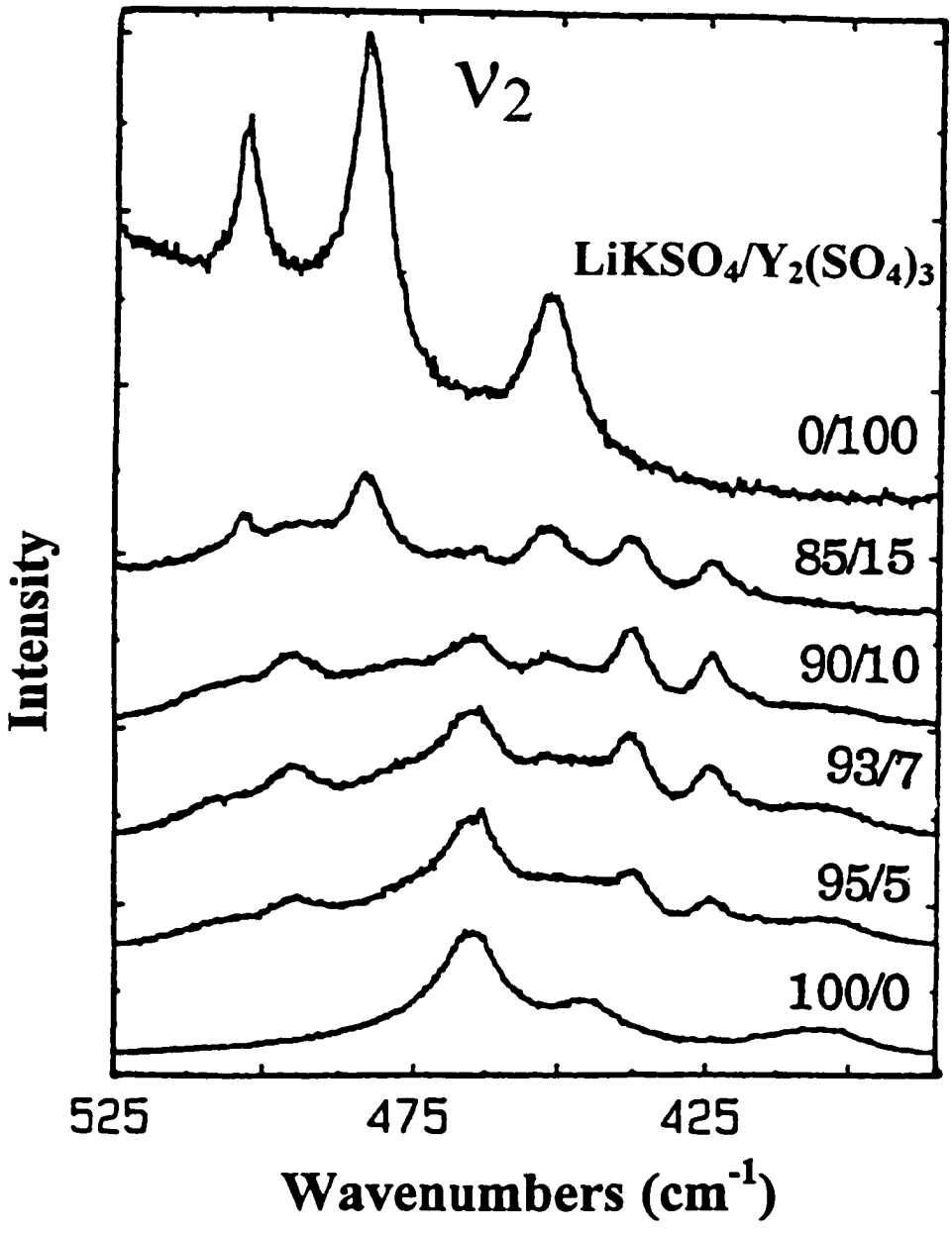

Figure 3.9. Raman spectra of $LiKSO_4$ substituted with Y^{3+} in the SO_4^{2-} ν_2 region with increasing concentration of $Y_2(SO_4)_3$.

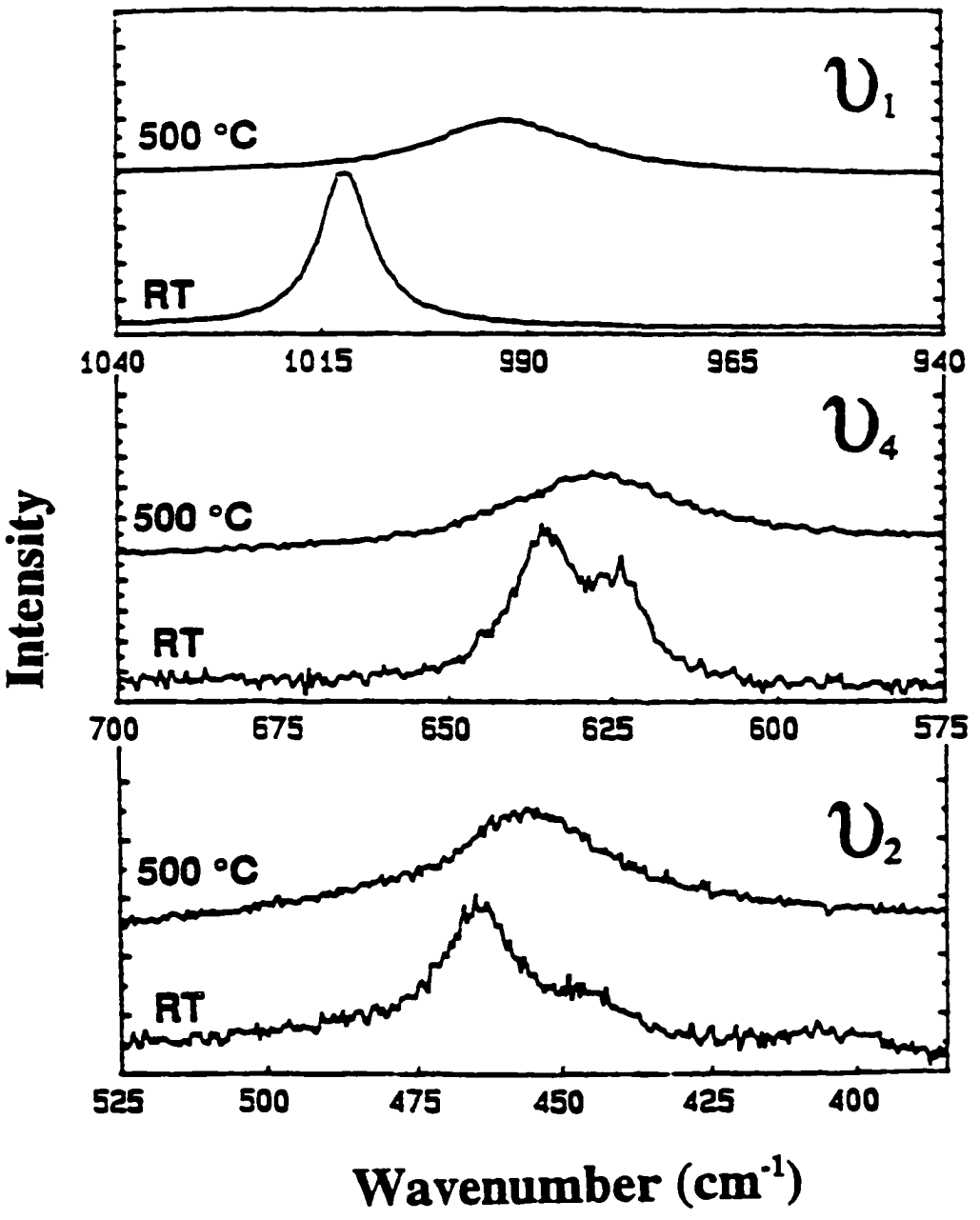

Figure 3.10. Temperature-dependent Raman spectra of $LiKSO_4$ in the SO_4^{2-} ν_1, ν_2 and ν_4 regions. The spectrum at 500°C corresponds to the high-temperature phase.

not coincide with any of the three new components in the substituted material. The spectrum of the ν_3 region (not shown) indicates a very broad, weak feature centered at roughly 1100 cm^{-1}. The frequencies are summarized in Table 3.2.

Lithium Potassium Sulfate: DSC and XRD

In order to more definitively determine the presence of a new compound or phase, both DSC and powder x-ray data were obtained. A thermal analysis was performed on the substituted $LiKSO_4$ compounds using a Perkin-Elmer DSC-2 differential scanning calorimeter. The samples were measured as finely ground powders over a temperature range of 37 to 475°C at a heating rate of 10°C/min. An endotherm was observed at 449°C in the pure $LiKSO_4$ which decreased to 444°C in the 85/15 $LiKSO_4/Y_2(SO_4)_3$ composition. However, an additional endotherm was observed in the 10% $Y_2(SO_4)_3$ substituted composition which increases in relative intensity in the more highly substituted compositions. No corresponding transition was observed in the unsubstituted compound.

Powder X-ray diffraction (XRD) patterns of pure $LiKSO_4$, $Y_2(SO_4)_3$ and the doped $LiKSO_4$ compositions were recorded with a Rigaku DMAX diffractometer using Cu Kα radiation (λ = 1.54 Å) monochromated with a graphite crystal. Table 3.3 shows the d-spacings and relative intensities of the diffraction peaks observed in the 90/10 $LiKSO_4/ Y_2(SO_4)_3$ composition and compares these data to those obtained for pure $LiKSO_4$ and $Y_2(SO_4)_3$. Diffraction peaks of the pure compounds can easily

Table 3-2. Frequencies (in cm^{-1}) of the SO_4^{2-} modes in $Y_2(SO_4)_3$-substituted $LiKSO_4$.

Spectral Region	$LiKSO_4$ (high-temperature phase)	$LiKSO_4$	New Compound	$Y_2(SO_4)_3$
ν_1		1013	1026	1013
	995		990	
ν_2	457	465	495	504
		445	438	484
		405	424	452
ν_3	1100	1201	1232	1184
		1121	1198	1145
			1153	1122
ν_4	628	636	675	654
		625	630	609

Table 3-3. Values of d-spacings and relative intensities of pure $LiKSO_4$, 90/10 $LiKSO_4/Y_2(SO_4)_3$, and pure $Y_2(SO_4)_3$.

$LiNaSO_4$	90/10 $LiKSO_4/Y_2(SO_4)_3$	$Y_2(SO_4)_3$
	7.369 (10)	
	6.702 (9)	
		6.320 (13)
	6.188 (28)	
	5.941 36)	
	5.007 (14)	
4.287 (20)	4.287 (10)	
	4.010 (18)	
3.948 (19)	3.940 (94)	3.931 (6)
	3.609 (15)	
	3.559 (42)	
	3.336 (10)	
	3.282 (17)	
	3.156 (13)	
3.092 (100)	3.087 (100)	
	3.025 (10)	
	2.981 (36)	
		2.952 (100)
	2.919 (13)	
		2.901 (80)
	2.869 (17)	2.873 (93)
	2.847 (14)	
	2.765 (10)	
	2.736 14)	
2.562 (12)	2.562 (57)	
2.456 (7)	2.456 (23)	
	2.387 (16)	
2.199 (7)	2.202 (24)	
	2.179 (13)	
	2.162 (12)	2.159 (11)

2.154 (9)	2.152 (27)	
	2.130 (7)	2.128 (15)
		2.109 (16)
		2.070 (20)
	2.056 (12)	
		2.002 (26)
	1.975 (11)	
		1.967 (17)
	1.899 (11)	
	1.823 (9)	1.819 (5)
1.757 (11)		
	1.700 (8)	1.703 (37)
	1.681 (7)	1.685 (42)
		1.658 (28)
	1.649 (11)	
	1.565 (14)	
	1.483 (20)	
		1.441 (13)
		1.334 (9)
		1.329 (10)
		1.271 (10)
	1.222 (13)	
1.187 (4)	1.186 (10)	
		1.111 (12)
		1.108 (10)

be distinguished in the substituted sample. However, the diffraction pattern appears to be dominated by additional peaks that are not due to either the pure host or the pure dopant compound.

Conclusion

It is clear from the spectral data of both $LiNaSO_4$ and $LiKSO_4$ that either a new phase or a new compound is formed upon substitution of $Y_2(SO_4)_3$ into the host compound. The appearance of new bands in the Raman spectra occurs between three and five mole percent $Y_2(SO_4)_3$ and is roughly coincident with the appearance of bands originating from the phase-separated, pure $Y_2(SO_4)_3$. Comparison of temperature-dependent Raman data of the pure host compounds with the substituted compounds show that in neither $LiNaSO_4$ nor $LiKSO_4$ can the new bands be attributed to a stabilized high temperature phase, unlike behavior previously observed in Na_2SO_4.

The data also argue against these new vibrational modes originating from the sulfate ions of the host lattice being locally perturbed by the substituent yttrium ions. The new bands appear with bandwidths which are comparable to the host bands, rather than being very broad with weak scattering intensity as would be expected for bands inhomogeneously broadened by a distribution of potential energy environments in a highly disordered system. Furthermore, the new bands exhibit a vibrational multiplet structure resembling the factor group components of the compound,

particularly in the ν_2, ν_3 and ν_4 spectral regions. In particular, the data in the ν_2 spectral region argue strongly for the formation of a compound.

In both substituted $LiNaSO_4$ and $LiKSO_4$ there are low frequency vibrations at 417 and 424 cm^{-1}, respectively, which may be tentatively assigned to a lithium translatory mode. It is known from studies of lithium modes in the pure compounds that such modes are highly sensitive to disorder in the local environment.[21] The local environment of the lithium ions is defined by the nearest neighbor oxygen atoms of the sulfate ions which tetrahedrally coordinate the lithium ions. With increasing temperature the lithium bands quickly broaden and decrease in scattering intensity, reflecting an increase in the librational amplitude of the sulfate ions. As the librational amplitude increases, the correlated motion of the sulfate ions decreases, and the potential energy environment of the lithium ions becomes increasingly dynamically disordered. Therefore the presence of sharp bands attributed to lithium ion translatory modes in the substituted compounds is a strong argument against any significant local disorder in those materials at the concentrations investigated in this study.

Finally, in the case of substituted $LiKSO_4$, both the differential scanning calorimetry and powder x-ray data clearly argue for the formation of a new compound.

References

1. Hofer, H.H., Eysel, W. & Alpen, U.v. *J. Solid State Chem.* **36**, 365-370 (1981).

2. Eysel, W., Hofer, H.H., Keester, K.L. & Hahn, T. *Acta Crystallogr., Sect. B* **41**, 5 (1985).

3. Keester, K.L., Eysel, W. & Hahn, T. *Acta Crystallographica A* **31**, S79 (1975).

4. Bandaranayake, P.W.S.K. & Mellander, B.-E. *Solid State Ionics* **26**, 33-36 (1988).

5. MacDonald, K.G., MacLean, C. & Secco, E.A. *Can. J. Chem.* **66**, 3132-3136 (1988).

6. Bandaranayake, P.W.S.K. & Mellander, B.-E. *Solid State Ionics* **40/41**, 31-33 (1990).

7. Murray, R.M. & Secco, E.A. *Can. J. Chem.* **56**, 2616-2619 (1978).

8. Dawson, P.C., Secco, E.A. & Oxner, W.M. *Can. J. Chem.* **67**, 1468-1471 (1989).

9. Imanaka, N., Yamaguchi, Y., Adachi, G.-y. & Shiowaka, J. *Solid State Ionics* **20**, 153-157 (1986).

10. Imanaka, N., Kuwabara, S., Adachi, G.-y. & Shiokawa, J. *Solid State Ionics* **23**, 15-19 (1987).

11. Rao, N., Schoonman, J. & Sorensen, O.T. *Solid State Ionics* **57**, 159-168 (1992).

12. Saito, Y., Kobayashi, K. & Maruyama, T. *Thermochim. Acta* **53**, 289-297 (1982).

13. Dharmasena, G. & Frech, R. *Solid State Ionics* **53-56**, 1274-1277 (1992).

14. Dharmasena, G. & Frech, R. *J. Chem. Phys.* **99**, 8929-8935 (1993).

15. Dharmasena, G., Schlindwein, W.S., Frech, R. & Linford, R.G. *J. Chem. Phys.* **101**, 9232-9235 (1994).

16. Morison, B. & Smith, D.L. *Acta Crystallogr.* **22**, 906 (1967).

17. Schroeder, K. & Kvist, A. *Z. Naturforsch. A* **23**, 773-774 (1968).

18. Josefson, A.-M. & Kvist, A. *Z. Naturforsch. A* **24**, 466-468 (1969).

19. Bradley, A.J. *Philos. Mag.* **49**, 1225-1237 (1925).

20. Schroeder, K. (University of Gothenburg, Göteborg, Sweden, 1975).

21. Teeters, D. & Frech, R. *Phys. Rev. B* **26**, 4132-4139 (1982).

22. Frech, R. & Teeters, D. *J. Phys. Chem.* **88**, 417-420 (1984).

CHAPTER 4

CHARACTERIZATION OF SODIUM PHOSPHATE

Introduction

When the attempt to stabilize lithium sodium sulfate and lithium potassium sulfate was unsuccessful, attention was turned to other anion systems. Previous studies[1-12] had shown that it is possible to stabilize the high-temperature phase of sodium phosphate (Na_3PO_4), but these systems had not been thoroughly characterized. However, before studying the phase stabilization of Na_3PO_4, it was necessary to first characterize the pure compound.

Na_3PO_4 has two anhydrous solid phases: a room-temperature tetragonal phase (designated α) and a high-temperature cubic phase (designated γ). α-Na_3PO_4 belongs to space group $P\bar{4}2_1c$[13] with cell dimensions a = 10.80 Å and c = 6.82 Å. It undergoes a reversible phase transition at 320°C to γ-Na_3PO_4, which is then stable to the melt at 1450°C. γ-Na_3PO_4 belongs to space group Fm3m with a = 7.42 Å. [14] The structure of γ-Na_3PO_4 is derived from a Li_3Bi-type structure and contains disordered PO_4^{3-} ions.

XRD and DSC Results

Differential scanning calorimetry (DSC) and powder x-ray diffraction (XRD) were used to confirm the synthesis of α-Na_3PO_4. Analysis of the Na_3PO_4 system is complicated by the fact that Na_3PO_4 forms several hydrates. There are four well-

known hydrates: the dodecahydrate, octahydrate, hexahydrate, and hemihydrate. However, the actual formula for the dodecahydrate is $Na_3PO_4 \cdot 12H_2O \cdot xNaOH$ where x varies from 1/11 to 2/9. [15, 16] There is also another "hydrate" phase (called the w-phase by Milne and West[8]), the exact composition of which is unknown. The hydrate phases, particularly the w-phase, will be discussed in more detail later.

The DSC trace is shown in Figure 4.1. There is a reversible thermal event at 325°C on heating and 319°C on cooling that is due to the α- to γ-Na_3PO_4 phase transition and an irreversible endotherm at 255°C. Kizilyalli and Welch[17] report a transition at 255°C that they attribute to β-Na_3PO_4 and speculate that β-Na_3PO_4 is an intermediate phase that cannot be isolated. Milne and West[8] examined the polymorphism of Na_3PO_4 and characterized this transition as a hydrate phase since there was a loss of mass associated with the transition in the DTA/TGA scans and water bands were observed in the IR spectrum. They also report that when the samples were exposed to air for increasing periods of time, the transition at 255°C would increase in relative intensity. This is in agreement with the results presented here as well. However, even two years after sample preparation, there is no indication of the presence of other hydrates of Na_3PO_4 in the samples analyzed for this work. The temperature of the α- to γ-Na_3PO_4 transition observed at 325°C is consistent with that observed in several previously published studies. [10, 14, 15, 17]

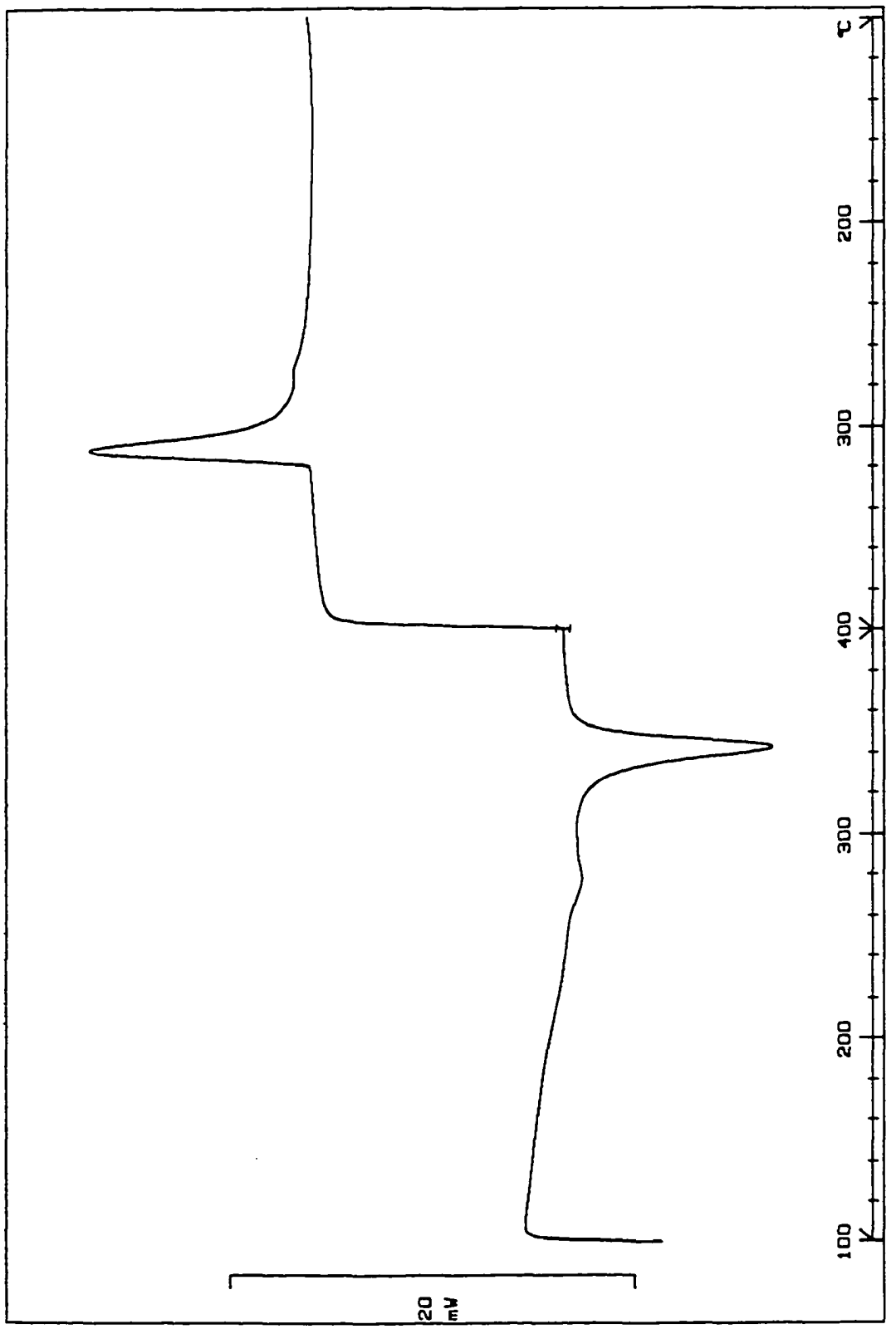

Figure 4.1. DSC thermogram of anhydrous Na_3PO_4.

The powder x-ray diffractogram for α-Na_3PO_4 is shown in Figure 4.2. Although the diffraction pattern is measured in terms of 2θ values, most patterns are reported in terms of d-spacings and relative intensities. This is done in order to facilitate comparisons and phase identification of compounds. d-spacings are a function of the lattice parameters of the crystal structure, while 2θ values are also dependent upon the wavelength of the x-ray source. The two can be related using the Bragg equation: $\lambda=2d\sin\theta$, where λ is the wavelength of the x-ray source. λ is equal to 1.54178 Å for Cu K-α radiation, which was used in these experiments. The d-spacings obtained for α-Na_3PO_4 in this work are compared to those from the literature in Table 4.1. The XRD pattern is consistent with the results published by several groups, [10,14,15,17] confirming that the bulk of the sample is α-Na_3PO_4. However, weak lines are also present in the pattern that can be assigned to the w-phase.

The minor discrepancies in the d-space values and relative intensities can be attributed to several factors. Preferred orientation effects can cause distortions in the relative intensities of the sample since some diffraction planes are measured preferentially to the others. In order to obtain accurate intensity measurements, it is necessary for the sample to be a completely random specimen. Microstrains in the material can produce two types of effects in the diffraction pattern. If there is a uniform tensile or compressive strain on the crystal structure, a shift in the diffraction peaks will be observed. If there are local strains in the crystallites due to a variety of defects, the net result will be a broadening of the diffraction peak. One of the most

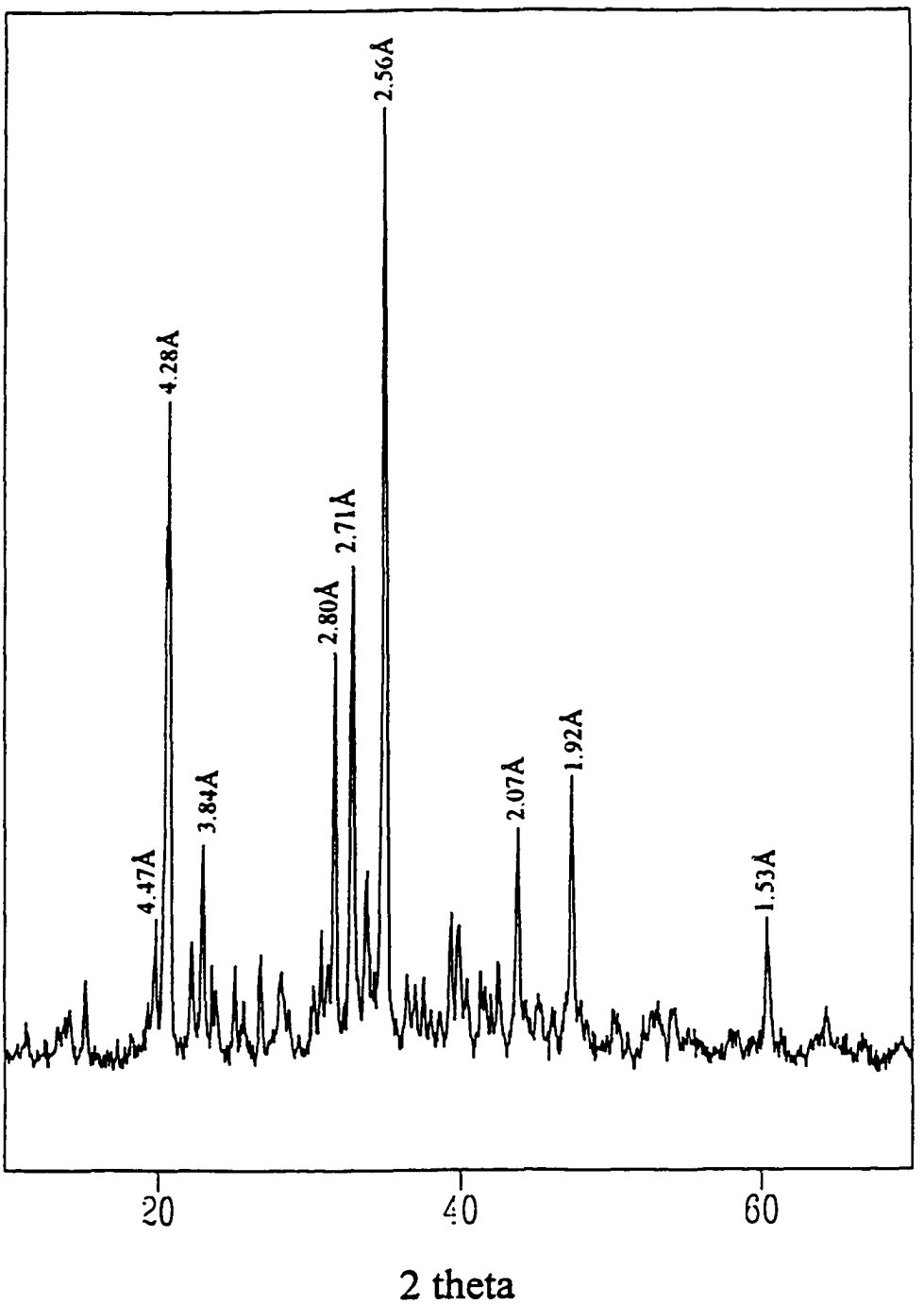

Figure 4.2. XRD pattern of α-Na_3PO_4. Some peaks are labeled in terms of d-spacings in Å.

Table 4.1. Comparison of d-spacings (in Å) and relative intensities of α-Na_3PO_4. The d-spacings of the w-phase are also included.

α-phase	α-phase	α-phase	α-phase	w-phase
Palazzi [10]	Kiziyalli [17]	Mair [15]	Present Work	Milne [8]
d (Å) (I/I_0)	d (Å) (I/I_0)	d (Å) (I/I_0)	d (Å) (I/I_0)	d (Å) (I/I_0)
7.648 (vvw)	7.615 (20)	7.660 (4)	7.771 (4)	7.026 (10)
				6.624 (30)
				6.422 (20)
			6.362 (7)	6.261 (35)
	5.753 (5)		5.841 (6)	5.850 (40)
				4.599 (40)
			4.472 (6)	4.475 (75)
4.244 (s)	4.230 (100)	4.244 (65)	4.284 (78)	4.314 (100)
3.955 (vw)	3.930 (50)	3.954 (12)	3.967 (10)	
3.825 (w)	3.817 (60)	3.833 (22)	3.839 (14)	
			3.712 (9)	3.701 (25)
			3.510 (6)	3.519 (45)
	3.401 (15)	3.422 (4)	3.438 (6)	3.392 (20)
				3.355 (20)
			3.287 (8)	3.296 (70)
				3.195 (20)
3.130 (vvw)	3.110 (50)	3.116 (10)	3.123 (16)	3.118 (30)
				3.083 (36)
			2.917 (6)	2.922 (30)
				2.879 (50)
				2.847 (30)
	2.779 (25)	2.790 (5)	2.796 (29)	2.803 (95)
2.705 (vs)	2.694 (90)	2.703 (50)	2.710 (40)	2.717 (10)
			2.640 (11)	2.650 (60)
				2.629 (40)
				2.617 (40)
				2.579 (70)
2.552 (vs)	2.540 (100)	2.547 (100)	2.556 (100)	2.562 (20)
2.450 vw)	2.442 (40)	2.449 (8)	2.453 (5)	2.530 (10)
2.420 (vvw)	2.409 (40)	2.416 (8)	2.388 (3)	2.393 (40)
				2.366 (20)
				2.331 (35)
2.280 (vvw)	2.274 (40)	2.281 (7)	2.285 (9)	2.293 (50)
2.257 (vw)	2.249 (60)	2.253 (16)		2.256 (20)
2.229 (vvw)	2.220 (40)	2.225 (8)	2.230 (6)	2.231 (35)
			2.182 (6)	2.189 (50)
2.163 (vvw)	2.158 (50)	2.165 (7)		2.153 (30)
2.122 (vvw)	2.115 (40)	2.120 (5)	2.124 (8)	2.133 (30)

	2.076 (5)			2.075 (55)
2.063 (w)	2.055 (60)	2.062 (20)	2.067 (27)	2.047 (35)
	2.018 (5)			2.015 (40)
	2.000 (5)		2.005 (6)	2.004 (50)
				1.969 (30)
	1.920 (10)	1.926 (3)		1.939 (20)
1.912 (s)	1.908 (80)	1.912 (30)	1.915 (32)	
	1.890 (10)	1.895 (4)		1.896 (30)
				1.882 (30)
	1.796 (20)	1.802 (5)	1.811 (6)	1.821 (30)
				1.789 (20)
	1.728 (20)	1.730 (5)		1.756 (40)
	1.716 (20)	1.720 (5)	1.720 (6)	
	1.702 (10)	1.706 (3)		1.697 (20)
	1.683 (20)	1.686 (3)	1.690 (5)	1.692 (20)
	1.663 (10)			
	1.654 (20)	1.658 (4)	1.661 (2)	1.655 (10)
	1.636 (20)			
	1.626 (10)			
	1.606 (5)			
	1.590 (5)		1.590 (2)	
	1.575 (20)	1.576 (4)		
	1.526 (60)	1.528 (16)	1.531 (13)	
	1.461 (20)	1.465 (3)		
	1.441 (30)	1.443 (6)	1.445 (4)	
	1.427 (5)			
	1.413 (5)			
	1.392 (5)		1.400 (5)	

common sources of error in diffraction patterns is due to specimen-displacement errors. This error arises when the sample surface lies either above or below the focusing circle of the goniometer. The major effects of specimen displacement are an asymmetric broadening of the peaks at low 2θ values and an absolute shift in 2θ peak positions. [18] However, a fixed error in 2θ values has a greater effect on d-spacings at low angles than at high angles. This occurs because the relationship between the errors in 2θ and d-spacings is of the form: $\frac{\Delta d}{d} = \Delta\theta \cot\theta$.

Vibrational Spectroscopy

Although the use of Na_3PO_4 for various medicinal and industrial purposes is extensive, it has not been thoroughly characterized using vibrational spectroscopy. Published Raman spectra have been limited to the dodecahydrate and aqueous solutions, although some averaged wavenumbers for the fundamental vibrational modes of Na_3PO_4 were reported by Lopez-Bote and Montero[19] in a paper investigating vibrational eigenvectors and force constants. These values are included in Table 4.2 along with the experimental values obtained in this study. These results agree with the range of values they reported. The only infrared spectra of anhydrous Na_3PO_4 reported are those by Zhu et al., [20, 21] and the results presented here do not agree with theirs for α-Na_3PO_4. This may be due to the difference in sample preparation. Samples in this study were prepared using solid state reactions, while they prepared samples of α-Na_3PO_4 by dehydrating the dodecahydrate, which has been shown to

Table 4.2. Frequencies of the PO_4^{3-} Raman vibrational modes of Na_3PO_4. Values at 24°C are for the α-phase, and values at 360°C are for the γ-phase.

Mode	Lopez-Bote [19] (cm^{-1})*	24°C	198°C	249°C	317°C	349°C	360°C
ν_1	936	943	943	943	941	941	943
ν_2	422	426(sh)	432	432	432	432	432
		435	496(sh)	496(sh)	491(sh)	491(sh)	
ν_3	1020	1013	1013	1010			
		1030	1030	1028	1028	1027	1028
		1048	1048	1043	1041	1039	
		1071	1071	1064	1062	1062	1061
		1082	1082	1078			
		1108	1108	1104	1102		
ν_4	563	573	573	573	573(sh)	573(sh)	
		586	586	586	582	582	582

contain significant amounts of NaOH.[15, 22] The results for stabilized γ-Na_3PO_4 are closer to those they report for pure γ-Na_3PO_4, but not identical. They are also reporting spectra for stabilized γ-Na_3PO_4 rather than spectra obtained from temperature-dependent measurements.[20, 21] The infrared spectrum for pure γ-Na_3PO_4 was not obtained due to experimental limitations which did not allow for high-temperature measurements.

The vibrational modes of Na_3PO_4 can be described using factor group analysis. PO_4^{3-} is a tetrahedral anion belonging to the Td point group. The symmetry of the PO_4^{3-} ion's potential energy environment is determined by the symmetry of the site occupied by the PO_4^{3-} ion. Therefore, the irreducible representations of the point group must be related to those of the site group. This site is generally taken to be the site of the center of mass of the ion, which would be the phosphorus atom in this case. However, in a multiply occupied unit cell the vibrational motions of the individual ions are not independent; they are correlated through intermolecular forces. Because the collective vibrational motions of the ions in the unit cell must reflect the symmetry of the unit cell, the irreducible representations of the site group must be correlated to those of the space group (factor group) of the crystal. The factor group analysis for α-Na_3PO_4 is shown on the following page.

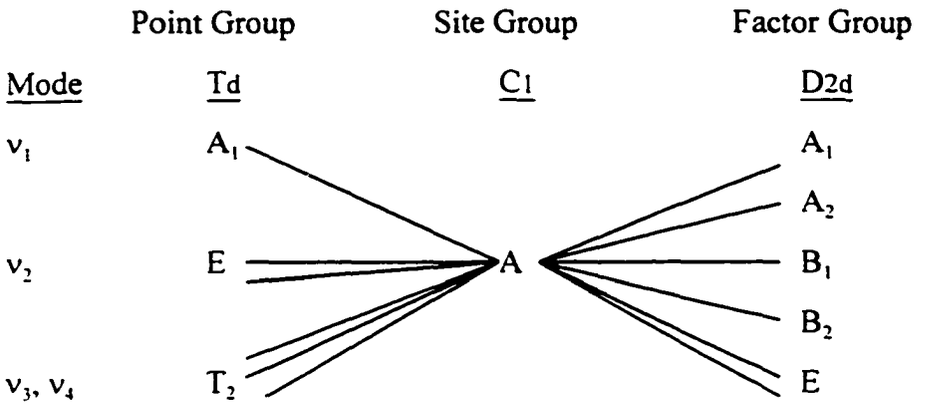

$$\Gamma\nu_1 = A_1 + A_2 + B_1 + B_2 + 2E$$

$$\Gamma\nu_2 = 2A_1 + 2A_2 + 2B_1 + 2B_2 + 4E$$

$$\Gamma\nu_3,\nu_4 = 3A_1 + 3A_2 + 3B_1 + 3B_2 + 6E$$

$$\Gamma_{vib} = 9A_1 + 9A_2 + 9B_1 + 9B_2 + 18E$$

This gives a total of 72 vibrational degrees of freedom. A quick check can be done to verify that the number of degrees of freedom is correct. There are 3n-6 degrees of freedom per molecule, which yields a total of nine degrees of freedom for each PO_4^{3-} ion. There are eight molecules per unit cell, resulting in a total of 72 degrees of freedom.

The factor group analysis for γ-Na_3PO_4 is much more complicated. A formal analysis is shown below.

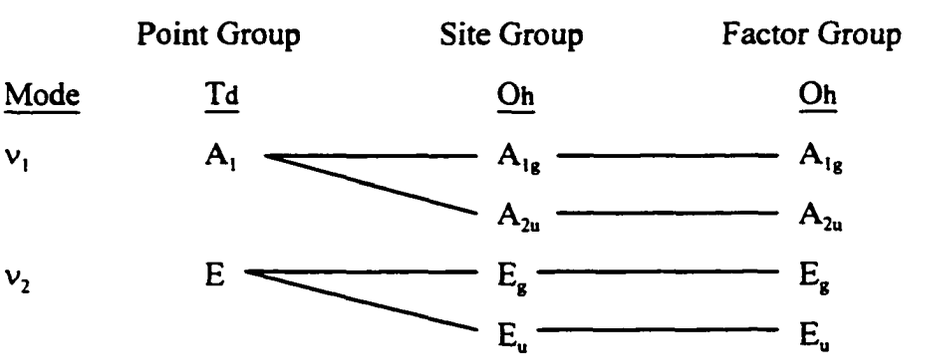

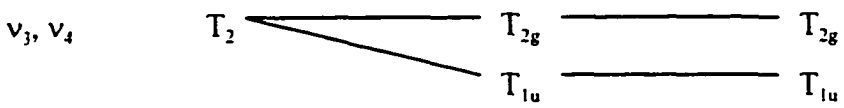

$$\Gamma\nu_1 = A_{1g} + A_{2u}$$

$$\Gamma\nu_2 = E_g + E_u$$

$$\Gamma\nu_3,\nu_4 = T_{2g} + T_{1u}$$

$$\Gamma_{vib} = A_{1g} + A_{2u} + E_g + E_u + 2T_{2g} + 2T_{1u}$$

This results in 18 vibrational degrees of freedom, but only nine degrees of freedom are allowed. Again, there are nine degrees of freedom for each PO_4^{3-} ion, but for γ-Na_3PO_4 there is effectively only one molecule per unit cell. Although Z=4 for the crystal structure, the crystallographic unit cell is not the same as the Bravais cell used for vibrational analysis. The crystallographic unit cell is identical to the Bravais cell for all structures whose space group is designated by a P (for primitive), as in the case of α-Na_3PO_4. But when the crystal structure is designated by any other letter (C, F, I, etc.), the crystallographic unit cell will contain two to four Bravais cells. The irreducible representations obtained using Z from the crystallographic unit cell will give more vibrations than are needed to represent the lattice vibrations of the crystal. Therefore, it is necessary to use the appropriate number of molecules from the Bravais cell using the formula below.[23]

$$Z^B = \frac{Z}{(LP)}$$

where Z^B is the number of molecules in the Bravais cell, Z is the number of molecules in the crystallographic unit cell, and LP is the number of lattice points. For an F space group, LP = 4, resulting in a Z^B of one for γ-Na_3PO_4.

The reason for the discrepancy between the formal factor group analysis and the allowed degrees of freedom becomes clearer when the crystal structure is examined more closely. The PO_4^{3-} ions do not experience a true Oh site symmetry. The phosphorus atoms sit on an Oh site, but the orientational disorder of the oxygen atoms breaks the Oh symmetry of the PO_4^{3-} ions. This results in a site group that is more accurately described by C_1 symmetry. This disorder extends to the factor group as well, which creates a breakdown in the correlation coupling between the site group and the factor group. This type of behavior has also been reported for $LiNaSO_4$[24] and Li_2SO_4.[25] Therefore, the vibrational analysis of γ-Na_3PO_4 is more accurately described by the following correlation:

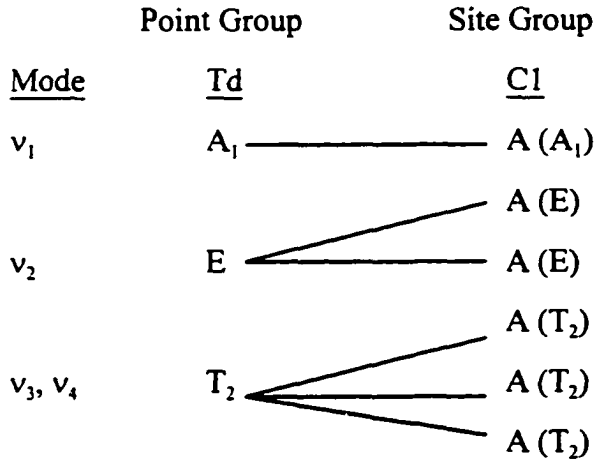

$\Gamma\nu_1 = A_1$

$\Gamma\nu_2 = 2A_1$

$\Gamma\nu_3,\nu_4 = 3A_1$

$\Gamma_{vib} = 9A_1$

This analysis results in nine degrees of freedom as required. Although the different modes all formally transform as A modes, they will retain a significant degree of tetrahedral character; this is indicated by the point group irreducible representation label in parentheses.

All ionized P^{+}-O^{-} linkages absorb in the ranges 1300 - 970 cm^{-1} for the stretching modes and 580 - 460 cm^{-1} for the deformation modes. The fundamental vibrational frequencies of the tetrahedral PO_4^{3-} ion occur at 1082 cm^{-1} (ν_3), 980 cm^{-1} (ν_1), 515 cm^{-1} (ν_4) and 363 cm^{-1} (ν_2).[26] The ν_1 and ν_2 modes are generally not infrared active. The orthophosphate salts that have been studied all show main bands in the region of 1060-1000 cm^{-1} and 580-520 cm^{-1}. [26-31]

Raman Results

Ideally, a single crystal Raman study should be included to more thoroughly investigate and analyze the temperature-dependence of the individual modes. However, single crystals of α-Na_3PO_4 could not be obtained. They cannot be grown from aqueous solution due to the formation of hydrates, nor can they be grown from the melt because the transition from high-temperature γ-Na_3PO_4 to low-temperature α-Na_3PO_4 prevents the formation of x-ray quality single crystals.

The temperature-dependent Raman spectra of the PO_4^{3-} ν_2 and ν_4 modes are shown in Figure 4.3. At room temperature the ν_4 mode has two peaks at 573 and 586 cm^{-1}. As the temperature increases, these two bands collapse into a single band at

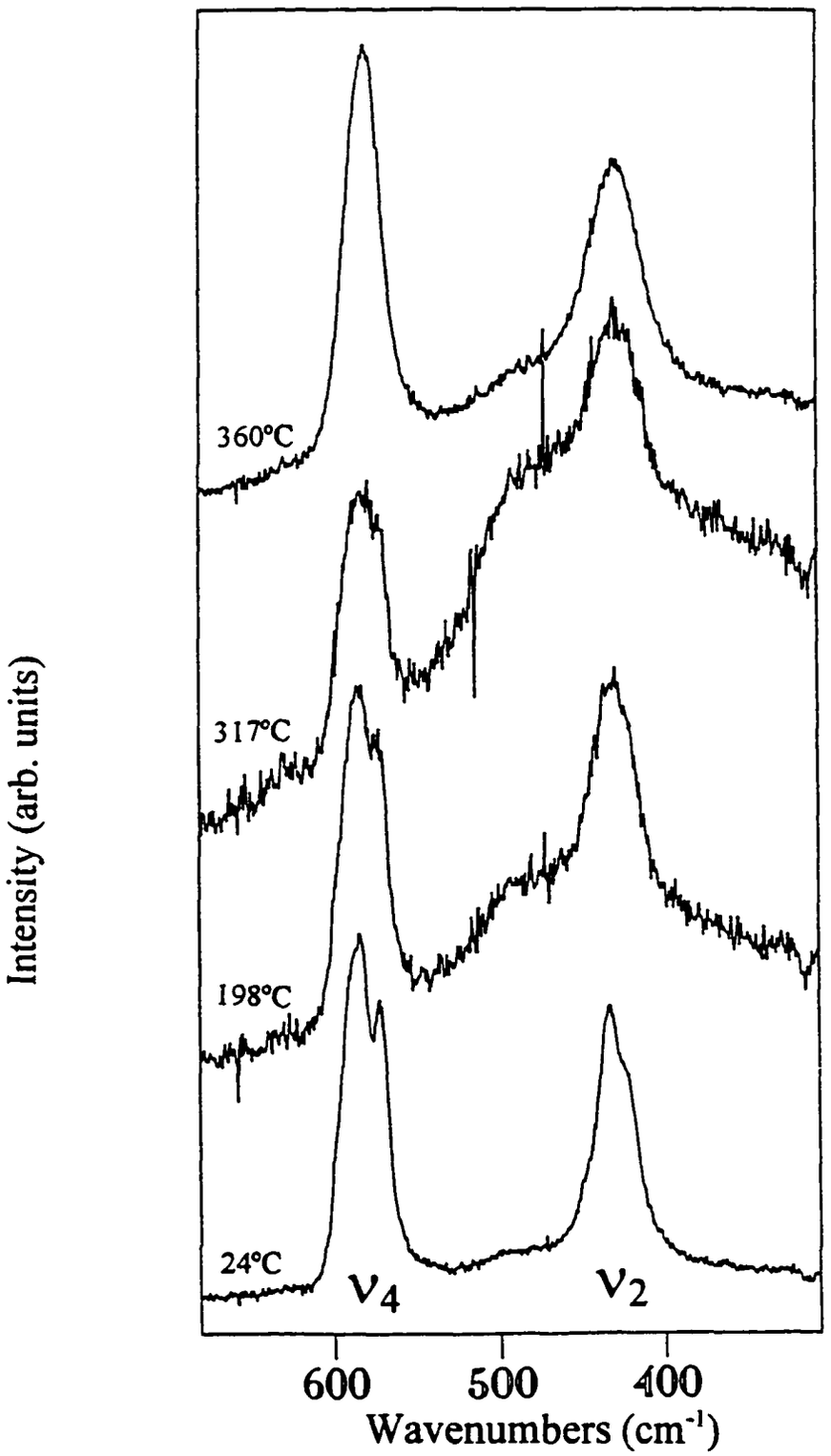

Figure 4.3. Temperature-dependent Raman spectra of Na_3PO_4 in the PO_4^{3-} ν_2 and ν_4 spectral regions. The spectrum at 360°C corresponds to the γ-phase.

582cm^{-1}. The ν_2 mode undergoes more complex behavior. α-Na_3PO_4 has a band at 435 cm^{-1} with a shoulder at 426 cm^{-1}. With increasing temperature, the band structure broadens into a single band at 432 cm^{-1}. A new feature also appears as a broad shoulder centered at 496 cm^{-1} in the 198°C spectrum. As the temperature increases, this shoulder merges into the band at 432 cm^{-1} and disappears once the transition to γ-Na_3PO_4 is complete.

The temperature-dependence of the PO_4^{3-} ν_1 region is shown in Figure 4.4. The band at 943 cm^{-1} broadens from 13 cm^{-1} to 22 cm^{-1} as the temperature increases. It also shifts to slightly lower frequency (941 cm^{-1}) in the intermediate temperature region, but returns to 943 cm^{-1} in the γ-phase. The band intensity also decreases significantly in the intermediate temperature region, but then increases to close to the room temperature intensity once the phase transition is complete.

The collapse of band structure with increasing temperature is seen most dramatically in the ν_3 region shown in Figure 4.5. α-Na_3PO_4 has five sharp bands at 1013, 1030, 1048, 1071 and 1108 cm^{-1}; a distinct shoulder at 1082 cm^{-1}; as well as a few indistinct shoulders on the bands mentioned above. Thermal broadening of the bands can be seen in the 84°C spectrum, and the beginning of the collapse of the band structure can be seen in the 249°C spectrum. The bands have shifted in frequency to 1028, 1043, 1064 and 1104 cm^{-1}. The band at 1013 cm^{-1} has essentially become a shoulder at 1010 cm^{-1}, while the shoulder at 1082 cm^{-1} has shifted to 1078 cm^{-1} and become less distinct. At 316°C the bands have become even less distinct with the

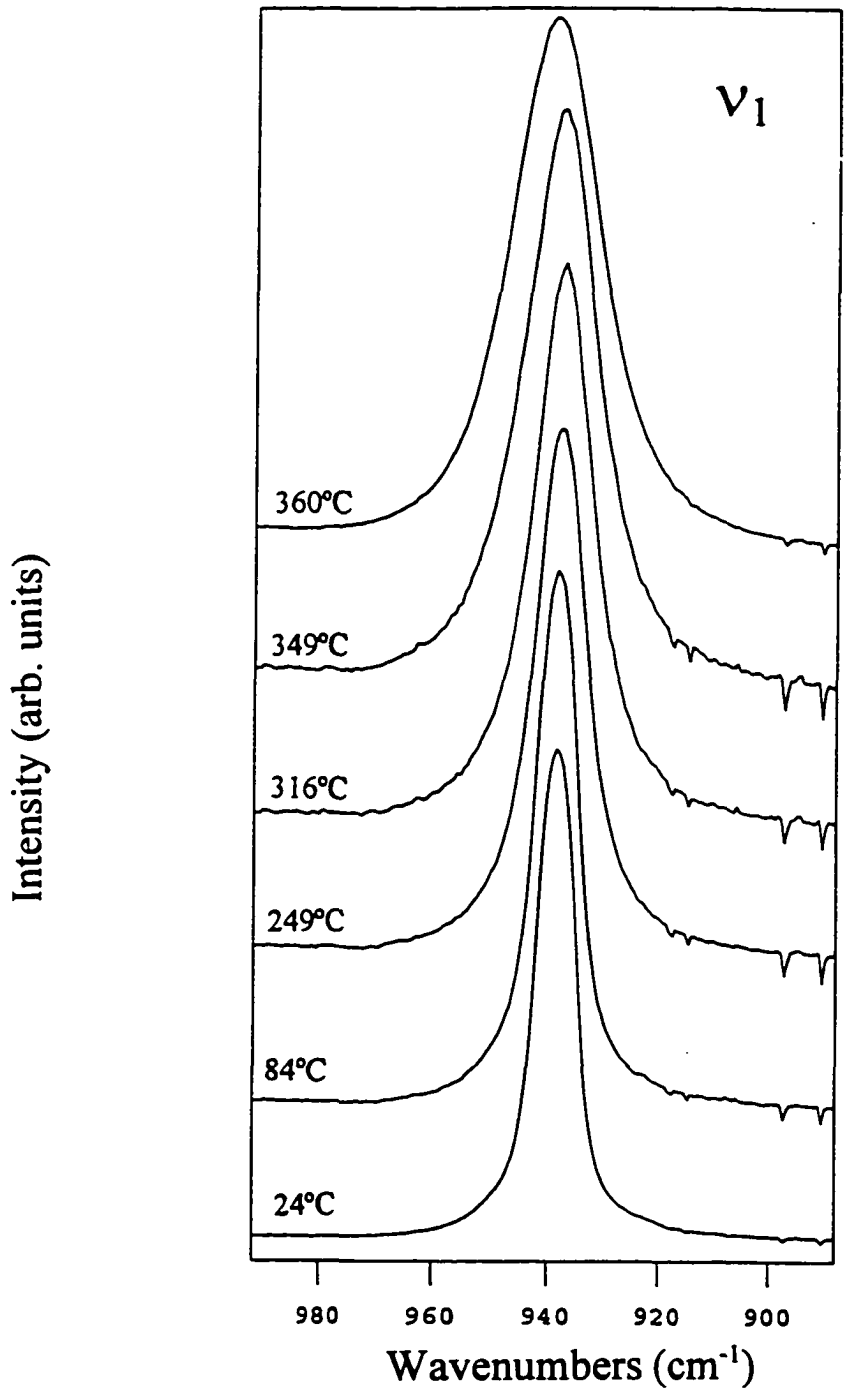

Figure 4.4. Temperature-dependent Raman spectra of Na_3PO_4 in the PO_4^{3-} ν_1 spectral region. The spectrum at 360°C corresponds to the γ-phase.

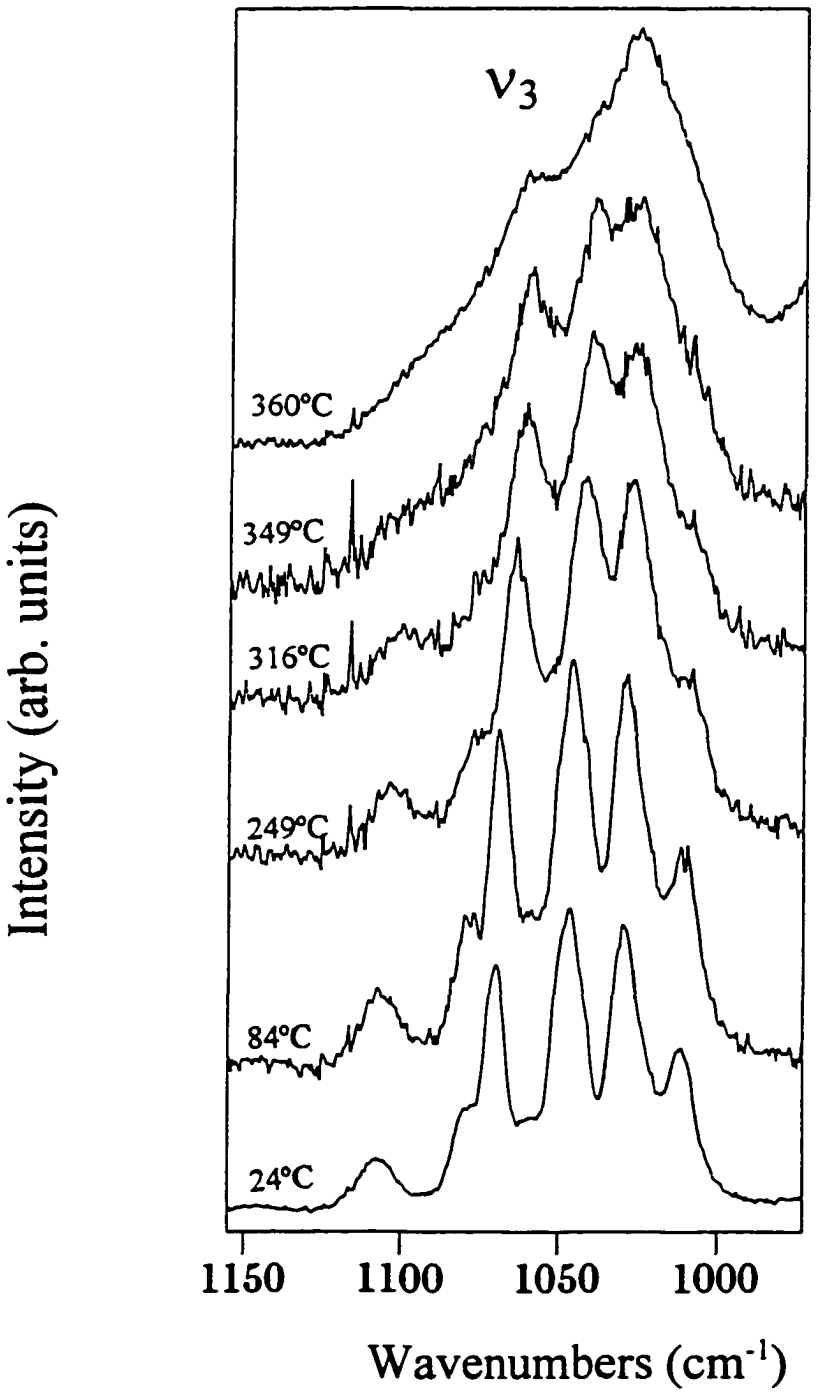

Figure 4.5. Temperature-dependent Raman spectra of Na_3PO_4 in the PO_4^{3-} ν_3 spectral region. The spectrum at 360°C corresponds to the γ-phase.

disappearance of the shoulders seen in the previous spectrum. The band at 1102 cm^{-1} has almost disappeared, and the bands at 1043 and 1064 cm^{-1} have shifted to 1041 and 1062 cm^{-1}, respectively. There are essentially three bands at 1027, 1039, and 1062 cm^{-1} that can be distinguished in the spectrum at 349°C. By 360°C these have collapsed to a single broad band centered at 1028 cm^{-1} with a shoulder at 1062 cm^{-1}.

The collapse of structure with increasing temperature seen in the Raman spectra reflects the change in symmetry as the crystal changes phase. The many sharp bands seen in the α-Na_3PO_4 spectrum are consistent with the factor group analysis. There is strong correlational coupling between molecules in the unit cell, which is seen particularly well in the structure of the ν_3 multiplet. As the temperature is increased and the ions become more orientationally disordered, this correlation breaks down. The perturbation of the α-phase before the transition to γ-Na_3PO_4 is complete can be seen in the frequency shift that occurs in the ν_1 mode. This perturbation is seen even more clearly in the new feature that appears, then disappears, in the ν_2 spectral region. The broad bands and collapsed band structure in γ-Na_3PO_4 are indicative of the high disorder present.

The infrared spectrum of α-Na_3PO_4 is shown in Figure 4.6. The frequencies are reported in Table 4.3 along with those of the fundamental frequencies of the isolated PO_4^{3-} ion [26] and the PO_4^{3-} ion in solution. [28] The fact that there is w-phase present in the sample can clearly be seen by the presence of the water bands at 3560, 3200, 2290 and 1668 cm^{-1}. Analysis of these water bands gives some insight into the

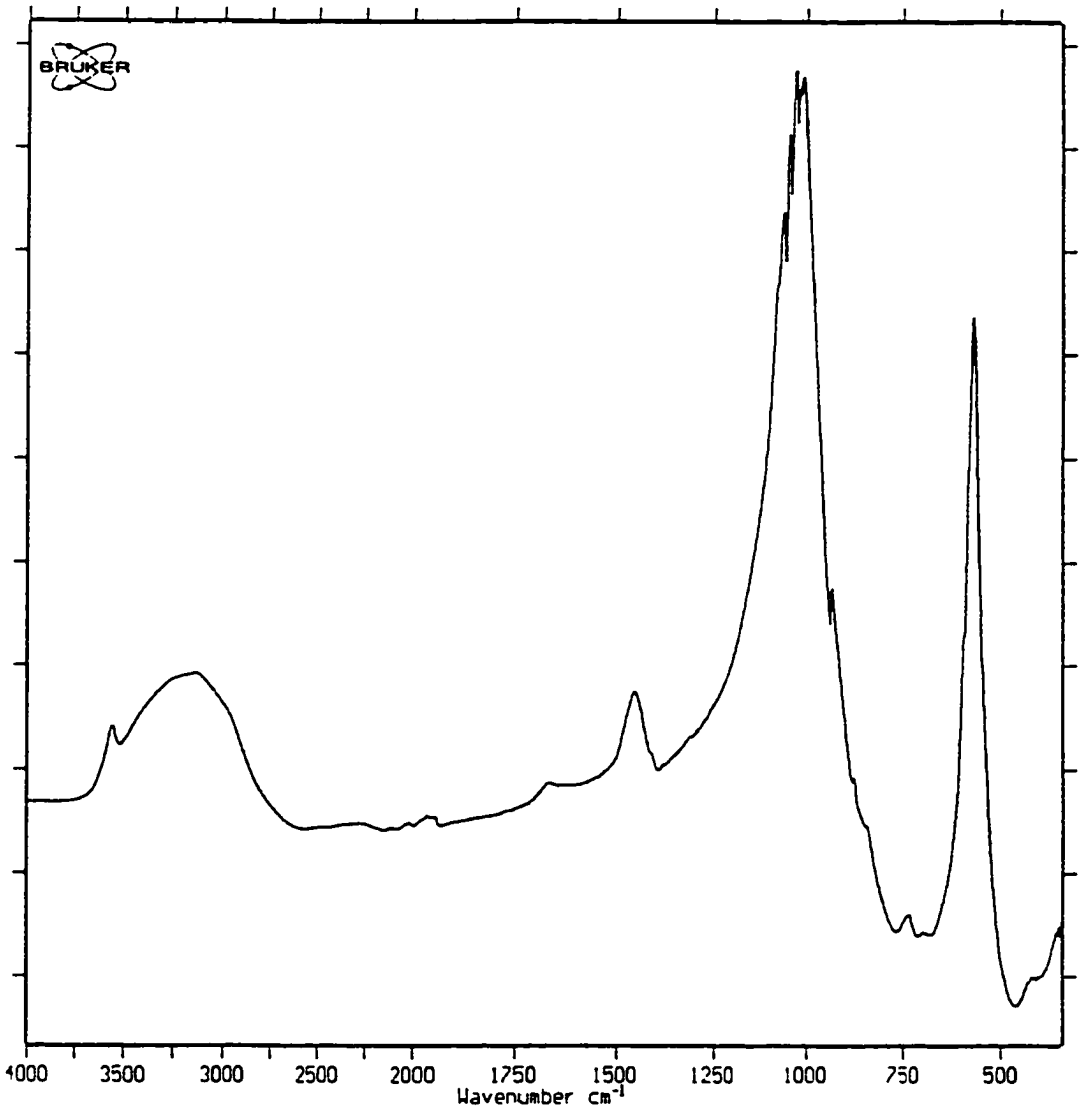

Figure 4.6. Infrared spectrum of α-Na_3PO_4.

Table 4.3. Frequencies of the PO_4^{3-} infrared vibrational modes.

Mode	Present work (cm^{-1})	fundamental frequencies (cm^{-1}) (Corbridge[26])	PO_4^{3-} in solution (cm^{-1}) (Steger)[28]
ν_1	935	980	938
ν_2	--	363	420
ν_3	1010 1032 1048 1065	1082	1017
ν_4	574	515	567
OH	1668 2290 3200 3560		
?	742 1456		

* Averaged values for the components of the crystal field splitting.

coordination of the water in the w-phase. The broad band centered at 3200 cm^{-1} is typical of the stretching vibration of OH when the water molecules are strongly bound to the PO_4^{3-} ions by hydrogen bridges. [27, 30, 32, 33] The OH deformation band at 1668 cm^{-1} is consistent with this description as well. However, the sharp band at 3560 cm^{-1} and the broad, weak band at 2290 cm^{-1} indicate the presence of free OH. [27, 31, 32] This has been explained by either interstitial water [27] or water with only one hydrogen strongly hydrogen bound to a phosphate oxygen.[32] The latter situation is more likely in this case, particularly in light of the high temperature (250°C) at which water loss occurs. The effect of the hydrogen bonding on the symmetry of the PO_4^{3-} ion can also be seen by the presence of the band at 935 cm^{-1}. The ν_1 symmetric stretching mode is not allowed in the infrared according to selection rules, but the hydrogen bonds perturb the symmetry enough to allow a weak ν_1 band to be seen.

References

1. Dollase, W.A., Merwin, L.H. & Sebald, A. *J. Solid State Chem.* **83**, 140-149 (1989).

2. Hooper, A., McGeehin, P., Harrison, K.T. & Tofield, B.C. *J. Solid State Chem.* **24**, 265-275 (1978).

3. Irvine, J.T.S. & West, A.R. *J. Solid State Chem.* **69**, 126-134 (1987).

4. Irvine, J.T.S. & West, A.R. *Mat. Res. Bull.* **22**, 1047-1054 (1987).

5. Irvine, J.T.S. & West, A.R. *Solid State Ionics* **28-30**, 214-219 (1988).

6. Irvine, J.T.S. & West, A.R. *Solid State Ionics* **37**, 73-78 (1989).

7. Kolsi, A.-W. *Rev. Chim. Miner.* **13**, 416-421 (1976).

8. Milne, S.J. & West, A.R. *J. Solid State Chem.* **57**, 166-177 (1985).

9. Newsam, J.M., Cheetham, A.K. & Tofield, B.C. *Solid State Ionics* **1**, 395-410 (1980).

10. Palazzi, M. & Rémy, F. *Bull. Soc. Chim. Fr.* **8**, 2795-2798 (1971).

11. Wiench, V.D.M. & Jansen, M. *Z. Anorg. Allg. Chem.* **486**, 57-60 (1982).

12. Irvine, J.T.S. & West, A.R. *J. Solid State Chem.* **74**, 385-392 (1988).

13. Lissel, E., Jansen, M., Jansen, E. & Will, G. *Z. Krist.* **192**, 233-243 (1990).

14. Wiench, V.D.M. & Jansen, M. *Zeitschrift fuer Anorganische und Allgemie Chemie* **461**, 101-108 (1980).

15. Mair, A.D. *N. Z. J. Sci.* **19**, 61-67 (1976).

16. Wendrow, B. & Kobe, K.A. *Chem. Rev.* **54**, 891-924 (1954).

17. Kizilyalli, M. & Welch, A.J.E. *J. Inorg. Nucl. Chem.* **38**, 1237-1240 (1976).

18. Jenkins, R. & Snyder, R.L. *Introduction to X-ray Powder Diffractometry* (John Wiley & Sons, Inc., New York, 1996).

19. Lopez-Bote, M.A. & Montero, S. *J. Raman Spectrosc.* **9**, 386-392 (1980).

20. Zhu, B., Mellander, B.-E. & Chen, J. *Mat. Res. Bull.* **28**, 321-328 (1993).

21. Mellander, B.E. & Zhu, B. *Solid State Ionics* **61**, 105-110 (1993).

22. Wendrow, B. & Kobe, K.A. *Industrial and Engineering Chemistry* **44**, 1439-1448 (1952).

23. Fateley, W.G., Dollish, F.R., McDevitt, N.T. & Bentley, F.F. *Infrared and Raman Selection Rules for Molecular and Lattice Vibrations: The Correlation Method.* (John Wiley & Sons, Inc., New York, 1972).

24. Frech, R. & Teeters, D. *J. Phys. Chem.* **88**, 417-420 (1984).

25. Cazzanelli, E. & Frech, R. *J. Chem. Phys.* **84**, 626-630 (1986).

26. Corbridge, D.E.C. *J. Appl. Chem.* **6**, 456-465 (1956).

27. Corbridge, D.E.C. & Lowe, E.J. *J. Chem. Soc.* , 493-502 (1954).

28. Steger, V.E. & Schmidt, W. *Ber. Bunsenges. Phys. Chem.* , 102-109 (1964).

29. Mutschin, A. & Maennchen, K. *Z. Anal. Chem* **156**, 241-248 (1957).

30. Chapman, A.C. & Thirlwell, L.E. *Spectrochim. Acta* **20**, 937-947 (1964).

31. Miller, F.A. & Wilkins, C.H. *Anal. Chem.* **24**, 1253-1294 (1952).

32. Zundel, G. *Hydration and Intermolecular Interaction: Infrared Investigations with Polyelectrolyte Membranes* (Academic Press, Inc., New York, 1969).

33. Ryskin, Y.I. & Stavistskaya, G.P. *Optics and Spectrosc.* **7**, 488-490 (1959).

CHAPTER 5

ANION STABILIZED SODIUM PHOSPHATE

Introduction

Previous studies[1-6] have shown that γ-Na_3PO_4 can be stabilized by the addition of a variety of anions including SO_4^{2-}, SeO_4^{2-}, SiO_4^{2-}, MoO_4^{2-} and WO_4^{2-}. However, these studies have focused on the ionic conductivity and variation in the lattice parameters of these systems and have not included vibrational spectroscopy as part of their analysis. I chose to concentrate on the Na_3PO_4/Na_2SO_4 system because both compounds have a fast-ion conducting phase and the two form an extended series of solid solutions. There is also the advantage that there have been extensive studies on the effects of aliovalent doping on Na_2SO_4 including structural, thermal and spectroscopic measurements.[7-26]

The extensive range of solid solutions formed by the Na_3PO_4/Na_2SO_4 system, represented by the formula $Na_{3-x}S_xP_{1-x}O_4$, is particularly significant because their phases do not belong to isostructural space groups. α-Na_3PO_4 is tetrahedral and belongs to $P\bar{4}2_1c$ (D_{2d}^4)[27]; γ-Na_3PO_4 is cubic and belongs to Fm3m (O_h^5)[28]. The three Na_2SO_4 phases that are thermodynamically stable between room temperature and the melt are phase V (RT to 180°C), phase III (180 to 237°C) and phase I (237 to the melt at 883°C). [29] Na_2SO_4 phases V and III are orthorhombic and belong to Fddd (D_{2h}^{24})[30] and Cmcm (D_{2h}^{17})[31] respectively, while Na_2SO_4 phase I is hexagonal and belongs to

$P6_3/mmc$ (D_{6h}^4)[14, 32]. Irvine and West[4] reported the phase diagram for $Na_{3-x}(S_xP_{1-x})O_4$ for $0 < x < 1$. For $0 < x < 0.3$, they observed a mixture of α- and γ-Na_3PO_4. In the range $0.3 < x < 0.6$ only γ-Na_3PO_4 is present. The range $0.6 < x < 1$ is a mixture of γ-Na_3PO_4 and Na_2SO_4 phase III. It should be noted that these ranges were reported with approximate limits. However, these limits are generally consistent with other studies[1-3] and with the results presented here.

Although the identification of phases is consistent in the literature, the reported conductivities and lattice parameters are not. Table 5.1 summarizes these results from the literature. Wiench & Jansen[2] and Irvine & West[4] report values for the lattice parameter *a* that increase with increasing x for $Na_{3-x}S_xP_{1-x}O_4$. There is reasonable correlation between the values from the two reports, but different overall behavior. Wiench and Jansen describe a linear relationship between x and the lattice parameter, and Irvine and West report a smooth curve with a slight downward curvature that levels out and becomes constant for $x > 0.60$. Majidi et al.[3] report very different behavior, with lattice parameters that decrease and then increase with a minimum value of 7.36Å at $x = 0.25$. The conductivities reported by Majidi et al. and Irvine & West, however, show good agreement, but differ from those reported by Hooper et al.[1] This discrepancy may be related to the method of preparation of the samples. Hooper et al. used dehydrated $Na_3PO_4 \cdot 12H_2O$ which contains significant amounts of NaOH. In the other studies Na_3PO_4 was prepared using synthetic routes that minimize this contamination. The best conductivity achieved was

Table 5.1. Summary of previous studies of $Na_{3-x}S_xP_{1-x}O_4$.

Reference	a vs x	σ vs x
Wiench & Jansen [2]	increases in a linear fashion	not measured
Irvine & West [4]	increasing curve that levels off	increases with x
Majidi et al. [3]	decreases then increases	increases with x
Hooper et al. [1]	not measured	decreases with x

σ = $1.3x10^{-2}$ $\Omega^{-1}cm^{-1}$ for x = 0.55 at 300°C.[4] Pure γ-Na_3PO_4 has a conductivity of $1x10^{-4}$ $\Omega^{-1}cm^{-1}$ at 370°C.[3]

Results

The Na_3PO_4/Na_2SO_4 system was examined over the entire range of solid solution compositions. As the composition of for $Na_{3-x}S_xP_{1-x}O_4$ is changed from x=0 to x=1 the transition from one phase to another can be observed using a variety of techniques. However, the composition and degree to which the transition between phases has taken place may appear to be different, depending on the technique used. This is due to complex structural changes taking place in these solid solutions and the fact that the domain size probed by the different techniques is not the same. Differential scanning calorimetry (DSC) data (shown in Figure 5.1) were used to identify the phase(s) present. These phases were confirmed using XRD analysis (patterns shown in Figure 5.2) by comparing the powder patterns obtained experimentally to the patterns published for the two anhydrous phases of Na_3PO_4 as well its hydrates[33-36] and to those of Na_2SO_4 phases V, III, and I.[7, 29, 30] Both DSC and XRD probe bulk structural characteristics. This is not the case for vibrational spectroscopy, which is more sensitive to small changes in the local structure that may not affect the global structure. This sensitivity is clearly seen by examining the infrared spectra (Figure 5.3) and particularly the Raman spectra (Figures 5.4 and 5.5). These results are discussed in more detail below.

Differential Scanning Calorimetry

The DSC thermograms for several compositions are shown in Figure 5.1. The thermogram for α-Na_3PO_4 is also included for comparison. The DSC thermogram for x=0.05 shows a broad endothermic transition at 257°C on heating, with no significant transition evident on cooling. There is no indication of a typical α- to γ-Na_3PO_4 phase transition at 330°C. The x=0.10 composition also has a very broad and shallow transition that is present on heating but not on cooling, but the transition occurs at 220°C in this case. The transition at 257°C is at least partially due to the presence of the w-phase. This can be seen by comparison to the transition at 257°C in the "pure" α-Na_3PO_4. As was discussed in the previous chapter, this phase is frequently present in small amounts. However, the broadness of the transition in the doped composition and the indication of a small transition on the cooling curve suggest that another thermal event due to an α- to γ-Na_3PO_4 phase transition is overlapping with the w-phase transition. This interpretation is further supported by the transition at 220°C in the x=0.10 composition. It is not uncommon for the addition of dopant ions to cause a decrease in the phase transition temperature since the ions introduce disorder into the structure. The lowering and broadening of the α- to γ-Na_3PO_4 phase transition in the for $Na_{3-x}S_xP_{1-x}O_4$ system, combined with the absence of the transition in the cooling curve, would indicate that any α-Na_3PO_4 present has significant disorder in the structure and is easily transformed and stabilized.

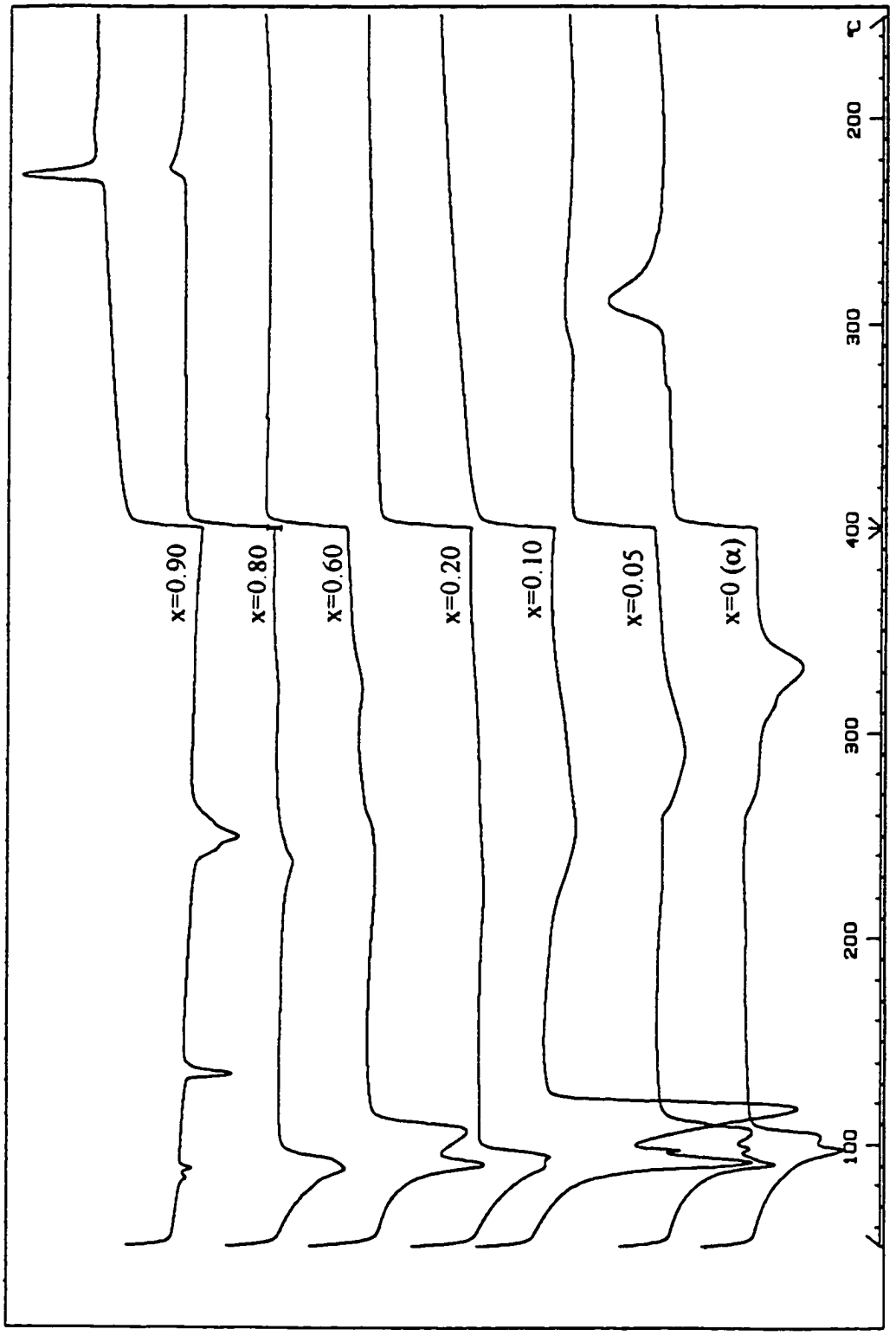

Figure 5.1. DSC thermograms of $Na_{3-x}S_xP_{1-x}O_4$ for increasing values of x.

The x=0.20 composition is more clearly γ-Na_3PO_4. The presence of hydrate(s) can be seen in the DSC trace in the transition at 80°C, but there are no transitions on either heating or cooling cycles after the initial loss of water on heating. The x=0.30, 0.40 and 0.50 compositions also have thermograms that show no transitions after the initial loss of water of hydration on heating. The DSC trace for the x=0.60 composition has a small but detectable transition at 223°C which is indicative of the transition from Na_2SO_4 phase III to phase I. The x=0.70 composition shows an increase in the amount of Na_2SO_4 phase III present, but there are no significant changes until a composition of x=0.80 is reached. At this point the system is clearly a mixture of γ-Na_3PO_4 and Na_2SO_4 phase III. There is a well-defined peak present in the DSC thermogram at 223°C on heating and at 231°C on cooling. The x=0.90 composition is almost entirely Na_2SO_4 phase III with some Na_2SO_4 phase V also present. The DSC thermogram has transitions at 130°C and 234°C on heating and a transition at 232°C on cooling. This behavior is typical of a V-III-I transition where all three phases are seen on the heating cycle but not on the cooling cycle since phase III can remain stable for months before reverting to phase V.[29]

Powder X-ray Diffraction

The XRD patterns for several for $Na_{3-x}S_xP_{1-x}O_4$ compositions are shown in Figure 5.2. The three Na_3PO_4 phases seen in the XRD patterns are α- and γ-Na_3PO_4 and the w-phase. The three phases can be differentiated by the presence of distinctive peaks and/or peak combinations. A table of the characteristic d-spacings and relative

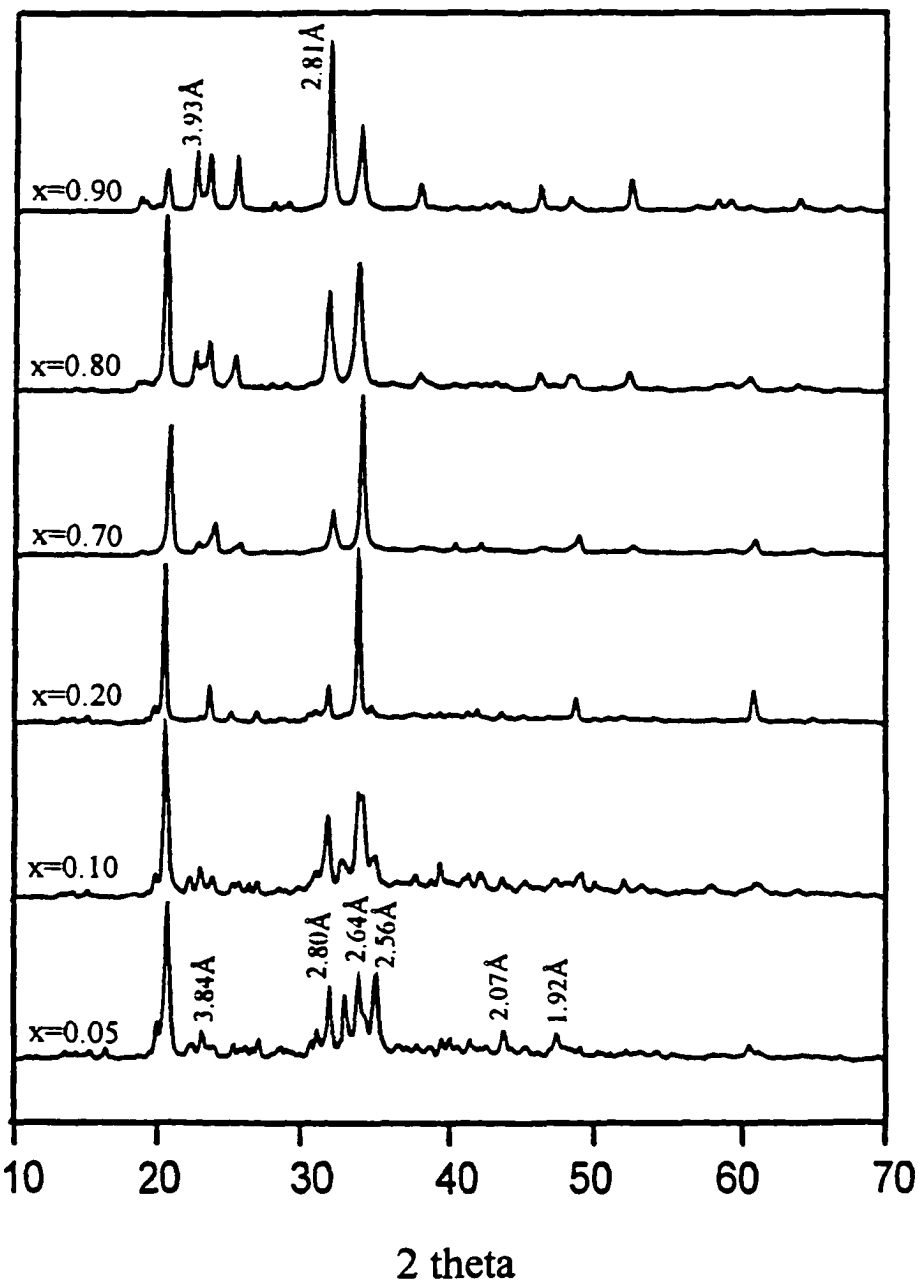

Figure 5.2. XRD patterns of $Na_{3-x}S_xP_{1-x}O_4$.

intensities for these phases is given in Table 5.2. This table is constructed from several XRD patterns reported in the literature. The values were combined in order to compensate for the minor variations in the reports. The strong peaks at 2.70 (60%) and 2.55 Å (100%) along with the weaker peaks at 3.82 (25%), 2.06 (25%) and 1.91 Å (35%) are characteristic of α-Na_3PO_4. The marker for the w-phase is a peak at 4.48Å. This peak does not appear in the other two phases and has a relative intensity of 75% in the pure compound. γ-Na_3PO_4 does not have any peaks that are unique identifiers since all of its peaks are also found in the other phases as well. However, the relative intensities of these peaks differ, and the phase can be distinguished by the presence of a strong peak at 2.62 Å combined with the absence of peaks found in the other phases. Although the phases can be distinguished without too much difficulty, it is not always possible to determine quantitatively the relative amounts of the phases present by comparing peak intensities. This is because there are near coincidental peaks occurring in the patterns. For example α-Na_3PO_4 has a peak at 4.24 Å with a relative intensity of 75%; γ-Na_3PO_4 has a peak at 4.28 with 50% relative intensity, and the w-phase has a peak at 4.31 Å with 100% relative intensity. These tend to overlap or blend into a single peak with an intermediate d-spacing and increased relative intensity.

The XRD pattern for the x=0.05 composition is a mixture of pure α-Na_3PO_4 and w-phase with what appears to be small amounts of γ-Na_3PO_4. The identification of α-Na_3PO_4 is based on the strong peaks at 2.56 and 2.71 Å, which have relative

Table 5.2. Powder x-ray diffraction data for Na_3PO_4 phases. Data are reported as d-spacings in Å with relative intensities in parentheses.

γ-phase [33-35]	α-phase [33-35]	1/2 H_2O [34]	6 H_2O [34]	8 H_2O [4,34]	w-phase [4]
4.28 (50)	7.64 (10)	8.33 (15)	6.57 (15)	8.47 (12)	7.03 (10)
3.70 (15)	4.24 (75)	4.70 (80)	6.37 (8)	8.06 (15)	6.62 (30)
2.62 (100)	3.95 (20)	4.54 (15)	6.21 (20)	6.42 (44)	6.42 (20)
2.23 (10)	3.82 (25)	4.40 (50)	5.81 (25)	6.21 (50)	6.26 (35)
2.14 (7)	3.41 (4)	4.30 (20)	4.58 (10)	5.24 (10)	5.85 (40)
1.85 (25)	3.12 (15)	4.16 (40)	4.45 (40)	5.11 (30)	4.60 (40)
1.51 (20)	2.78 (10)	3.91 (10)	4.29 (100)	4.85 (50)	4.48 (75)
1.43 (5)	2.70 (60)	3.75 (15)	3.68 (10)	4.55 (35)	4.31 (100)
	2.55 (100)	3.51 (20)	3.50 (25)	4.48 (80)	3.70 (25)
	2.45 (15)	3.30 (10)	3.28 (30)	4.35 (100)	3.52 (45)
	2.42 (15)	2.76 (60)	3.18 (4)	4.09 (20)	3.39 (20)
	2.28 (15)	2.71 (100)	3.10 (8)	3.78 (25)	3.35 (20)
	2.16 (20)	2.67 (30)	3.07 (10)	3.67 (40)	3.30 (70)
	2.12 (15)	2.64 (50)	2.91 (15)	3.62 (15)	3.20 (20)
	2.06 (25)	2.60 (10)	2.86 (25)	3.50 (25)	3.12 (30)
	1.91 (35)	2.50 (8)	2.83 (15)	3.22 (15)	3.08 (36)
	1.80 (5)	2.35 (10)	2.79 (100)	3.15 (15)	2.92 (30)
	1.72 (5)	2.32 (8)	2.64 (35)	2.93 (30)	2.88 (50)
	1.57 (10)	2.27 (80)	2.60 (8)	2.91 (60)	2.85 (35)
	1.52 (20)		2.57 (35)	2.82 (60)	2.80 (95)
	1.44 (10)		2.52 (8)	2.74 (20)	2.72 (10)
			2.38 (15)	2.70 (50)	2.65 (60)
			2.32 (10)	2.68 (65)	2.63 (40)
			2.28 (15)	2.64 (15)	2.62 (40)
			2.25 (8)	2.61 (15)	2.58 (70)
			2.22 (5)	2.58 (15)	2.56 (20)
			2.18 (20)	2.56 (40)	2.53 (10)
			2.14 (5)	2.52 (12)	2.39 (40)
			2.12 (6)	2.50 (15)	2.37 (20)
			2.07 (15)	2.47 (20)	2.33 (35)
			2.04 (8)	2.38 (15)	2.29 (50)
				2.35 (20)	2.26 (20)
				2.29 (20)	2.23 (20)
				2.26 (15)	2.19 (50)
					2.15 (30)
					2.13 (30)
					2.08 (55)

intensities of 54 and 30%, and the weaker peaks at 3.84, 2.07 and 1.92 Å. The presence of the w-phase is clearly indicated by the peaks at 4.45 (18%) and 2.80 Å (31%). The reason for identifying γ-Na_3PO_4 as a possible component is the intensity of the peak at 2.64 Å. The most intense peak in γ-Na_3PO_4 occurs at 2.62 Å. The w-phase is reported to have peaks at 2.62, 2.63, and 2.64 Å, but with relative intensities of about 40%. The peak at 2.64 Å in the XRD pattern for the x=0.05 composition has a relative intensity of 39%. To put this in perspective, the peak in this pattern at 4.45 Å has a relative intensity of 18%, but the correlating peak in pure w-phase has a relative intensity of 75%. Therefore, if no γ-Na_3PO_4 was present and this peak was due only to the presence of w-phase, it would be expected to be much lower in intensity. This is the case for the peak at 3.51 Å which has a relative intensity of 4% in the x=0.05 composition and 45% in the pure w-phase.

The x=0.10 composition has an XRD pattern which indicates that the primary phase present is γ-Na_3PO_4 but with w-phase and α-Na_3PO_4 components. The most intense peak is at 4.28 Å, but this gives relatively little information for phase identification since all three phases have peaks close to this value. However, the second most intense peak occurs at 2.62 Å with a relative intensity of 69%. The number of intense peaks has also decreased significantly from the previous pattern. The fact that there is a notable amount of w-phase present can be determined by the intensity of the peaks at 4.43 Å (7%) and 2.79 Å (43%). The presence of a small amount of α-Na_3PO_4 is indicated by the peaks at 2.55 Å (23%) and 2.70 Å (19%).

The x=0.20 composition appears to be almost entirely γ-Na_3PO_4 solid solution. The XRD pattern has very little noise and only a few intense peaks, although there are a few small peaks that correspond to those of a hydrate phase. In this case, it is harder to determine which hydrate phase is present. The DSC results do not show the presence of the w-phase for compositions with more than ten percent Na_2SO_4. The hydrate peaks in the XRD pattern seem to match the pattern of the w-phase most closely but are also generally in agreement with $Na_3PO_4 \cdot 6H_2O$ pattern. The latter assignment would be more consistent with the DSC results. The x=0.30, 0.40 and 0.50 compositions also have XRD patterns that indicate the presence of γ-Na_3PO_4 with small amounts of a hydrate phase present.

The XRD patterns for the x=0.60 and 0.70 compositions indicate the presence of very small amounts of Na_2SO_4 phase III. The d-spacings for the three thermodynamically stable phases of Na_2SO_4 are shown in Table 5.3. There are peaks at 3.91 (8%) and 2.80 Å (32%) that can be attributed to Na_2SO_4 phase III. The peak at 2.80 Å can be unambiguously assigned to Na_2SO_4 phase III rather than to the w-phase because there is no peak at 4.48 Å.

The x=0.80 composition is clearly a mixture of γ-Na_3PO_4 and Na_2SO_4 phase III. This easily seen in the XRD pattern by the increased intensity of the peaks at 3.93 (21%) and 2.81 Å (70%). The XRD pattern for the x=0.90 composition is dominated by the Na_2SO_4 phase III peaks with small peaks present that correspond to γ-Na_3PO_4 and perhaps a small amount of w-phase.

Table 5.3. Powder x-ray diffraction data for Na_2SO_4 phases. Data are reported as d-spacings in Å with relative intensities in parentheses.

Phase V [29,30]	Phase III [7,29]	Phase I [29]
4.66 (73)	4.73 (20)	4.68 (30)
3.84 (18)	4.47 (10)	3.92 (100)
3.18 (51)	3.93 (70)	3.62 (60)
3.08 (47)	3.76 (60)	2.86 (90)
2.78 (100)	3.47 (40)	2.70 (90)
2.65 (48)	2.80 (100)	2.35 (20)
2.33 (21)	2.63 (80)	2.21 (20)
2.19 (20)	2.37 (70)	1.96 (70)
1.86 (31)	2.23 (10)	1.81 (20)
1.79 (30)	2.13 (20)	1.58 (20)
1.68 (12)	2.08 (20)	1.55 (30)
1.55 (10)	1.96 (60)	1.50 (40)
	1.88 (40)	
	1.74 (70)	
	1.69 (20)	
	1.62 (20)	
	1.58 (50)	
	1.56 (40)	
	1.53 (20)	
	1.48 (10)	
	1.45 (50)	
	1.40 (30)	

Infrared Spectroscopy

The infrared spectrum for the for $Na_{3-x}S_xP_{1-x}O_4$ x=0.05 composition (shown in Figure 5.3) closely resembles that of α-Na_3PO_4, although the PO_4^{3-} ν_3 multiplet has been reduced from five distinct bands to two with broad shoulders. There are only minor changes as x is increased to 0.10. The shoulder at 1146 cm^{-1} is more distinct, and the shoulder at 632 cm^{-1} has become a distinct band. The spectrum for the x=0.20 composition is very similar to that of the previous spectra with the only differences being an increase in the intensity of the band at 632 cm^{-1} and a broadening of the band at 545 cm^{-1}. The infrared spectra for the x=0.30 and 0.40 compositions are virtually identical although there are small differences compared to previous spectra. The band at 549 cm^{-1} has become a shoulder while the band at 565 cm^{-1} has become sharper, and the spectral structure in the PO_4^{3-} ν_3 region has been reduced to two bands at 1010 and 1039 cm^{-1}. In the x=0.50 composition, the infrared spectrum shows a further broadening of the PO_4^{3-} ν_3 bands as the SO_4^{2-} band shifts towards 1140 cm^{-1} from its initial position at 1158 cm^{-1}. The spectrum of the x=0.60 composition now has two well-defined bands at 613 and 632 cm^{-1} instead of a single, broad band. There is also the appearance of a sharp band at 994 cm^{-1}. The PO_4^{3-} ν_3 band has almost completely disappeared in the x=0.80 composition. The infrared spectrum of the x=0.90 composition is almost the same as the previous spectrum except for further decreases in the PO_4^{3-} band intensities.

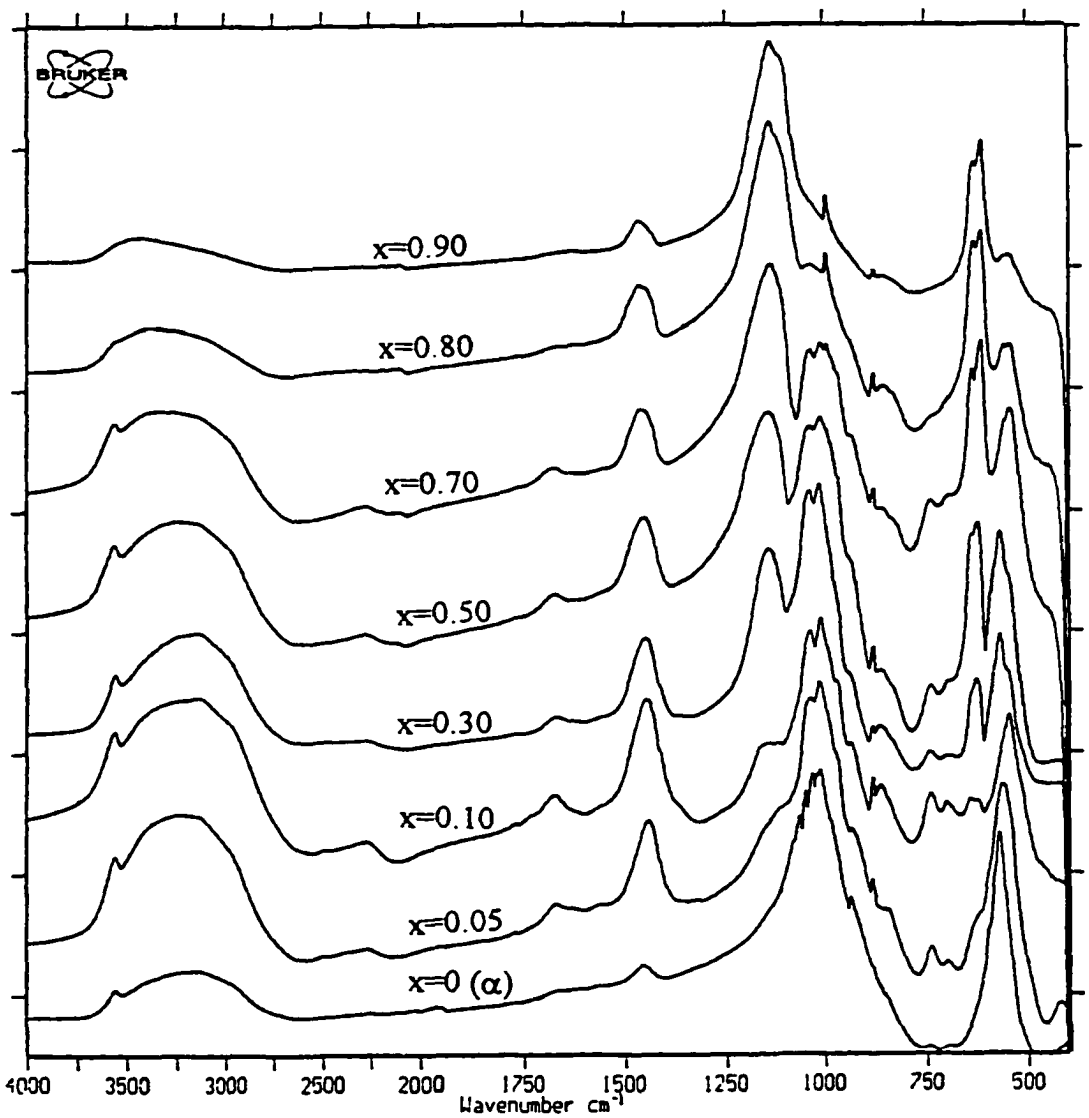

Figure 5.3. Infrared spectra of $Na_{3-x}S_xP_{1-x}O_4$ for increasing values of x.

Although the infrared spectra show the sensitivity of the vibrational modes to changes in the local structure of the solid solutions, they essentially do not provide any information that can not be obtained from the Raman spectra. This is largely due to the fact that temperature-dependent infrared spectra could not be obtained. The lack of a γ-Na_3PO_4 spectrum made it impossible to thoroughly interpret the changes in band structure relative to the pure phases. For this reason infrared spectra are not used in the characterization of the cation and cation/anion stabilized systems.

Raman Spectroscopy

The Raman spectra (shown in Figures 5.4 and 5.5) clearly show the change from α-Na_3PO_4 to γ-Na_3PO_4 to Na_2SO_4 phase III. It is not always clear which phases are present using vibrational spectroscopy alone. The presence of a new phase or compound can be determined by the appearance of additional bands in the spectrum which are unique to the new phase or compound. Although in this system sulfate bands can be seen in all compositions regardless of which phase is present, the frequencies, band shapes and intensities of the dopant SO_4^{2-} modes change in a distinctive manner as the structure changes from SO_4^{2-} in a host-Na_3PO_4 phase to an identifiable Na_2SO_4 phase.

The Raman spectrum of the for $Na_{3-x}S_xP_{1-x}O_4$ x=0.05 composition is almost identical to that of pure α-Na_3PO_4 with the exception of a very small ν_1 SO_4^{2-} band at

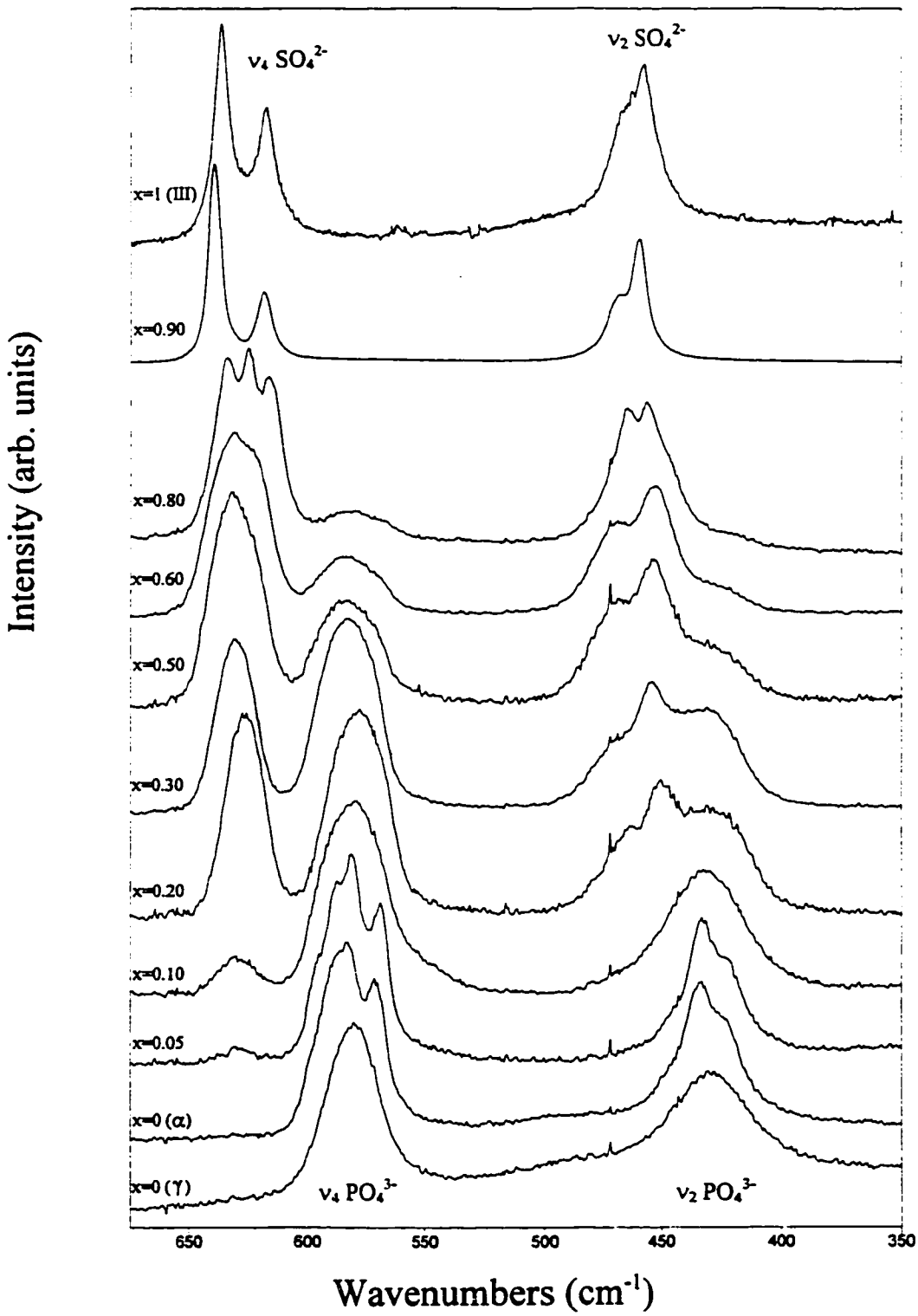

Figure 5.4. Raman spectra of $Na_{3-x}S_xP_{1-x}O_4$ in the ν_2 and ν_4 spectral regions for increasing values of x.

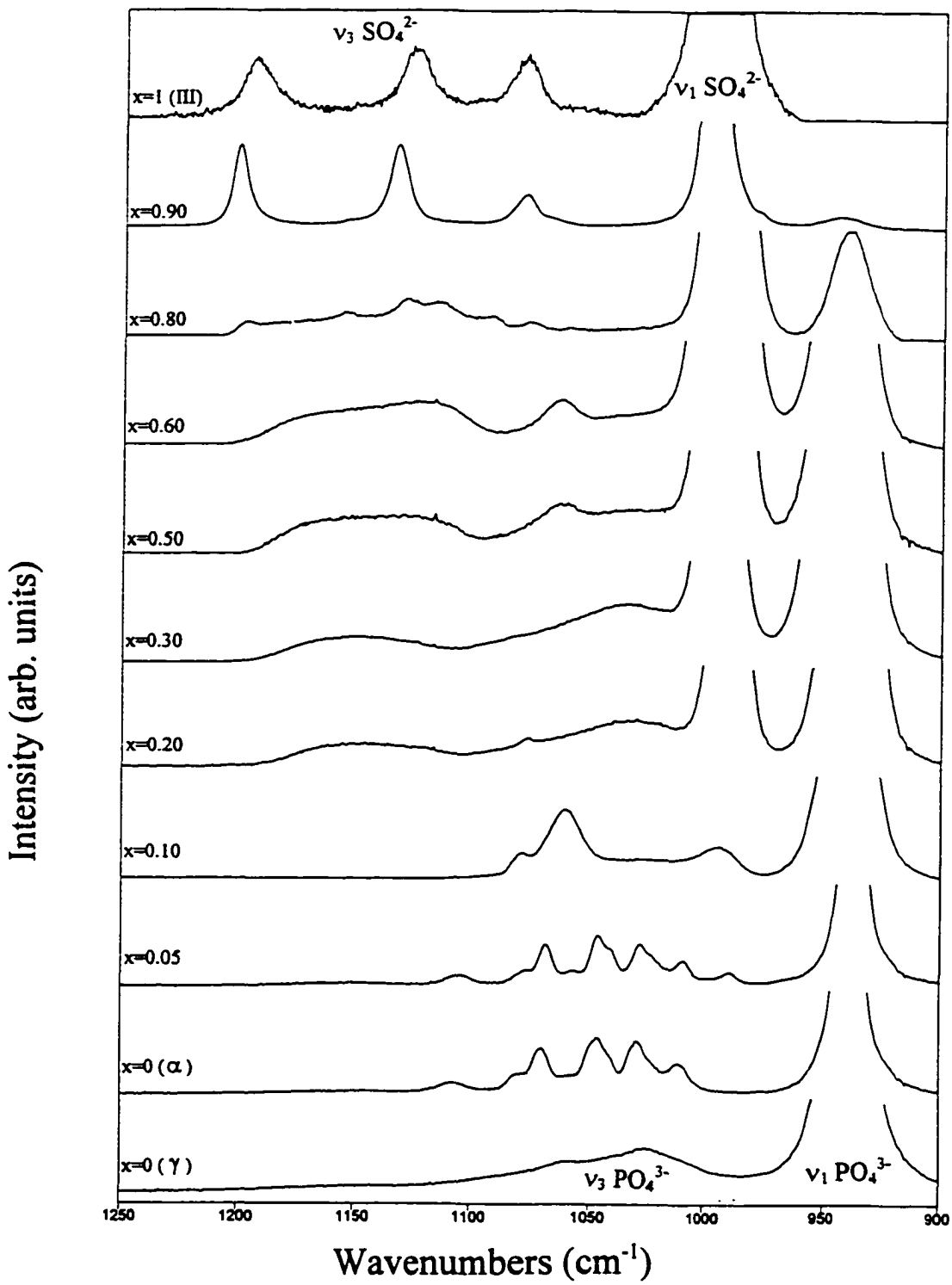

Figure 5.5. Raman spectra of $Na_{3-x}S_xP_{1-x}O_4$ in the ν_1 and ν_3 spectral regions for increasing values of x.

997 cm^{-1}, which can be attributed to the vibrational frequency of an isolated SO_4^{2-} in an α-Na_3PO_4 host matrix. Several changes occur in the spectrum when x is increased. The ν_1 SO_4^{2-} band at 997 cm^{-1} has increased in intensity, and a small ν_4 SO_4^{2-} band appears at 633 cm^{-1}. The ν_1, ν_2 and ν_4 PO_4^{3-} bands have the same band shape and occur at the same frequencies of the ν_1, ν_2 and ν_4 PO_4^{3-} bands in pure γ-Na_3PO_4. However, the ν_3 PO_4^{3-} spectral region does not have the structure observed in γ- or α-Na_3PO_4. Instead, it appears as a broad, weak feature with a sharper band at 1062 cm^{-1} and a shoulder at 1082 cm^{-1}. This alteration of band shape suggests a structure which is a perturbed γ-phase.

This type of behavior, where the structure indicated by the ν_2 and ν_4 regions is not completely consistent with that indicated by the ν_3 region has also been seen in the Na_2SO_4/Na_2CrO_4 system [37] where it was attributed to the differing nature of the modes. The ν_2 and ν_4 bending modes are sensitive to changes in bond angles and are therefore primarily influenced by the immediate potential energy environment of the anion. In contrast, ν_3 is an antisymmetric stretching mode with a very large dipole moment derivative, and hence the intermolecular coupling between PO_4^{3-} ions occurs over a larger domain size.

The Raman spectrum of the x=0.20 composition undergoes a significant change from that of the x=0.10 composition in the ν_2 and ν_3 regions while the ν_1 and ν_4 regions are essentially the same. The ν_1 PO_4^{3-} band at 942 cm^{-1} decreases in intensity, while the intensity of the SO_4^{2-} band at 997 cm^{-1} increases. Similar behavior

is seen in the ν_4 region. The PO_4^{3-} band at 583 cm^{-1} and the SO_4^{2-} band at 633 cm^{-1} are now equal in intensity. The ν_2 region still shows the PO_4^{3-} band at 432 cm^{-1}, but new bands have appeared at 452 and 466 cm^{-1} and the band structure has also become very broad. In the ν_3 region, the PO_4^{3-} band now has the same structure and frequency as that seen in pure γ-Na_3PO_4, while a very broad ν_3 SO_4^{2-} band centered at 1151 cm^{-1} has appeared. This band does not resemble the ν_3 SO_4^{3-} mode in any of the phases of Na_2SO_4, and so must reflect the vibrational potential energy environment of SO_4^{2-} in the γ-Na_3PO_4 host lattice.

The Raman spectra of the x=0.30 and 0.40 compositions are very similar to that of the x=0.20 compositions. This is also generally true for the x=0.50 composition. The biggest change in the Raman spectrum is in the ν_3 PO_4^{3-} bands. Instead of single broad band at 1032 cm^{-1}, there is a new peak at 1065 cm^{-1} and the rest of the band is considerably "flattened". There are several changes in the Raman spectrum of the x=0.60 composition compared to previous spectra. The ν_2 PO_4^{3-} band at 432 cm^{-1} has almost entirely disappeared and the SO_4^{2-} bands at 453 and 471 cm^{-1} have narrowed. The SO_4^{2-} ν_4 band has broadened and is beginning to develop a shoulder at 625 cm^{-1}. In the ν_3 region, the PO_4^{3-} band has almost entirely disappeared with only a small peak at 1062 cm^{-1}. The SO_4^{2-} band has developed some asymmetry with a more pronounced peak at 1126 cm^{-1}. The x=0.70 composition shows no significant changes when compared to the x=0.60 composition.

There is a dramatic change in the Raman spectrum of the x=0.80 composition compared to previous spectra. The ν_2 region now consists of a doublet band with peaks at 456 and 472 cm^{-1}. The ν_4 region has gone from a single band to a triplet with peaks at 617, 626, and 637 cm^{-1}. The ν_3 region has transformed from a broad, featureless band to a band having distinct peaks at 1080, 1097, 1120, 1132, 1158 and 1202 cm^{-1}. The Raman spectrum of the x=0.90 composition is almost identical to that of Na_2SO_4 phase III[38] with no trace of PO_4^{3-} modes except for a very small ν_1 band at 942 cm^{-1}. The ν_2 region has a peak at 456 cm^{-1} with a small shoulder at 472 cm^{-1}. The ν_4 region has now been reduced to two bands at 620 and 640 cm^{-1}. The ν_3 region has sharpened into three bands at 1081, 1135 and 1203 cm^{-1}.

Discussion

The differences in the structure detected by the various techniques are seen immediately in the $Na_{3-x}S_xP_{1-x}O_4$ x=0.05 composition. The XRD pattern indicates that only α-Na_3PO_4 and the w-phase are present, the Raman spectrum is in agreement with the assignment of α-Na_3PO_4 as is the infrared spectrum with only small changes in the PO_4^{3-} ν_3 spectral region. However, the DSC thermogram shows no endotherm indicative of the α- to γ-Na_3PO_4 phase transition. These results would indicate that although the local environment around the PO_4^{3-} ions has not changed significantly, there has been enough disorder introduced into the bulk structure to lower the transition temperature and broaden the α- to γ-Na_3PO_4 phase transition. This description is also consistent with the failure to observe a transition on the cooling

curve. If the structure is already close to the γ-phase, it is likely that it would remain metastable and not immediately make the transition back to the α-phase. This disorder is also seen in the infrared spectrum where the factor group multiplet structure seems to be highly sensitive to even a small degree of disorder, particularly in the ν_3 mode of PO_4^{3-}, as evidenced by the collapse of the band structure from a multiplet structure to a broadened doublet.

An increasing degree of disorder is also evident in the x=0.10 composition where the α- to γ- phase transition has been further broadened and the temperature lowered again. While the infrared spectrum does not change much from the x=0.05 composition, the Raman spectrum for this composition is somewhat more complicated. The ν_2 and ν_4 spectral regions have the same band shape and occur at the same frequencies as those of pure γ-Na_3PO_4. However, the ν_3 PO_4^{3-} region does not have the structure observed in either α- or γ-Na_3PO_4. The alteration of the band shape in the Raman spectrum along with the DSC and infrared data suggests a structure that is a perturbed γ-phase. The XRD pattern indicates that the primary phase present is γ-Na_3PO_4 but with w-phase and α-Na_3PO_4 components.

Compositions from x=0.20 to 0.60 in the $Na_{3-x}S_xP_{1-x}O_4$ system appear to be almost entirely γ-Na_3PO_4 solid solutions. In this range of compositions it is interesting to observe the changes taking place in the vibrational spectra, particularly the SO_4^{2-} Raman spectral regions. Although the bulk structural characteristics remain constant in this range, the Raman spectra undergo significant changes as the

percentage of SO_4^{2-} ions increases. These changes reflect the different potential energy environments of both the PO_4^{3-} and SO_4^{2-} ions in the various γ-phase solid solution compositions.

The x=0.70 composition shows an increase in the amount of Na_2SO_4 phase III present along with the dominant γ-Na_3PO_4, but there are no significant changes until a composition of x=0.80 is reached. At this point the $Na_{3-x}S_xP_{1-x}O_4$ system is clearly a mixture of γ-Na_3PO_4 and Na_2SO_4 phase III. This is easily seen in the XRD pattern and DSC thermogram, but the most dramatic difference is in the Raman spectrum. As was detailed earlier, the spectral regions have transformed from broad bands to multiplet structures.

The x=0.90 composition is almost entirely Na_2SO_4 phase III with a little Na_2SO_4 phase V and γ-Na_3PO_4 mixed in. This is verified by all the techniques used to characterize the compounds.

Conclusion

The results of this study have confirmed that the stabilization of γ-Na_3PO_4 by Na_2SO_4 occurs over a wide range of solid solution compositions extending from 20% to more than 60% Na_2SO_4. The amount of Na_2SO_4 that can be accommodated in the γ-Na_3PO_4 lattice is particularly interesting. Even with a composition of x=0.70, the predominant phase is γ-Na_3PO_4 with only a small amount of a true Na_2SO_4 phase present.

The difference in structure detected by the different techniques is perhaps a more important phenomenon. It is clear that the system undergoes complex structural changes that cannot be completely characterized using a single technique. This is primarily due to the difference in domain size probed by each technique, and in the case of Raman spectroscopy, the difference in domain size "probed" by different modes. The XRD results indicate a complete transition from α- to γ-Na_3PO_4 with no intermediate structures present. The DSC thermograms show the presence of a perturbed α- or γ-phase, but generally agree with the phases identified by the XRD patterns. Vibrational spectroscopy provides a richer description of the structural changes, particularly local structural changes, occurring as the composition changes. This is particularly true in the Raman scattering spectra where the presence of the SO_4^{2-} bands in the γ-Na_3PO_4 host lattice could be identified.

References

1. Hooper, A., McGeehin, P., Harrison, K.T. & Tofield, B.C. *J. Solid State Chem.* **24**, 265-275 (1978).
2. Wiench, V.D.M. & Jansen, M. *Z. Anorg. Allg. Chem.* **486**, 57-60 (1982).
3. Majidi, B., Brice, J.-F. & Kessler, H. *Mat. Res. Bull.* **19**, 1599-1606 (1984).
4. Irvine, J.T.S. & West, A.R. *J. Solid State Chem.* **69**, 126-134 (1987).
5. Irvine, J.T.S. & West, A.R. *Mat. Res. Bull.* **22**, 1047-1054 (1987).
6. Irvine, J.T.S. & West, A.R. *Solid State Ionics* **28-30**, 214-219 (1988).
7. Fischmeister, H.F. *Acta Crystallogr.* **7**, 776 (1954).

8. Fischmeister, H.F. *Monat. Chem.* **93**, 420-434 (1962).

9. Mehrotra, B.N. *Neues Jahrb. Mineral. Abh.* **11**, 485-490 (1978).

10. Hofer, H.H., Eysel, W. & Alpen, U.v. *J. Solid State Chem.* **36**, 365-370 (1981).

11. Saito, Y., Kobayashi, K. & Maruyama, T. *Thermochim. Acta* **53**, 289-297 (1982).

12. Kumari, M.S. & Secco, E.A. *Can. J. Chem.* **61**, 2804-2808 (1983).

13. Imanaka, N., Adachi, G.-y. & Shiokawa, J. *Can. J. Chem.* **61**, 1557-1561 (1983).

14. Eysel, W., Hofer, H.H., Keester, K.L. & Hahn, T. *Acta Crystallogr., Sect. B* **41**, 5 (1985).

15. Gundusharma, U.M. & Secco, E.A. *Can. J. Chem.* **65**, 1205-1208 (1987).

16. Imanaka, N., Kuwabara, S., Adachi, G.-y. & Shiokawa, J. *Solid State Ionics* **23**, 15-19 (1987).

17. Prakash, G. & Shahi, K. *Solid State Ionics* **23**, 151-163 (1987).

18. Bandaranayake, P.W.S.K. & Mellander, B.-E. *Solid State Ionics* **26**, 33-36 (1988).

19. MacDonald, K.G., MacLean, C. & Secco, E.A. *Can. J. Chem.* **66**, 3132-3136 (1988).

20. Bandaranayake, P.W.S.K. & Mellander, B.-E. *Solid State Ionics* **40/41**, 31-33 (1990).

21. Rao, N., Schoonman, J. & Sorensen, O.T. *Solid State Ionics* **57**, 159-168 (1992).

22. Frech, R. & Dharmasena, G. *Solid State Ionics* **70/71**, 191-195 (1994).

23. Dharmasena, G. & Frech, R. *Solid State Ionics* **53-56**, 1274-1277 (1992).

24. Dharmasena, G. & Frech, R. *J. Chem. Phys.* **99**, 8929-8935 (1993).

25. Dharmasena, G., Schlindwein, W.S., Frech, R. & Linford, R.G. *J. Chem. Phys.* **101**, 9232-9235 (1994).

26. Dissanayake, M.A.K.L. *Solid State Ionics* **23**, 49-51 (1987).

27. Lissel, E., Jansen, M., Jansen, E. & Will, G. *Z. Krist.* **192**, 233-243 (1990).

28. Wiench, V.D.M. & Jansen, M. *Z. Anorg. Allg. Chem.* **461**, 101-108 (1980).

29. Kracek, F.C. & Ksanda, C.J. *J. Phys. Chem.* **34**, 1741 (1930).

30. Nord, A.G. *Acta Chemica Scandanavica* **27**, 814-822 (1973).

31. Mehrotra, B.N. *Z. Krist.* **155**, 159-163 (1981).

32. Naruse, H., Tanaka, K., Morikawa, H., Marumo, F. & Mehrotra, B.N. *Acta Crystallogr.* **B43**, 143-146 (1987).

33. Palazzi, M. & Rémy, F. *Bull. Soc. Chim. Fr.* **8**, 2795-2798 (1971).

34. Mair, A.D. *N. Z. J. Sci.* **19**, 61-67 (1976).

35. Kizilyalli, M. & Welch, A.J.E. *J. Inorg. Nucl. Chem.* **38**, 1237-1240 (1976).

36. Milne, S.J. & West, A.R. *J. Solid State Chem.* **57**, 166-177 (1985).

37. Doyen, L. & Frech, R. *J. Chem. Phys.* **104**, 7847-7853 (1996).

38. Choi, B.-K., Labbé, H.J. & Lockwood, D.J. *Solid State Commun.* **74**, 109-113 (1990).

CHAPTER 6

CATION STABILIZED SODIUM PHOSPHATE

INTRODUCTION

A variety of cations have been investigated to determine if they can stabilize the high-temperature cubic phase of Na_3PO_4 (γ-Na_3PO_4) and to determine how they affect the conductivities of the γ-Na_3PO_4 solid solutions. Divalent (Ba^{2+}, Ca^{2+}, Cd^{2+}, Mg^{2+}, Sr^{2+}, Zn^{2+}), trivalent (Al^{3+}), and tetravalent (Ce^{4+}, Hf^{4+}, Sn^{4+}, Th^{4+}, Ti^{4+}, Zr^{4+}) cations have all been studied as dopant ions in Na_3PO_4 with varying degrees of stabilization being achieved.

There is considerable variation in the effect of doping Na_3PO_4 with divalent cations. These systems are represented by the formula $Na_{3-2x}M_xPO_4$, where M is the dopant ion. The addition of Ba^{2+} ions did not stabilize γ-Na_3PO_4 to any extent.[1] Some degree of stabilization was attained with Ca^{2+} and Sr^{2+} as dopant ions,[1, 2] although the γ-phase could not be stabilized to room temperature. Instead, there is a transformation to an ordered tetragonal phase below ~250°C. It should be noted that this phase is different than the tetragonal α-Na_3PO_4. This phase change is reflected in the discontinuity in the conductivity plots as well as in the DTA data.[2] Cd^{2+} [1], Mg^{2+} [2] and Zn^{2+} [1-3] all stabilize γ-Na_3PO_4 to room temperature. Mg^{2+} and Zn^{2+} have solid solution limits of x=0.27 and 0.30, respectively.[2] In both systems the lattice parameter decreases to about 7.4 Å, the maximum conductivities occur in the range of

x=0.17 to 0.20, and the Arrhenius conductivity plots show similar sigmoidal behavior. Irvine and West attribute the behavior seen in the conductivity plots to a second order (order-disorder) transition that occurs between 100 and 250°C. They suggest that there is local tetragonal distortion/ordering of the γ-phase, while the overall symmetry remains cubic.

Trivalent Al^{3+} is probably the most thoroughly studied of the cation dopants [4-7] and is represented by the formula $Na_{3-3x}Al_xPO_4$. For x<0.05, a mixture of α- and γ-Na_3PO_4 is obtained. Between x=0.05 and 0.50, γ-Na_3PO_4 solid solution is obtained as the only phase. In concentrations where x>0.50, a glass forms upon cooling. Hooper et al. [4] primarily measured the conductivity of the solid solutions. Newsam et al.[5, 6] used powder neutron diffraction to determine the structure for the x=0.025 and 0.2 compositions. Analysis of the structure for the latter system was consistent with the structure of pure γ-Na_3PO_4. Dollase et al.[7] used NMR and XRD analyses to investigate compositions ranging from x=0 to 0.5. They report that the PO_4^{3-} ions undergo a reorientation as the amount of Al^{3+} is increased. In pure γ-Na_3PO_4 the PO_4^{3-} tetrahedra are more likely to have corners pointing in the (100) direction toward Na^+ ions in octahedral sites. As the Na^+ ions are replaced by Al^{3+} in the tetrahedral sites and vacancies in the octahedral sites, the PO_4^{3-} groups turn to point more in the (111) direction in order to form stronger bonds with the Al^{3+} ions.

The systems doped with tetravalent ions have the formula $Na_{3-4x}M_xPO_4$. Irvine and West[8] surveyed the influence of tetravalent cations on the formation and

conductivity of Na_3PO_4 solid solutions and found that the different cations substitute to a different extent in the sequence $Zr^{4+}>Hf^{4+}>Sn^{4+}=Th^{4+}>Ce^{4+}>Ti^{4+}$. They also found an apparent correlation between the solid solution limit and the rate of change in the host lattice parameter with x. The conductivity increases rapidly with x and reaches a maximum at or near the solid solution limit for all the tetravalent cations studied. Of these ions, Zr^{4+} has been the most thoroughly studied, and it also has the highest conductivity of any of the γ-Na_3PO_4 solid solutions. At 300°C and $x \cong 0.13$, the conductivity is $2.5 \times 10^{-2}\ \Omega^{-1}cm^{-1}$, which is three orders of magnitude greater than pure γ-Na_3PO_4 and less than one order of magnitude smaller than that of Nasicon or β-alumina at 300°C.[9, 10]

The study presented here focused on Mg^{2+}- and Zn^{2+}-doped Na_3PO_4. Both of these cations have been shown to stabilize the high-temperature γ-phase, and they both exhibit interesting behavior that can been attributed to the presence of local structural changes. Analysis of these systems using vibrational spectroscopy provides another approach in describing these structural changes.

RESULTS

The $Na_{3-2x}Mg_xPO_4$ System

Powder X-ray Diffraction

The d-spacings from the powder x-ray diffraction (XRD) patterns were compared to those for α-Na_3PO_4, γ-Na_3PO_4 and the Na_3PO_4-hydrates to determine the phase(s) present for the different compositions. The d-spacings for the different

compounds were presented in the previous chapter and are listed in Table 5.2. The XRD patterns for some $Na_{3-2x}Mg_xPO_4$ compositions are shown in Figure 6.1. The d-spacings for several samples are also tabulated in Table 6.1. At a dopant level of x=0.04 the structure is primarily α-Na_3PO_4 with some γ- and w-phase present. The most intense peak in the XRD pattern occurs at 4.29 Å. All three phases have strong peaks close to this value (relative intensities are given in parentheses): γ-Na_3PO_4 at 4.28 Å (50); α-Na_3PO_4 at 4.24 Å (75); w-phase at 4.31 Å (100). Therefore the fact that the most intense peak occurs at 4.29 Å does not necessarily mean that the w-phase is present in the largest amount. It is more likely that the intensity is due to an additive effect from the three phases. The best indication of this is that other strong peaks occurring at 4.48 Å and 2.80 Å with relative intensities of 75% and 95% in the pure w-phase, occur in the x=0.04 sample with relative intensities of 7 and 24%. The second most intense peak in the pattern occurs at 2.56 Å with a relative intensity of 69% followed by a peak at 2.63 Å with a relative intensity of 54%. These data indicate that the dominate phase present is α-Na_3PO_4, particularly when combined with the presence of relatively strong peaks at 2.70 (34%), 3.83 (12%), 2.07 (14%) and 1.91 Å (20%). It is harder to determine the relative amounts of the w-phase and γ-Na_3PO_4 present because their dominant peaks are coincident or near coincident with peaks in other phases.

With a dopant increase to x=0.06, there is a dramatic change in the XRD pattern (see Figure 6.1). There are significantly fewer peaks in the pattern, and the strong peaks correspond to those seen in pure γ-Na_3PO_4. The presence of the w-phase

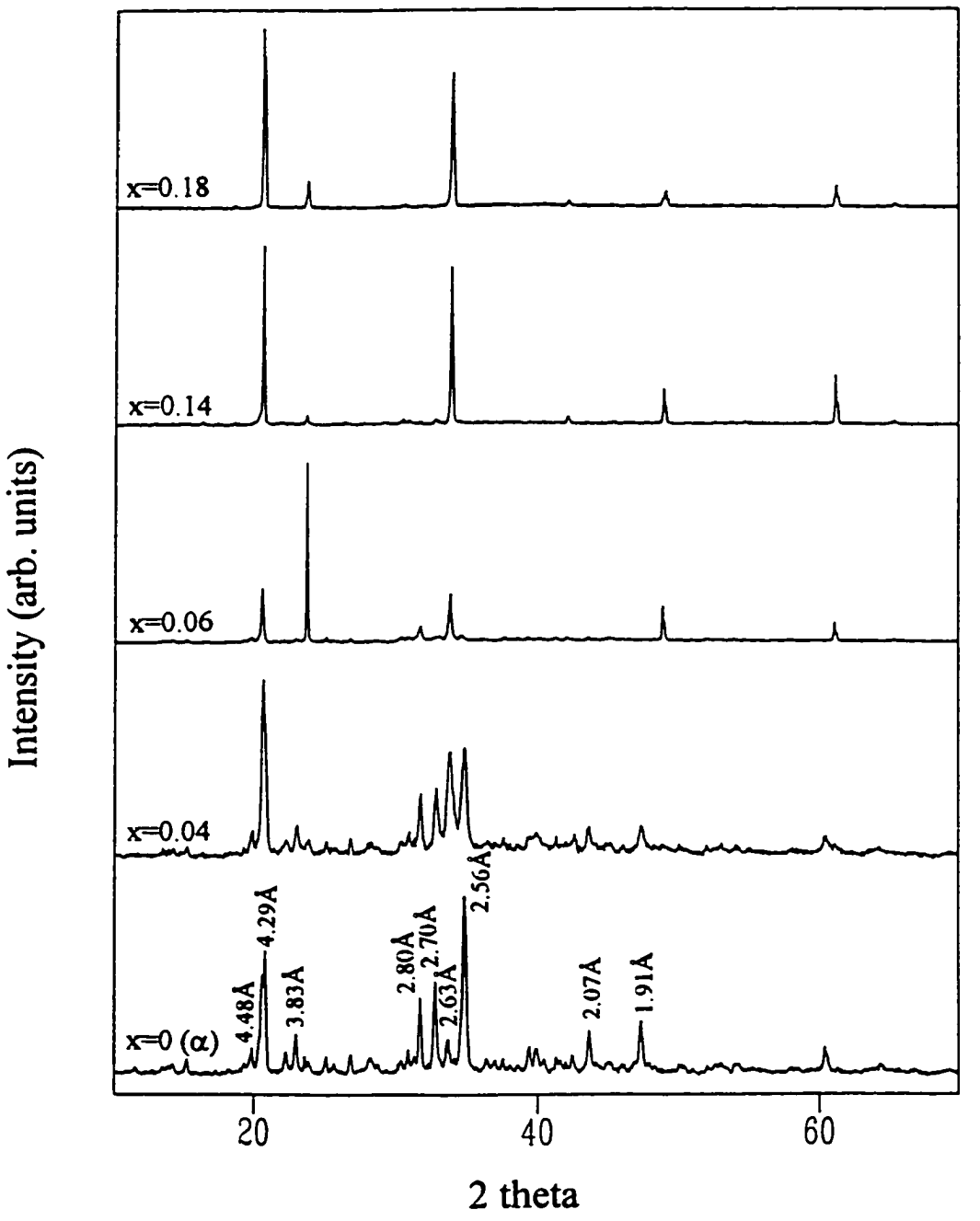

Figure 6.1. XRD patterns of $Na_{3-2x}Mg_xPO_4$ for increasing values of x.

Table 6.1 Powder x-ray diffraction data for $Na_{3-2x}Mg_xPO_4$. Data are reported as d-spacings in Å with relative intensities in parentheses.

x=0.04	x=0.06	x=0.08	x=0.10	x=0.14
5.85 (6)	4.48 (3)	4.84 (5)	4.46 (5)	4.30 (100)
4.46 (7)	4.31 (52)	4.48 (11)	4.30 (68)	3.72 (8)
4.28 (100)	3.83 (5)	4.27 (72)	3.70 (31)	2.70 (6)
3.97 (8)	3.71 (100)	3.70 (16)	3.49 (5)	2.62 (94)
3.83 (12)	3.29 (5)	3.28 (5)	3.28 (5)	2.14 (8)
3.70 (8)	2.92 (6)	2.91 (10)	2.91 (7)	1.85 (24)
3.51 (5)	2.80 (17)	2.79 (20)	2.79 (13)	1.51 (33)
3.29 (5)	2.70 (6)	2.69 (14)	2.69 (9)	1.43 (5)
3.12 (8)	2.63 (44)	2.61 (100)	2.62 (100)	
2.91 (5)	2.57 (7)	2.56 (9)	2.57 (7)	
2.80 (24)	2.14 (8)	2.48 (9)	2.14 (6)	
2.70 (34)	1.86 (28)	2.38 (7)	1.85 (19)	
2.63 (54)	1.51 (19)	2.18 (5)	1.51 (36)	
2.56 (69)		2.14 (8)	1.43 (5)	
2.39 (5)		2.01 (6)		
2.29 (5)		1.85 (11)		
2.12 (8)		1.51 (11)		
2.07 (14)				
2.01 (9)				
1.91 (20)				
1.81 (6)				
1.72 (6)				
1.53 (13)				
1.51 (7)				
1.45 (11)				

is indicated by the small peaks at 4.48 Å and 2.80 Å. The reason for the inversion of intensity for the bands at 2.63 Å and 3.71 Å is not clear but could be due to orientational effects resulting from sample preparation or it could be indicative of structural distortions in the sample.

The XRD pattern for the x=0.10 sample is clearly γ-Na_3PO_4 with some w-phase present. The peaks that stand out from the noise occur at 4.46 (5%), 4.30 (68%), 3.70 (31%), 2.79 (14%), 2.62 (100%), 1.85 (19%) and 1.51 Å (36%). With the exception of the peaks at 4.46 Å and 2.79 Å, which indicate the w-phase, these peaks are characteristic of γ-Na_3PO_4.

The patterns for the x=0.14 and x=0.18 samples are consistent with γ-Na_3PO_4 and do not indicate the presence of the w-phase. The patterns for these two samples have very little noise so that even the weaker peaks in the pattern at 2.14 Å (8%) and 1.43 (5%) stand out clearly from the baseline. There are, however, deviations from the literature values for pure γ-Na_3PO_4 in the relative intensities of some bands. In both samples, the peak at 4.30 Å is more intense than is typical and the peak at 3.72 Å is less intense in the x=0.14 sample. However, this increased intensity of the peak at 4.30Å is seen in a majority of the XRD patterns measured for this study. This phenomenon could be attributed to the overlapping of peaks from different phases, but that would not be an adequate explanation in this case. It is more likely due to structural distortions or sample orientation effects.

Differential Scanning Calorimetry

The DSC data (shown in Figure 6.2) are more difficult to analyze than the XRD patterns because of the presence of broad transitions that cannot be assigned to any known phase transition. The presence of some of the hydrates can be identified in several traces by the irreversible transitions around 100°C, although they cannot be specifically be identified in the XRD patterns due to overlap with the w-phase. The x=0.04 sample has two broad transitions at 208 and 274°C on the heating cycle after the initial loss of water and a single broad transition at 266°C on the cooling cycle. The reversible transition is due to the α- to γ-Na_3PO_4 phase transition although the temperature at which it occurs has been depressed by more than 50°C. This depression of the transition temperature clearly indicates that that significant disorder has been introduced into the tetragonal lattice structure.

There is no reversible transition in the thermogram for the x=0.06 sample, however there is a very small transition at 220°C and a much broader transition at 273°C. The fact that there are broad transitions that begin at roughly the same temperature in the heating cycles of the x=0.04 and 0.06 compositions is striking in light of the absence of a transition on the cooling cycle of the x=0.06 sample. It seems reasonable to assume that there are structural similarities between the two samples, although one seems to be a disordered tetragonal phase and the other an ordered cubic phase. The shapes of the transitions, which are almost mirror images,

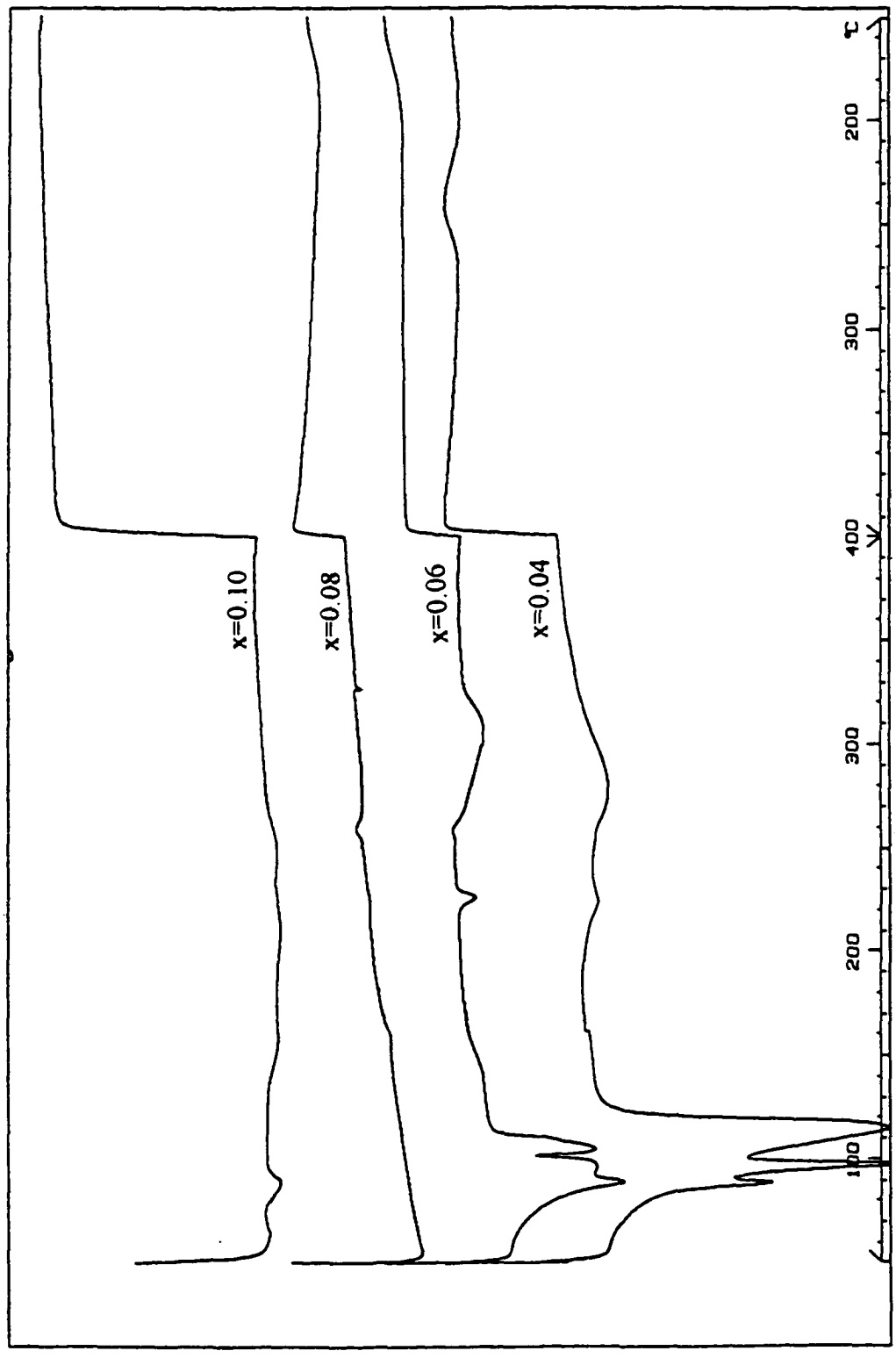

Figure 6.2. DSC thermograms of $Na_{3-2x}Mg_xPO_4$ for increasing values of x.

may reflect this difference in structure. The transition at 220°C is due to the presence of the w-phase. This was made clear when the DSC thermogram of the x=0.08 sample was measured again after several months. The second time the sample was run it had an almost identical transition at 220°C while there was no indication of the presence of other hydrate phases. This result is also consistent with previous experiments that indicate that the w-phase forms after the samples have been exposed to air for several months, however there is no trace of the other hydrates. The x=0.08 sample also has a very small transition that begins at about 273°C, indicating that while its structure is essentially identical to γ-Na_3PO_4 there are still regions of structural distortion.

The series of very weak, broad transitions occurring at 137, 186 and 232°C in the x=0.10 sample is also suggestive of the presence of regions exhibiting varying degrees of ordering in the γ-phase. The x=0.18 sample does not show any significant transitions beyond the initial loss of water of hydration, but does have a hint of a transition at 133°C which may indicate the presence of very small regions of local structural distortion.

Raman Spectroscopy

Raman spectra were measured for the $Na_{3-2x}Mg_xPO_4$ system beginning with the x=0.01 sample and continuing in 0.01 increments to x=0.10. The concentration of dopant ion was then increased to a level of x=0.20, although the increment size was 0.02 from x=0.10 to 0.20. The temperature-dependent Raman spectra for pure

Na_3PO_4 (shown in Figures 4.3, 4.4 and 4.5) show a gradual breakdown of the band structure with increasing temperature. Since the α- to γ-phase transition is an order-disorder transition, there was a question of whether increasing the dopant concentration would have the same effect on the structure, and therefore the Raman spectra, as increasing the temperature. However, this is not what I observed. Instead of a gradual transition from one phase to the other, the doped systems exhibit an abrupt transition from the α-phase to the γ-phase

The ν_2 spectral region (shown in Figure 6.3) shows very little change as x increases from 0.01 to 0.05. For x=0.06 the mode changes from a band at 435 cm^{-1} with a shoulder at 425 cm^{-1} to a single band at 432 cm^{-1}. This band structure corresponds to that seen for γ-Na_3PO_4. There are essentially no changes in band shape in this region for the x=0.06 to x=0.20 samples.

The ν_4 spectral region is also shown in Figure 6.3. An interesting behavior is observed in this region with the addition of small amounts of dopant. Pure α-Na_3PO_4 has two bands at 572 and 586 cm^{-1}. This region in the x=0.01 to 0.05 samples consists of three distinct bands at 572, 584 and 590 cm^{-1}. The bands then collapse into a single band at 577 cm^{-1} in the x=0.06 sample. This band shape and position are consistent with γ-Na_3PO_4. There is very little change in the band structure with increasing x from a dopant level of x=0.06 to x=0.15. However, a broad shoulder appears in the spectra at 620 cm^{-1} in the x=0.15 to 0.20 samples.

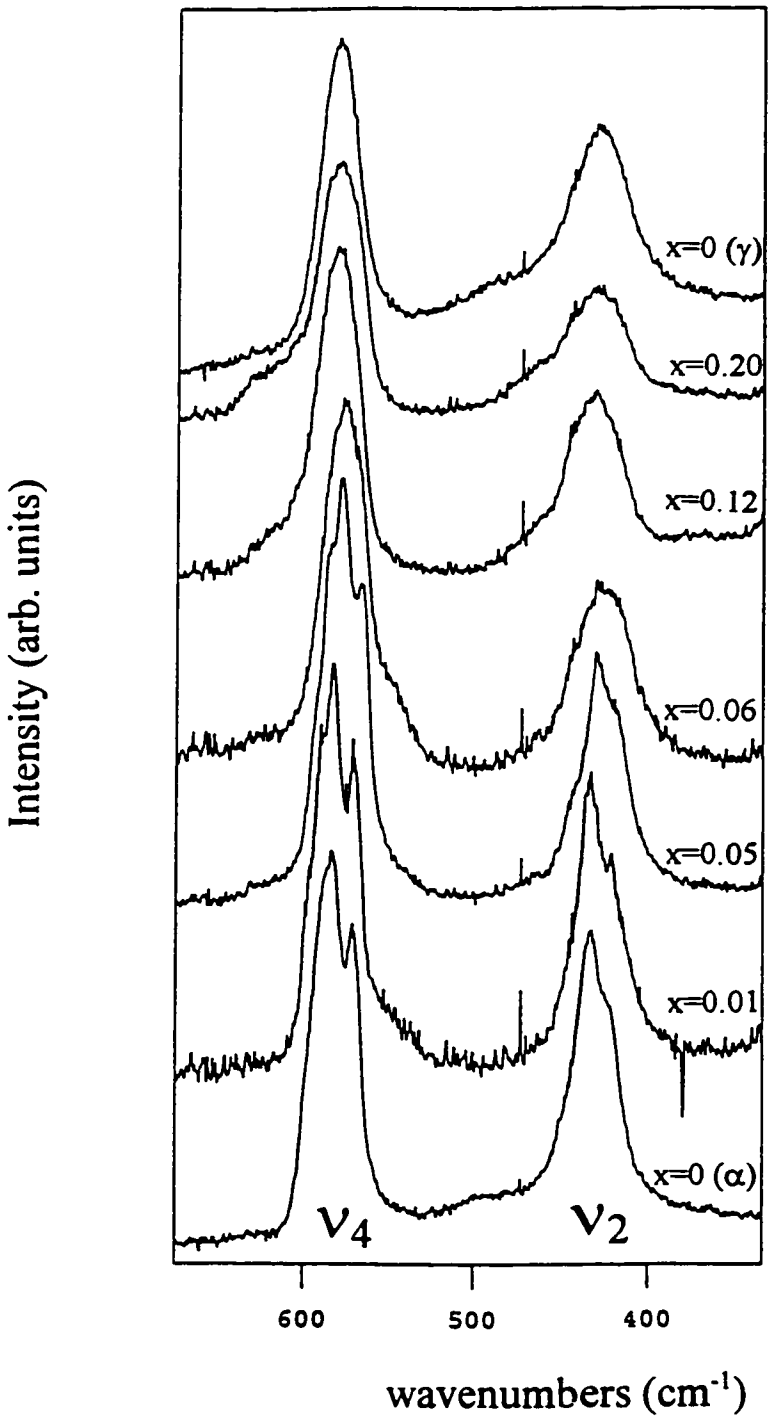

Figure 6.3. Raman spectra of $Na_{3-2x}Mg_xPO_4$ in the ν_2 and ν_4 spectral regions for increasing values of x.

The changes in the ν_1 spectral region with increasing x, seen in Figure 6.4, are very interesting particularly when compared to the pure compound. In the pure compound, essentially the only change in the ν_1 band with increasing temperature is some broadening of the bandwidth. In this case, the peak not only broadens, but it also shifts to higher wavenumbers and becomes asymmetric. The lowest doping concentrations (x=0.01 to 0.04) do not show any significant change in band shape or width, but at x=0.05, the band shifts from 939 cm^{-1} to 936 cm^{-1}. As x increases after this point, the band shifts to higher wavenumbers. The band also abruptly broadens from a bandwidth of 7 cm^{-1} to a bandwidth of 20 cm^{-1} when x is increased from 0.05 to 0.06. The asymmetry of the band toward higher frequencies also begins to be seen in the x=0.05 composition and increases with increasing x.

The ν_3 spectral region is shown in Figures 6.5 and 6.6. Initially this region follows a pattern of behavior similar to that seen in the ν_4 region. The band structure seems to be more well defined for the x=0.01 to x=0.05 samples than it does in pure α-Na_3PO_4, although there is also some degree of broadening in these samples. The spectrum abruptly changes when a dopant level of x=0.06 is reached. The band structure transforms from a complex multiplet structure to a broad band centered at 1032 cm^{-1} with a steeper shoulder at 1012 cm^{-1}. There is also a sharp band at 1068 cm^{-1} that is probably related to the presence of the w-phase. The band shape has smoothed out in the x=0.07 sample and more closely resembles that of γ-Na_3PO_4. The x=0.08 spectrum has a single broad band centered at 1034 cm^{-1}. This sample was prepared under an argon atmosphere and was initially free of any hydrates or w-phase.

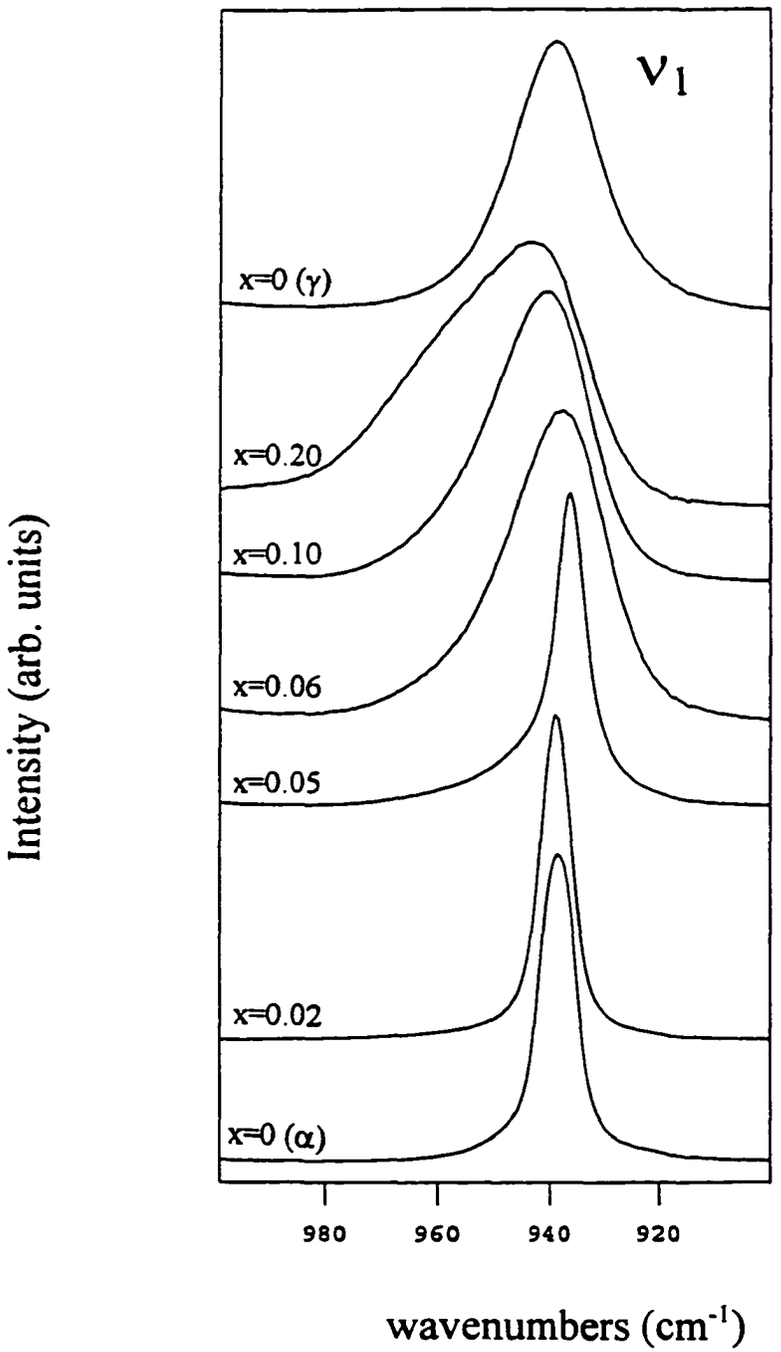

Figure 6.4. Raman spectra of $Na_{3-2x}Mg_xPO_4$ in the ν_1 spectral region for increasing values of x.

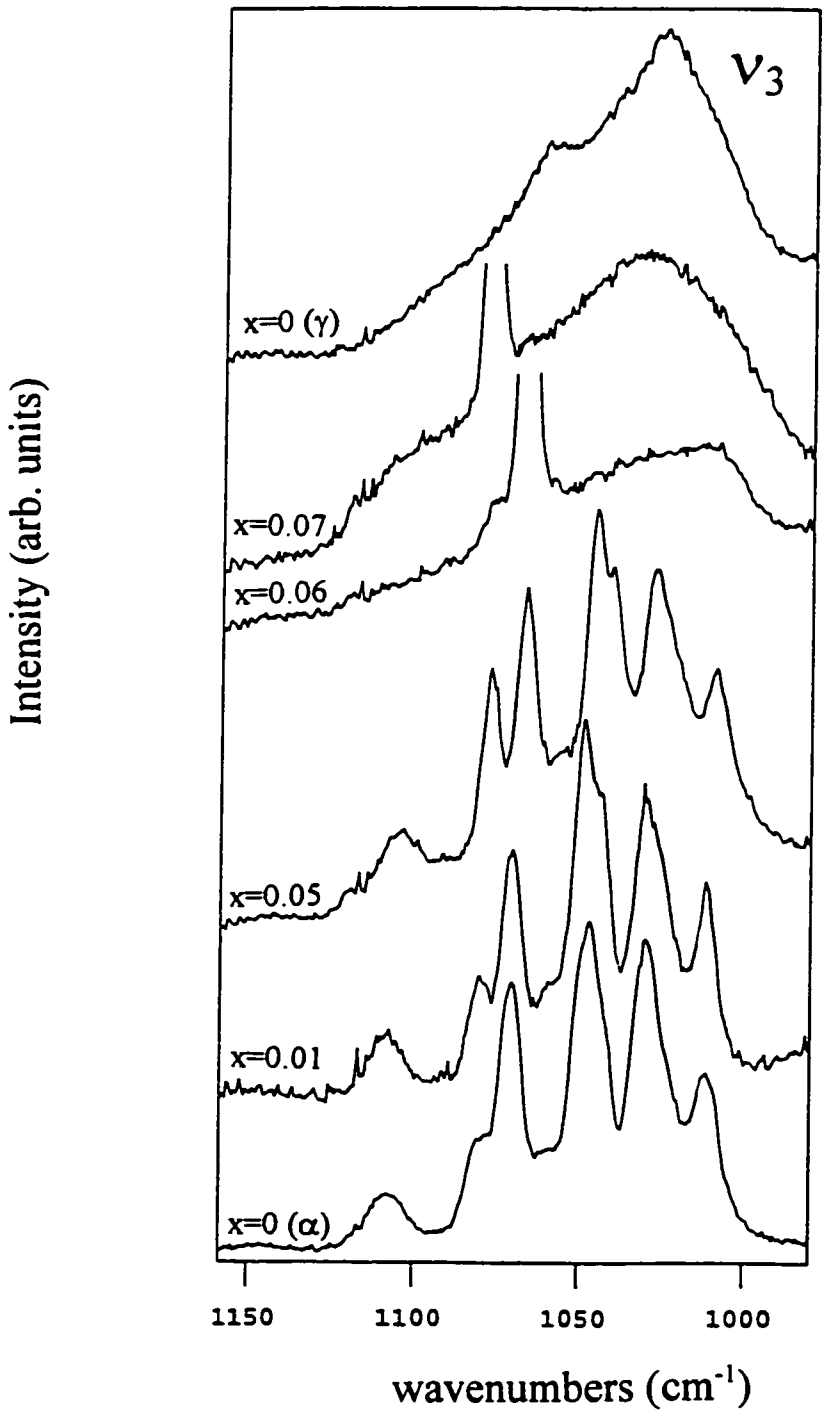

Figure 6.5. Raman spectra of $Na_{3-2x}Mg_xPO_4$ in the ν_3 spectral region for increasing values of x.

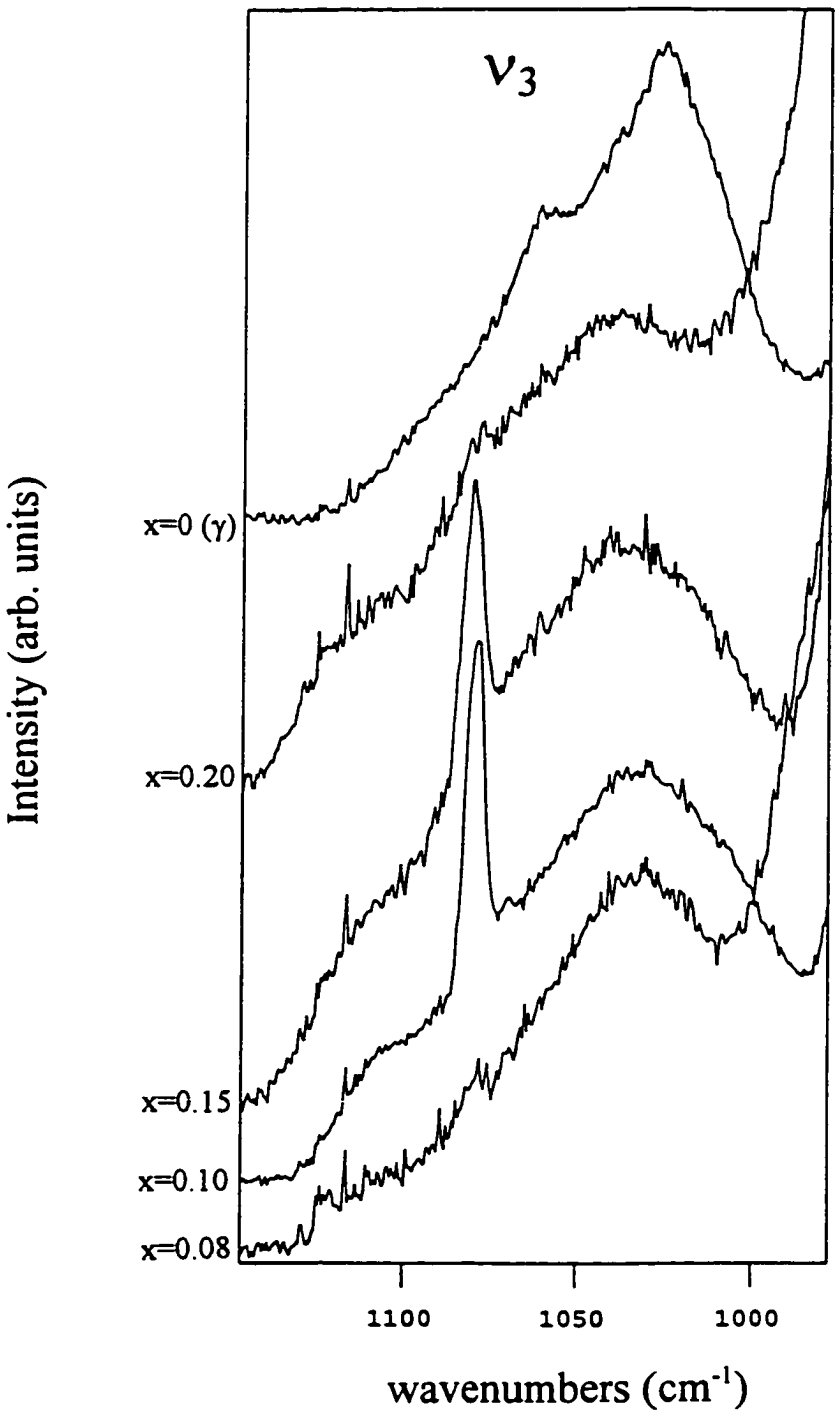

Figure 6.6. Raman spectra of $Na_{3-2x}Mg_xPO_4$ in the ν_3 spectral region for increasing values of x.

The spectra for x=0.10 to 0.20 samples also look like γ-Na_3PO_4 with a broad band centered at 1034 cm^{-1} although they have an additional sharp band at 1080 cm^{-1}.

The presence of the w-phase in these solid solutions raises the question of its effects on the Raman spectra. This question became particularly important when sharp, relatively intense bands at 1080 cm^{-1} superimposed on the broader ν_3 band structure were observed in many of the compositions. In order to address the question, several samples were prepared under Ar to prevent the formation of hydrate phases and analyzed very soon thereafter. Three spectra from the same x=0.08 sample are shown in Figure 6.7. The sample was prepared under Ar and the first spectrum was measured immediately after sample preparation. The second spectrum was taken two and a half months later, and the appearance of a sharp, relatively intense band can be seen at 1080 cm^{-1}. The third spectrum, taken a month after the second, does not show any significant change from the previous spectrum. These results are consistent with DSC analysis as well, which shows no trace of the hydrate phase immediately after sample preparation but has a transition at 250°C after a couple of months. The other effect seen in this sequence of spectra is the improvement in differentiation between the ν_1 and ν_3 bands. This could be due to structural distortions caused by the w-phase, but are more likely due to the structure reaching an equilibrium state with less dynamical disorder present.

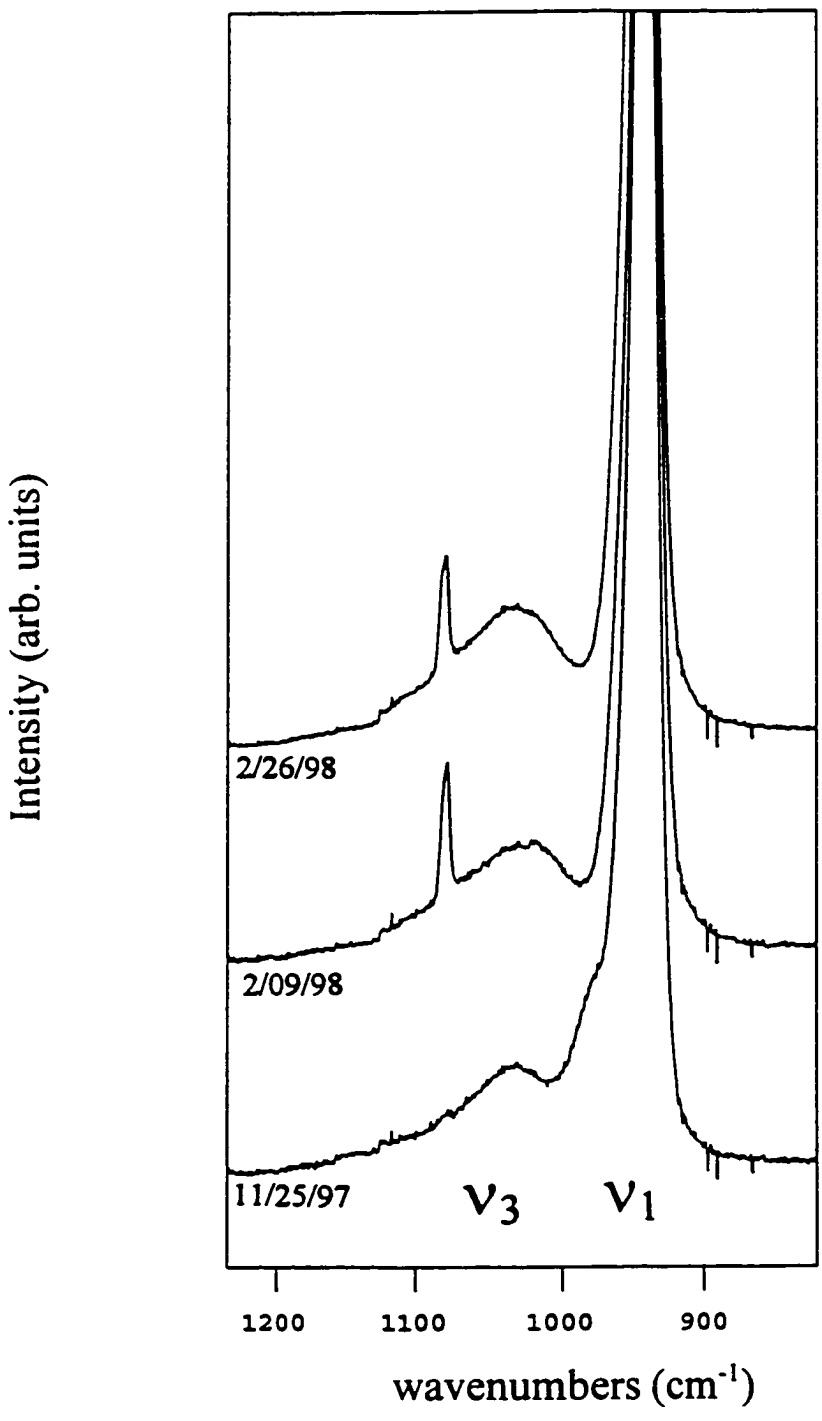

Figure 6.7. Raman spectra of $Na_{2.84}Mg_{0.08}PO_4$ in the ν_1 and ν_3 spectral regions.

The $Na_{3-2x}Zn_xPO_4$ System

Powder X-ray Diffraction

Some representative XRD patterns are shown in Figure 6.8 and the d-spacings for several samples are presented in Table 6.2. The x=0.02 sample is mostly α-Na_3PO_4, but there is a significant amount of w-phase present and possibly some γ-Na_3PO_4. The presence of the w-phase is to be expected since the samples had been prepared for some time before the XRD experiments were performed. The x=0.04 sample is still primarily α-Na_3PO_4 although there is more γ-Na_3PO_4 present compared to the x=0.02 sample. As has been mentioned previously, it is hard to determine relative amounts of the phases present in a quantitative manner by simply analyzing the relative intensities of the peaks but some general qualitative evaluations can be made. The relative intensities of the w-phase marker peaks are inconsistent in going from the x=0.02 to the x=0.04 sample. The peak at 4.46 Å has an intensity of 9% for x=0.02 and 14% for x=0.04 while the peak at 2.80 Å has an intensity of 35% in both samples. The fact that the peak at 2.63Å has significantly increased in relative intensity (from 43% for x=0.02 to 100% for x=0.04) indicates the increased presence of γ-Na_3PO_4. This is supported by the appearance of peaks at 3.71 (11%), 1.86 (13%) and 1.53Å (16%). The x=0.06 sample is almost entirely γ-Na_3PO_4 with some w-phase present (noted by the peaks at 4.44 (7%) and 2.79Å (15%). The x=0.08, 0.09 and 0.10 samples also have γ-Na_3PO_4 as the dominant phase with some w-phase present.

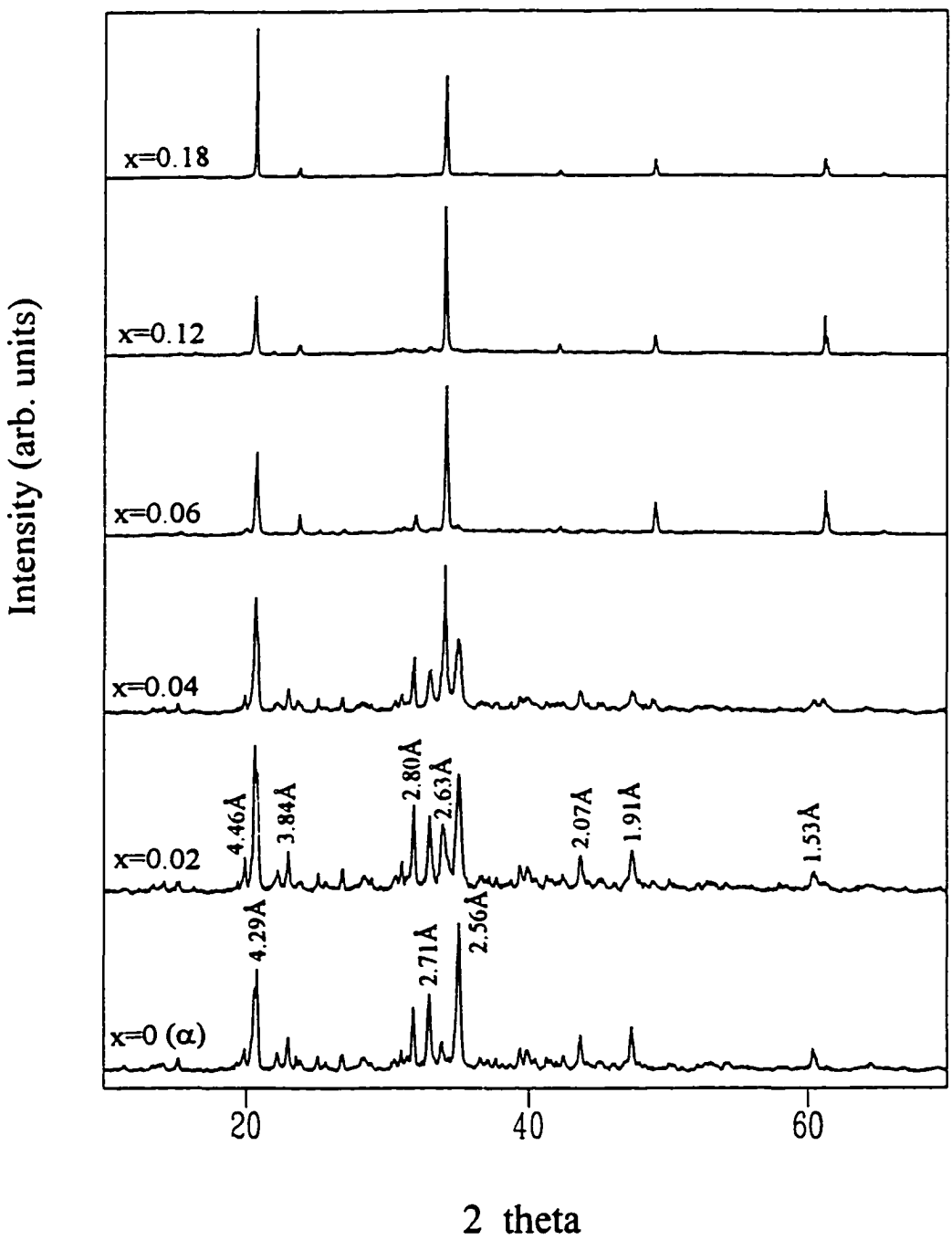

Figure 6.8. XRD patterns of $Na_{3-2x}Zn_xPO_4$ for increasing values of x.

Table 6.2 Powder X-ray diffraction data for $Na_{3-2x}Zn_xPO_4$. Data are reported as d-spacings in Å with relative intensities in parentheses.

x=0.02	x=0.04	x=0.06	x=0.09	x=0.12	x=0.20
6.27 (5)	5.84 (7)	4.44 (7)	5.44 (6)	4.47 (3)	5.44 (5)
5.84 (7)	4.46 (12)	4.28 (73)	4.46 (7)	4.30 (52)	4.30 (69)
4.46 (9)	4.29 (100)	3.71 (13)	4.29 (85)	3.71 (9)	3.73 (13)
4.29 (100)	3.96 (8)	3.28 (5)	4.01 (5)	2.71 (7)	3.33 (6)
3.97 (13)	3.83 (12)	2.79 (15)	3.71 (11)	2.62 (100)	2.90 (5)
3.84 (15)	3.71 (9)	2.62 (100)	2.79 (19)	2.14 (6)	2.70 (7)
3.70 (6)	3.50 (6)	2.57 (6)	2.70 (15)	1.85 (16)	2.63 (100)
3.51 (6)	3.29 (8)	2.14 (7)	2.62 (100)	1.51 (24)	2.14 (3)
3.29 (8)	3.14 (10)	1.85 (25)	2.56 (18)	1.43 (4)	1.86 (44)
3.12 (12)	2.91 (5)	1.51 (35)	2.14 (5)		1.51 (24)
2.91 (7)	2.80 (29)	1.43 (6)	2.07 (6)		1.43 (4)
2.80 (36)	2.70 (34)		1.91 (6)		
2.71 (35)	2.63 (83)		1.85 (23)		
2.63 (43)	2.56 (83)		1.51 (27)		
2.56 (90)	2.45 (7)		1.43 (8)		
2.45 (7)	2.39 (5)				
2.28 (10)	2.28 (7)				
2.26 (6)	2.13 (5)				
2.17 (8)	2.07 (19)				
2.13 (10)	2.00 (7)				
2.07 (24)	1.91 (26)				
2.00 (9)	1.86 (11)				
1.91 (36)	1.81 (6)				
1.86 (5)	1.75 (5)				
1.81 (6)	1.73 (7)				
1.53 (16)	1.53 (13)				
1.51 (9)	1.52 (16)				
1.45 (7)	1.45 (6)				

The samples in the range x=0.12 to 0.20 appear to be entirely γ-Na_3PO_4 with very little or no w-phase present.

Differential Scanning Calorimetry

DSC thermograms for a range of x values are shown in Figure 6.9. The x=0.04 sample has a reversible transition at 290°C on the heating cycle and 268°C on the cooling cycle. This indicates the presence of α-Na_3PO_4, although the transition temperature has been decreased. There is also an irreversible transition at 203°C. The x=0.06 sample has two irreversible transitions at 220 and 250°C. The transition at 220°C is most likely due to the presence of the w-phase, while the transition at 250°C is suggestive of structural distortion present in the γ-Na_3PO_4 structure. The x=0.10 and higher samples have no reversible transitions, but most have at least one irreversible transition. The x=0.10 sample has a very weak, very broad transition at 133°C and a sharper transition at 242°C. The x=0.14 sample has two very weak, broad transitions at 137 and 232°C. The x=0.18 sample has a hint of a transition at 152°C. The x=0.20 sample has two weak transitions at 139 and 223°C. The x=0.16 and 0.20 samples were prepared under an argon atmosphere, and the DSC thermograms were measured within a day or two of sample preparation. These two samples show no transitions that would indicate the presence of hydrates. They do exhibit two very small irreversible transitions at 160 and 259°C.

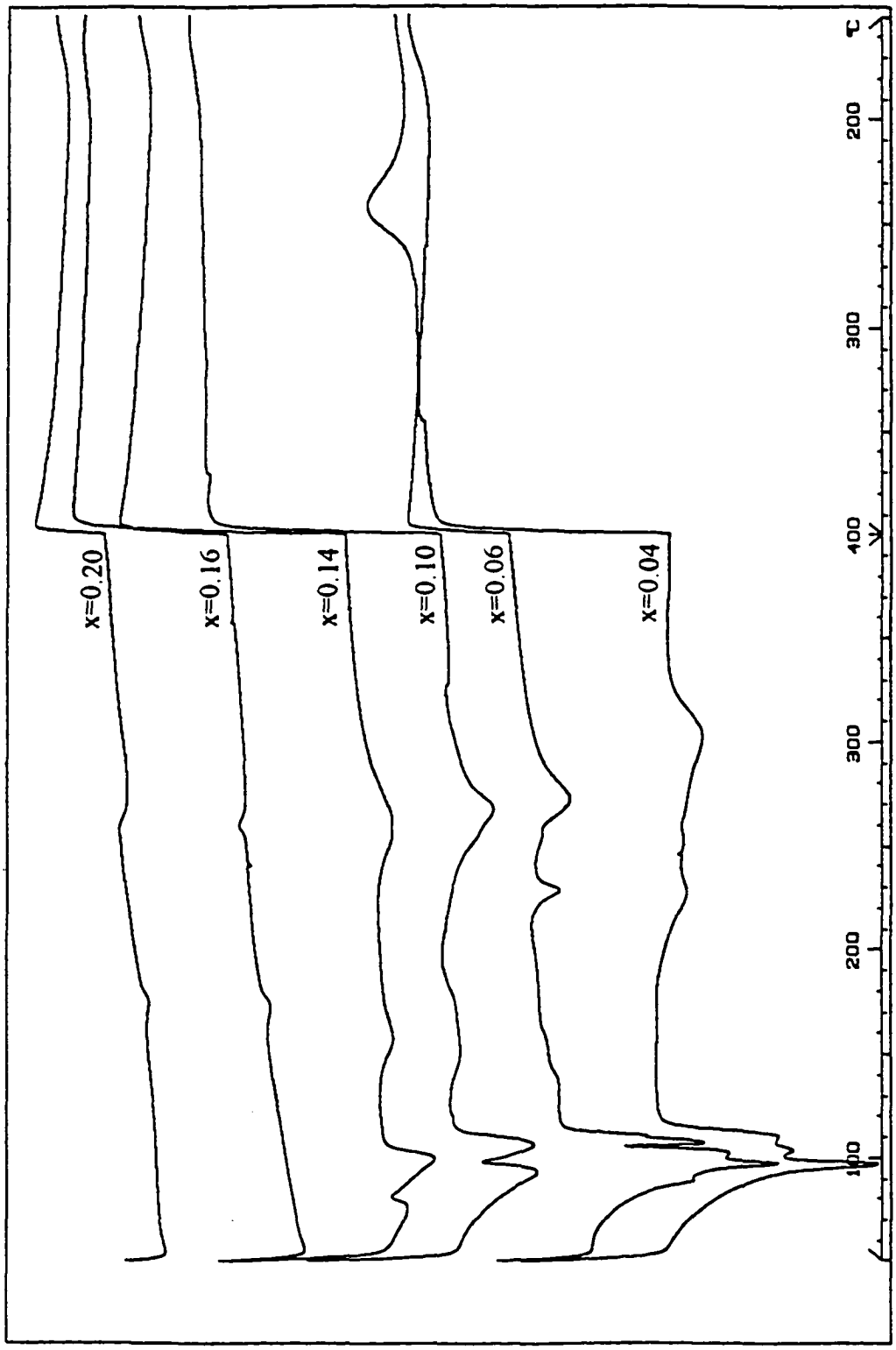

Figure 6.9. DSC thermograms of $Na_{3-2x}Zn_xPO_4$ for increasing values of x.

Raman Spectroscopy

The ν_1 spectral region (shown in Figure 6.10) does not exhibit the dramatic changes with increasing x that are seen in the other modes. The bandwidth broadens from 10 cm^{-1} to 20 cm^{-1} and develops some asymmetry toward higher frequencies. The x=0.02 sample has a band that is very similar to that of α-Na_3PO_4, although the peak has shifted from 939 cm^{-1} to 941 cm^{-1}. At a dopant concentration of x=0.04 the band is still very similar to that seen in lower concentrations, but it has begun to display the asymmetry toward higher frequencies. The band broadens significantly from 11 cm^{-1} to 20 cm^{-1} in the x=0.06 sample and the peak shifts to 943 cm^{-1}. The band shape remains essentially constant as x increases from 0.06 to 0.20, although the peak gradually shifts back to 939 cm^{-1}.

The ν_2 spectral region is shown in Figures 6.11 and 6.12. The spectrum for the x=0.02 sample looks very much like that of pure α-Na_3PO_4 with a peak at 435 cm^{-1} and a shoulder at 427 cm^{-1}. The band has broadened and the shoulder at 425 cm^{-1} looks more like a distinct second peak in the x=0.04 sample. The appearance of the band changes again in the x=0.06 sample to a single peak at 434 cm^{-1}. This peak position is consistent with γ-Na_3PO_4. The only changes seen in the spectra from x=0.06 to x=0.20 are a broadening of the band and the formation of a wing on the high frequency side of the peak. This wing has become a distinct band in the x=0.20 spectrum.

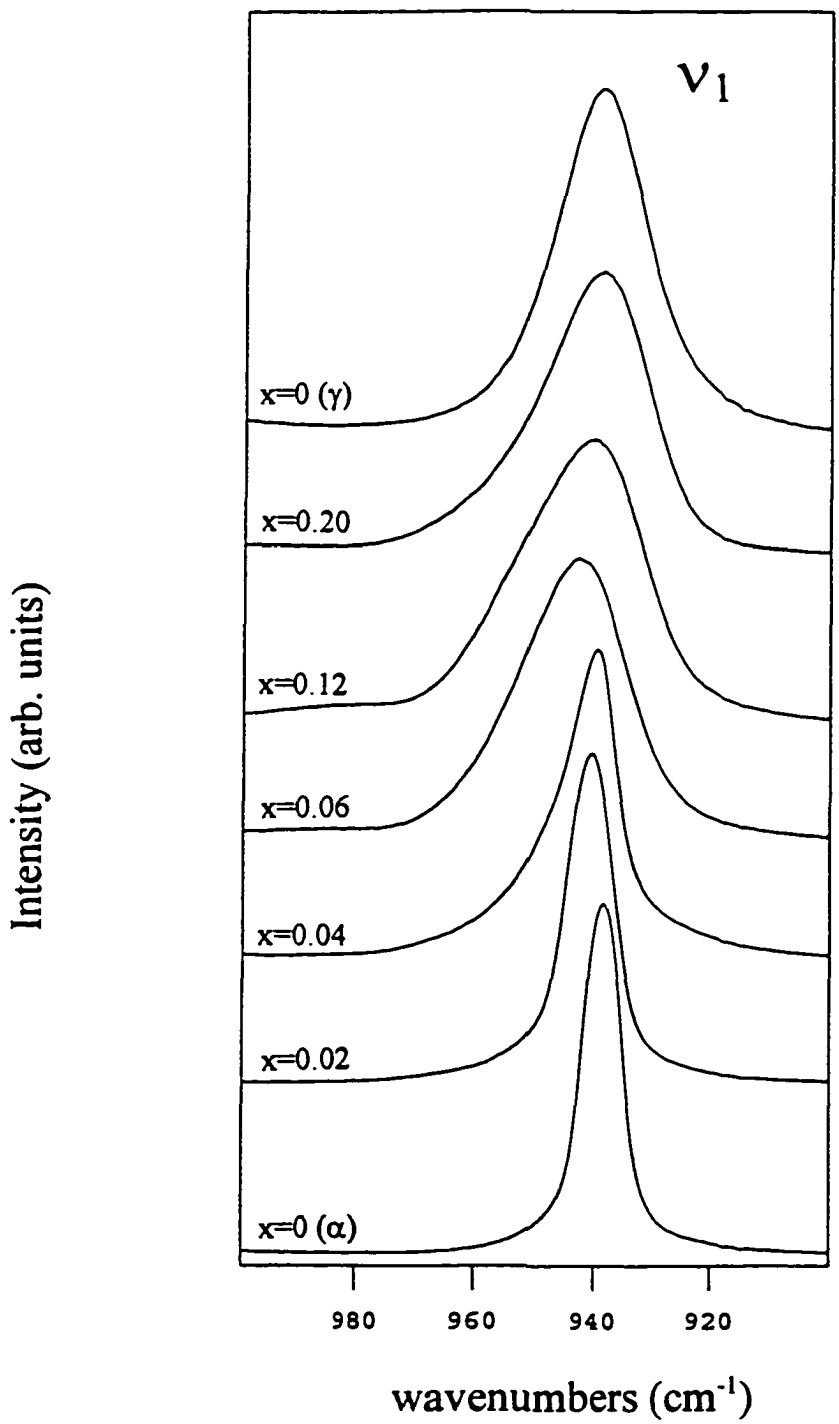

Figure 6.10. Raman spectra of $Na_{3-2x}Zn_xPO_4$ in the ν_1 spectral region for increasing values of x.

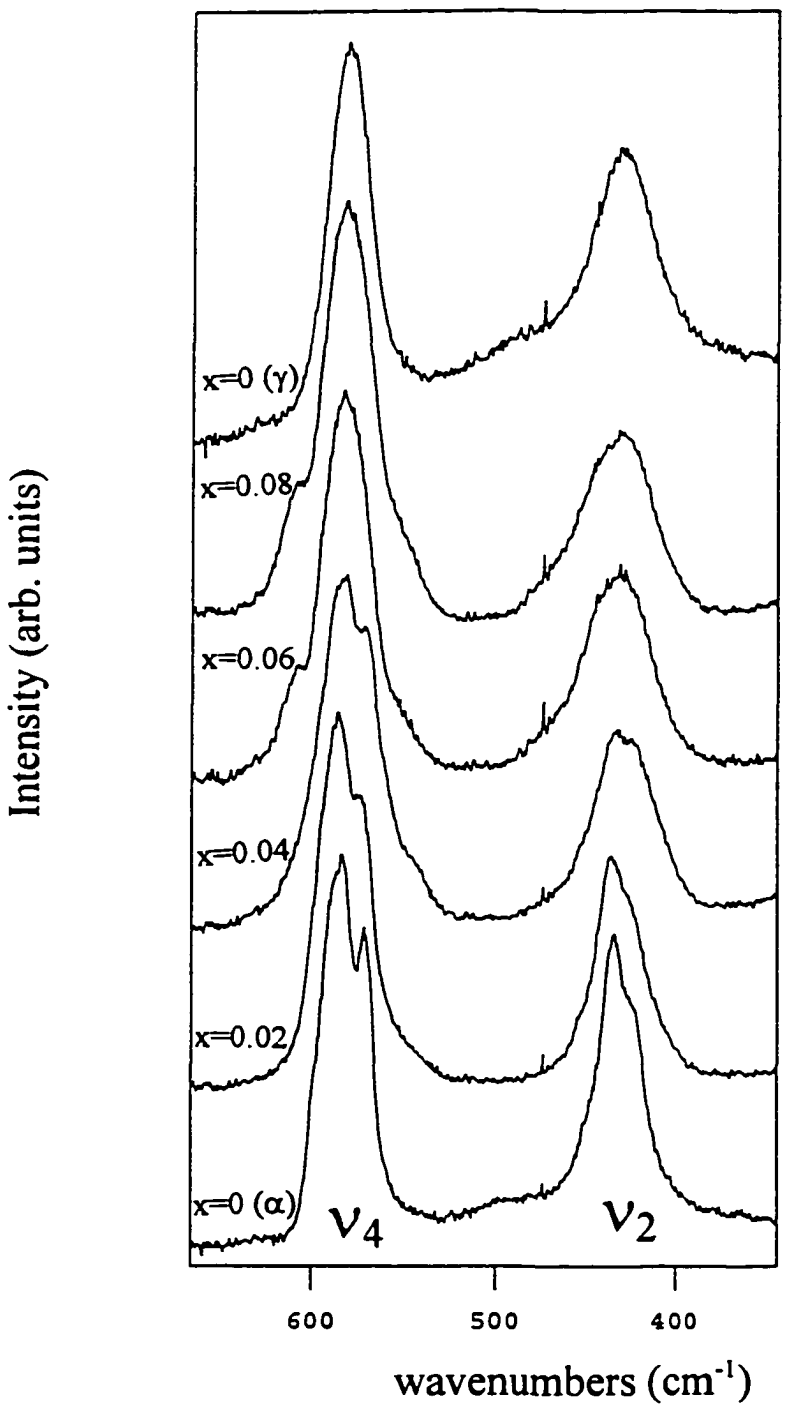

Figure 6.11. Raman spectra of $Na_{3-2x}Mg_xPO_4$ in the ν_2 and ν_4 spectral regions for increasing values of x.

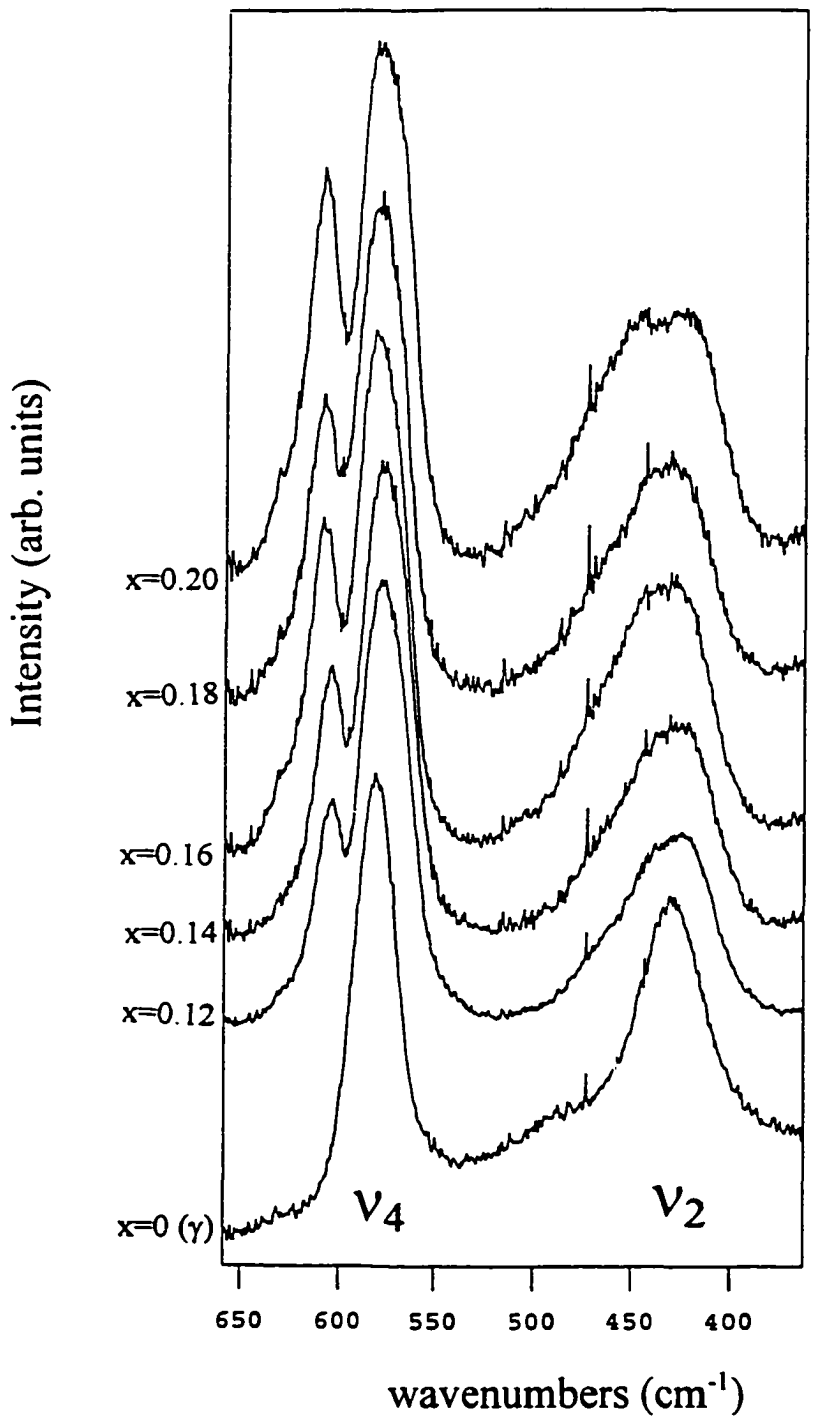

Figure 6.12. Raman spectra of $Na_{3-2x}Zn_xPO_4$ in the ν_2 and ν_4 spectral regions for increasing values of x.

An interesting phenomenon is observed in the ν_4 spectral region (also shown in Figures 6.11 and 6.12). The spectra for the x=0.02 and 0.04 samples are very similar to that of α-Na_3PO_4 with peaks at 575 and 586 cm^{-1}. At a concentration of x=0.06, the doublet becomes a single band at 584 cm^{-1} and a shoulder appears at 610 cm^{-1}. The peak shifts to 581 cm^{-1} and the shoulder increases in relative intensity and becomes more clearly defined with increasing x. This shoulder appears as a distinct band for $x \geq 0.12$ samples.

The ν_3 region (shown in Figures 6.13 and 6.14) also displays interesting behavior. The x=0.02 sample is very like α-Na_3PO_4 with peaks at 1015, 1032, 1050, 1074, 1081 and 1110 cm^{-1}. The multiplet structure has begun to broaden and the band at 1110 cm^{-1} has significantly decreased in intensity in the x=0.04 sample. The spectrum for the x=0.06 sample no longer shows a multiplet structure but has a sharp, relatively intense band at 1082 cm^{-1} and a very broad band centered at 1032 cm^{-1}. The x=0.08 sample has the same broad band at 1032 cm^{-1}, but the band at 1082 cm^{-1} is much weaker and there is a sharp band at 1070 cm^{-1}. The rest of the samples have a broad band that shifts from 1034 to 1050 cm^{-1} with increasing dopant concentrations, and most of the samples also have a band at 1081 cm^{-1} that varies in intensity. The x=0.16 and 0.20 samples that were characterized soon after sample preparation have very weak shoulders at 1081 cm^{-1}, which again indicates that this band is connected to the w-phase.

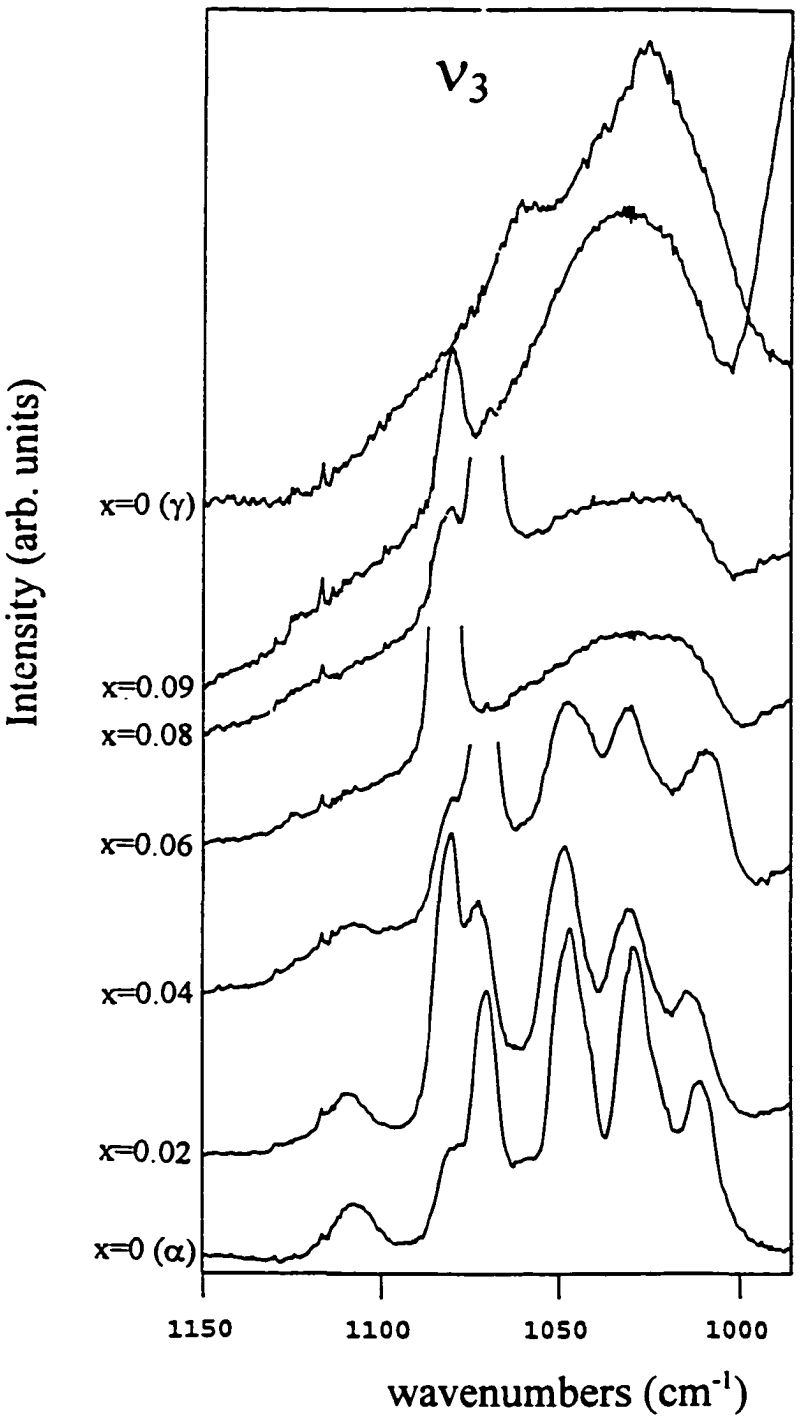

Figure 6.13. Raman spectra of $Na_{3-2x}Zn_xPO_4$ in the ν_3 spectral region for increasing values of x.

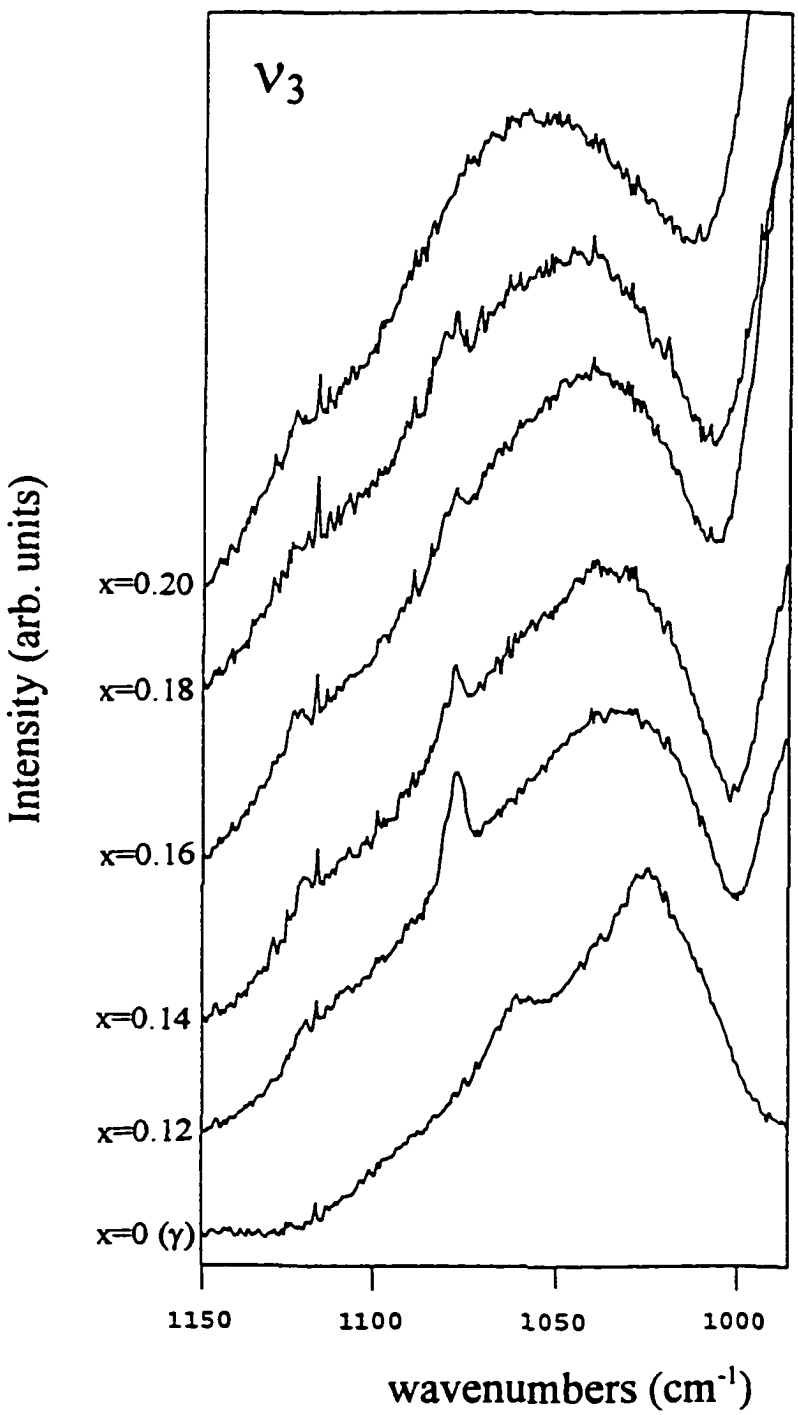

Figure 6.14. Raman spectra of $Na_{3-2x}Zn_xPO_4$ in the ν_3 spectral region for increasing values of x.

DISCUSSION

Although there are some significant differences in the $Na_{3-2x}Mg_xPO_4$ and $Na_{3-2x}Zn_xPO_4$ systems when comparing the effect of increasing dopant concentration on the Raman spectra, the results of the XRD and DSC analyses are very similar. The XRD patterns indicate that both systems are composed of a mixture of phases with α-Na_3PO_4 the dominant phase at x=0.04 followed by an abrupt change to γ-Na_3PO_4 at x=0.06. The w-phase is also seen in most of these samples. The XRD results also show very little if any hydrate phase(s) present for concentrations of $x \geq 0.12$. This is an interesting result considering that there are transitions in the DSC thermograms below 100°C that indicate the presence of some hydrate(s) in the samples. This would imply that the hydrates are present in very small amounts in those samples but still show up in the DSC traces because the loss of water is such an energetic transition. It is not clear why the hydrate phases are not seen as strongly in the samples with higher dopant concentrations. It may be a coincidence due to environmental conditions, or there may be something about the structure in those samples that does not accommodate water as well. The DSC thermograms for both systems also show a series of broad, weak transitions occurring at temperatures between 130° and 260°C for samples with $x \geq 0.06$. These results are consistent with those reported by Irvine and West[2] in which they attribute the transitions to the creation of partial disorder and regions of local tetragonal ordering in the γ-phase.

The analysis of the Raman spectra of the $Na_{3-2x}Mg_xPO_4$ and $Na_{3-2x}Zn_xPO_4$ systems indicates that the Zn^{2+} ions interact more strongly with the PO_4^{3-} ions than the Mg^{2+} ions do. The best evidence for this is seen in the appearance of a new peak at 610 cm^{-1} in the ν_4 spectral region of the Zn^{2+}-doped samples. This interpretation is further supported by the change in band shape observed in the ν_2 region and the shift of the ν_3 band. However, this difference in interaction does not seem to affect the overall symmetry of the structures (indicated by the XRD patterns) or the formation of local structural distortions (indicated by the DSC thermograms). Further support for this difference in interaction is seen in the low frequency Raman spectra. The $Na_{3-2x}Mg_xPO_4$ system (spectra shown in Figure 6.15) does not have any low frequency peaks although there is perhaps the beginning of peak in the x=0.20 sample. In comparison, the $Na_{3-2x}Zn_xPO_4$ system has a low frequency peak that is clearly seen in the x=0.06 composition and continues to increase in intensity with increasing x (see Figures 6.16).

One thing that must be taken into consideration when working with the cation doped systems is the problem with sample preparation and impurities. Samples in which the composition or structure was discordant with the other samples in the sequence occurred in both the $Na_{3-2x}Mg_xPO_4$ and $Na_{3-2x}Zn_xPO_4$ systems. New samples were prepared at these compositions with results consistent with the trends observed in the other compositions. These discrepancies in structure are not seen in the XRD patterns but can be seen in the DSC thermograms and Raman spectra. Dollase et al. reported similar problems with their sample preparations.[7] This problem was

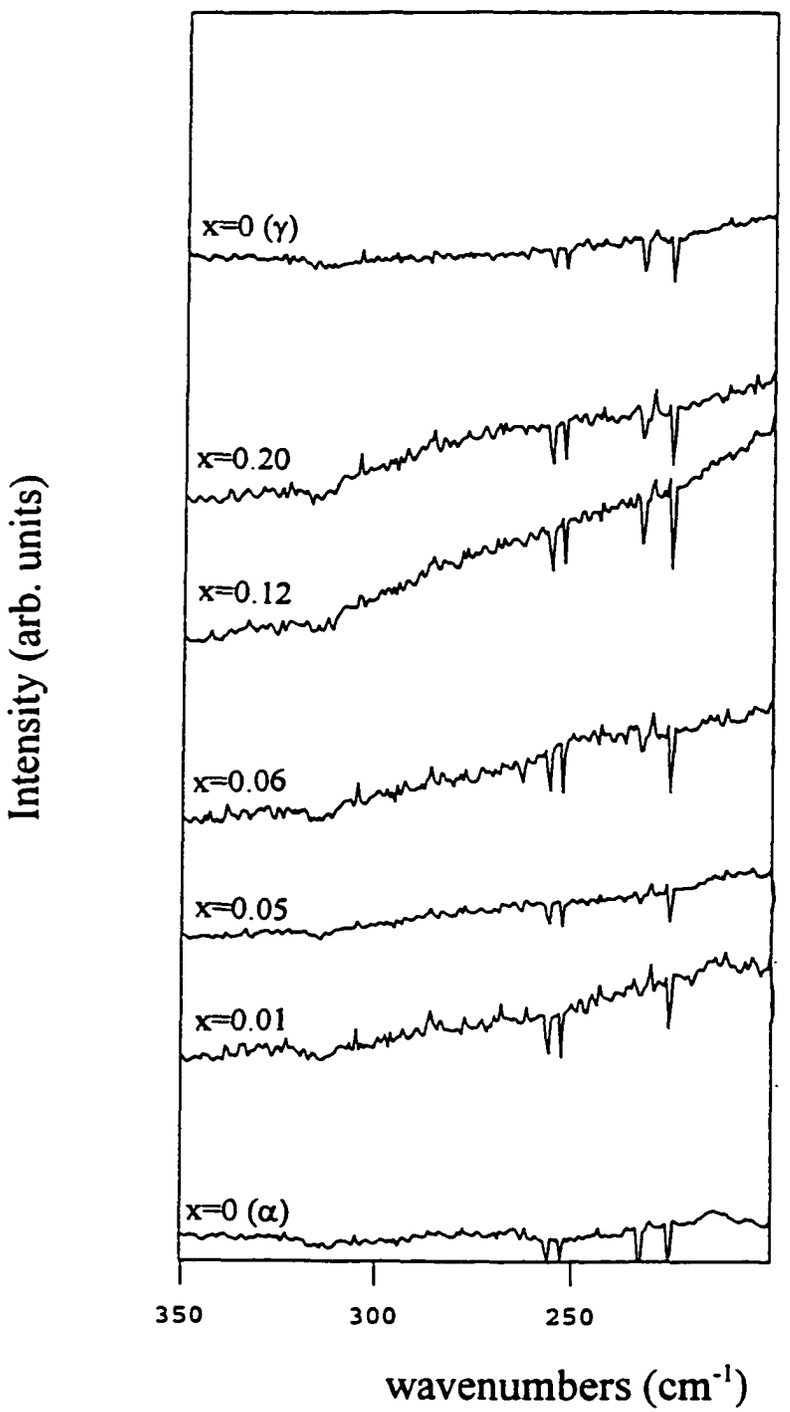

Figure 6.15. Raman spectra of $Na_{3-2x}Mg_xPO_4$ in the low frequency region for increasing values of x.

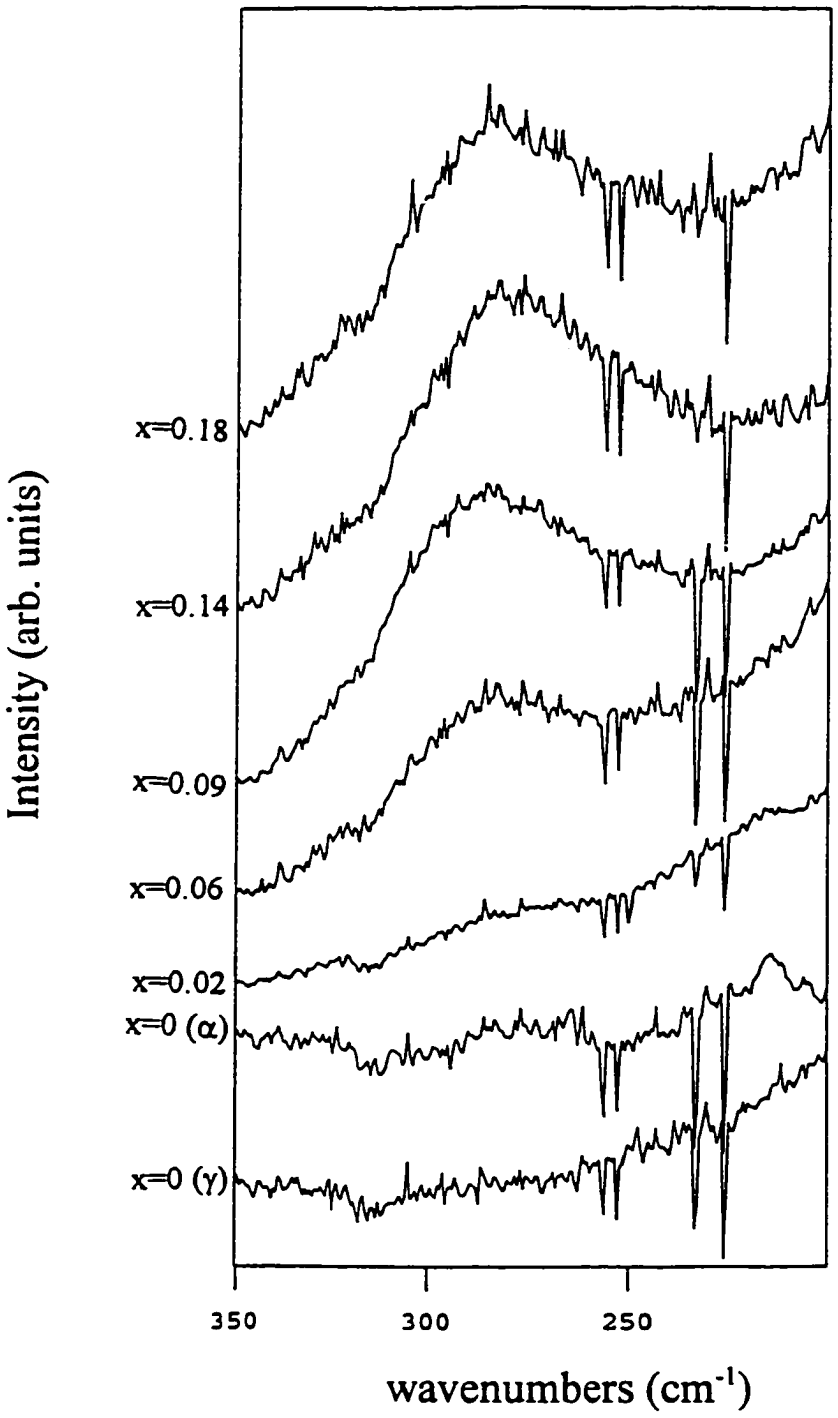

Figure 6.16. Raman spectra of $Na_{3-2x}Zn_xPO_4$ in the low frequency spectral region for increasing values of x.

observed for x=0.04 and 0.08 in the $Na_{3-2x}Mg_xPO_4$ system. One sample for each of these compositions show striking differences in the ν_3 spectral region when compared to other spectra. The discrepant spectra for both compositions are very similar and have two strong peaks at 1080 and 1062 cm^{-1} and a broad shoulder at 1023 cm^{-1}. The x=0.04 sample was prepared twice more with both of the resulting spectra resembling the α-Na_3PO_4 spectrum. When a subsequent x=0.08 sample was analyzed, the resulting spectrum was very similar to that of γ-Na_3PO_4 with a broad band centered at 1034 cm^{-1}. The DSC thermogram of the first x=0.08 sample also had two broad irreversible transitions at 173 and 252°C. The discordant samples in the $Na_{3-2x}Zn_xPO_4$ system occurred at x=0.16 and 0.20. These two samples were prepared at the same time, which supports the theory that the discrepancies are due to sample preparation. These samples did not have the peak at 581 cm^{-1} in the ν_4 region seen in all of the other spectra in this system. New samples prepared at these concentrations do have peaks at 581 cm^{-1}.

CONCLUSION

The results of this study have confirmed the stabilization of γ-Na_3PO_4 by the addition of Zn^{2+} or Mg^{2+} ions. Analysis of these systems using vibrational spectroscopy has also provided another description of the local structural distortions present in the cubic structure. The ν_1 mode displays a distinctive asymmetry in both the Mg^{2+} and Zn^{2+} doped systems and the broadening of the band in the Mg^{2+} doped systems exhibits a 50% increase over that seen in pure γ-Na_3PO_4. The ν_3 spectral

region displays similar behavior for the two systems with an intermediate structure seen in the compositions that first appear as the γ-phase in the XRD patterns. These results would support the conclusion that there are local structural distortions while the overall structure remains cubic.

REFERENCES

1. Kolsi, A.-W. *Rev. Chim. Miner.* **13**, 416-421 (1976).
2. Irvine, J.T.S. & West, A.R. *Solid State Ionics* **37**, 73-78 (1989).
3. Kolsi, A.-W., Erb, A. & Freundlich, W. *Comptes Rendus Acad Sc Paris, Serie C* **282**, 575-577 (1976).
4. Hooper, A., McGeehin, P., Harrison, K.T. & Tofield, B.C. *J. Solid State Chem.* **24**, 265-275 (1978).
5. Newsam, J.M., Cheetham, A.K. & Tofield, B.C. in *Fast Ion Transport in Solids* (eds. Vashishta, Mundy & Shenoy) 435-437 (Elsevier North Holland, Inc., 1979).
6. Newsam, J.M., Cheetham, A.K. & Tofield, B.C. *Solid State Ionics* **1**, 395-410 (1980).
7. Dollase, W.A., Merwin, L.H. & Sebald, A. *J. Solid State Chem.* **83**, 140-149 (1989).
8. Irvine, J.T.S. & West, A.R. *J. Solid State Chem.* **74**, 385-392 (1988).
9. Milne, S.J. & West, A.R. *Mat. Res. Bull.* **19**, 705-710 (1984).
10. Milne, S.J. & West, A.R. *J. Solid State Chem.* **57**, 166-177 (1985).

CHAPTER 7

CATION/ANION STABILIZED SODIUM PHOSPHATE

INTRODUCTION

Na_3PO_4 doped with $ZnSO_4$ has not been studied before. The effect of a combination of cation and anion dopants on phase stabilization has not been studied for any crystal system. The reasons behind this are likely due to the complexity of analyzing the doubly doped systems and problems with phase separation. There have been some reports of solid solubility studies of metal oxides in Si_3N_4.[1,2] The resulting compounds are called Sialons and occur as mixed phases composed of the pure Si_3N_4 and new phase similar to Si_3N_4. The goal of the Sialon studies was to replace N^{3-} with O^{2-} in order to improve the properties of the original ceramic. Cation dopants were included in order to achieve charge compensation.

In the current study of phase stabilization in Na_3PO_4, I was interested in the effect of combining both Zn^{2+} and SO_4^{2-} as dopants on the stabilization of γ-Na_3PO_4. Each ion stabilizes the γ-phase individually, but there is a great degree of difference in the extent of solid solution formation. The local structure observed in the Raman spectra is also different in the cation and anion systems, and the effect of a combination of dopants on the local structure was of interest. This system can be represented by the formula $Na_{3-3x}Zn_xS_xP_{1-x}O_4$.

RESULTS

The $ZnSO_4$ doped systems were examined over a range of compositions varying from x=0.005 to 0.40. The limit of solid solution is at approximately x=0.30. The x=0.40 sample phase separated into several compounds including γ-Na_3PO_4, Na_2SO_4 phase III, and several unidentified components.

Differential Scanning Calorimetry

DSC thermograms for several values of x are shown in Figure 7.1. Almost all of the samples have an irreversible transition at approximately 80°C and a very small irreversible transition at approximately 250°C. These transitions are likely due to the presence of hydrate phases with the latter transition attributed to the w-phase. The presence of α-Na_3PO_4 can be seen by the reversible transitions in the x=0.005 and 0.01 samples, but there are no reversible transitions for higher values of x. These transitions occur in the heating cycle at 290°C for x=0.005 and at 284°C for x=0.01 and in the cooling cycle at 289°C and 268°C, respectively. Since the α- to γ-Na_3PO_4 phase transition takes place at 330°C in the pure compound, the depressed temperature of transition in the doped compounds indicates that disorder has been introduced into the α-Na_3PO_4 structure. The x=0.02 sample has two irreversible transitions at 195 and 230°C. It is not immediately clear what is causing these transitions. The latter transition is almost certainly related to the w-phase although the transition temperature is somewhat low, particularly when compared to the other

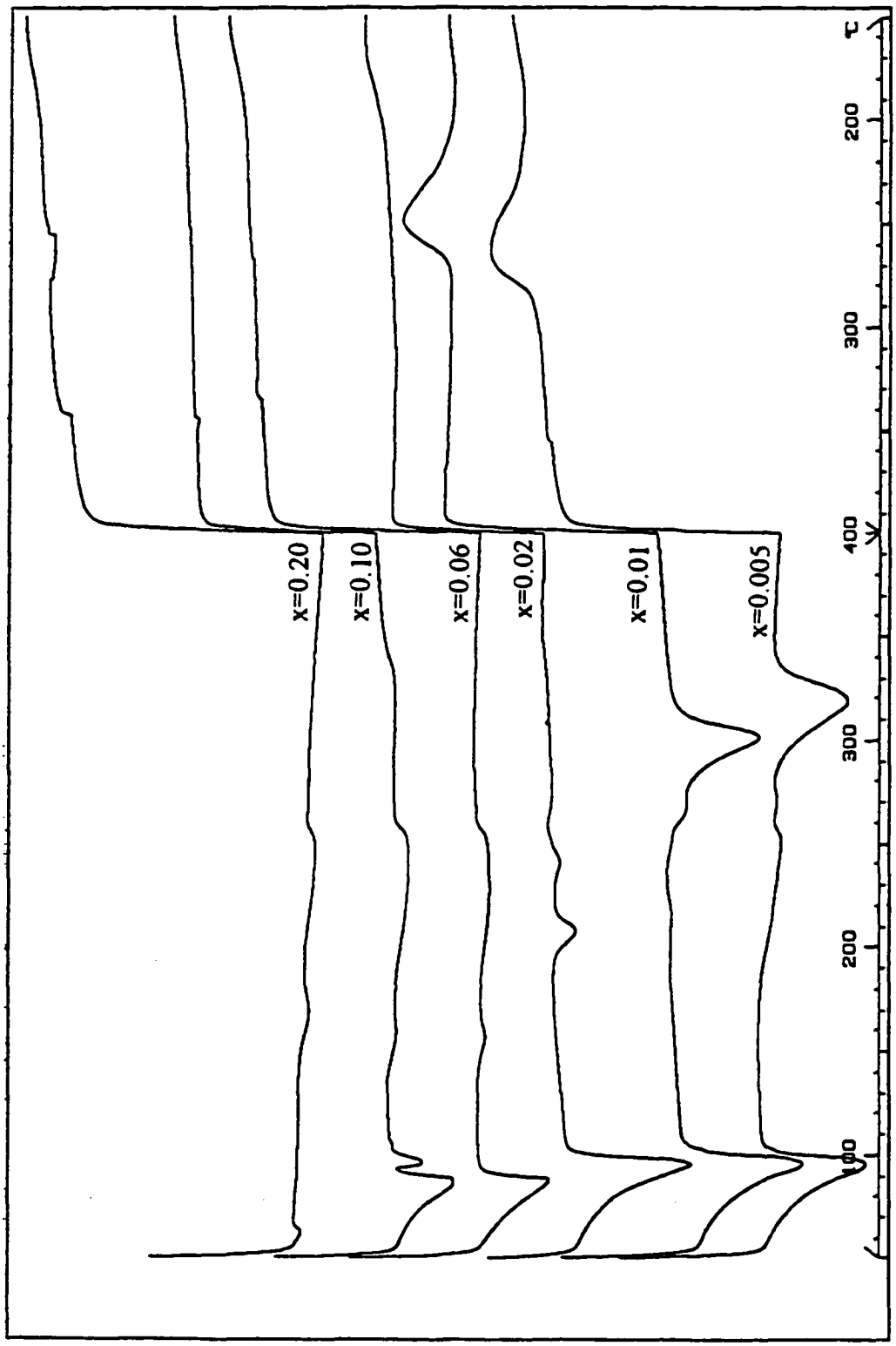

Figure 7.1. DSC thermograms of $Na_{3-3x}Zn_xS_xP_{1-x}O_4$ for increasing values of x.

samples. The transition at 195°C is likely due to structural distortions in the cubic structure of the γ-phase that are not present at higher concentrations of dopant. The samples for which x≥0.6 do not exhibit any significant transitions, although there is a very small transition at 140°C and the transition due to the w-phase at 250°C.

Powder X-ray Diffraction

The diffractograms for several values of x are shown in Figure 7.2 and summarized in Table 7.1. The pattern for the x=0.005 sample is clearly dominated by the presence of α-Na_3PO_4, although there is a significant amount of w-phase present as well. The anomalous intensity of the peak at 4.29 Å is seen in this pattern and in several other concentrations in this system. The pattern for the x=0.01 sample is very similar to that for the x=0.005 sample, but there are indications that some γ-Na_3PO_4 is also present in the x=0.01 sample. This can be seen by the increased intensities of the peaks at 3.72, 2.63 and 1.86 Å. The x=0.02 sample consists of phase-stabilized γ-Na_3PO_4 and some w-phase. The pattern is a close match to that of pure γ-Na_3PO_4 with a few additional peaks present that correspond to the strongest lines of the w-phase. There is very little difference between the x=0.02 and 0.04 patterns. The only difference is in the relative amount of w-phase present which is greater in the x=0.04 sample. The x=0.06 sample consists of γ-Na_3PO_4 with a trace of w-phase present. This diffractogram has well-defined peaks and very little noise. The relative intensities of the γ-Na_3PO_4 peaks are also very close to those published for the pure compound. The x=0.08 sample is γ-Na_3PO_4, but the peak at 4.31 Å has an unusually

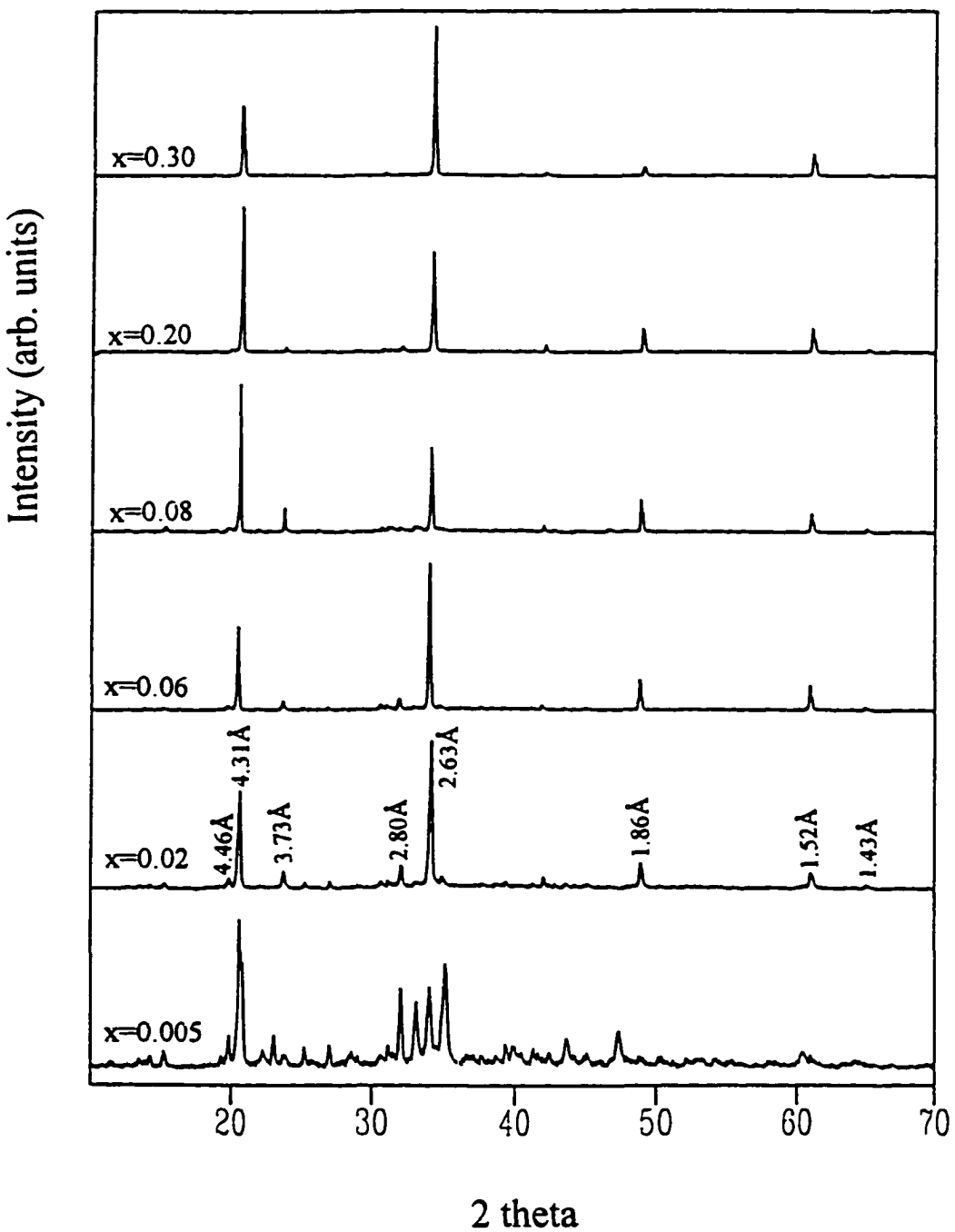

Figure 7.2. XRD patterns of $Na_{3-3x}Zn_xS_xP_{1-x}O_4$ for increasing values of x.

Table 7.1 Powder x-ray diffraction data for $Na_{3-3x}Zn_xS_xP_{1-x}O_4$. Data are reported as d-spacings in Å with relative intensities in parentheses.

x=0.005	x=0.02	x=0.06	(2/19/97) x=0.20	(5/27/97) x=0.20	x=0.30
6.27 (6)	4.46 (5)	4.49 (4)	4.29 (100)	4.30 (70)	4.29 (62)
5.84 (9)	4.31 (68)	4.34 (57	3.72 (7)	3.72 (4)	2.62 (100)
4.46 (8)	3.73 (15)	3.74 (9)	2.91 (6)	2.90 (3)	2.91 (2)
4.29 (100)	2.91 (5)	2.81 (8)	2.80 (8)	2.80 (3)	2.14 (4)
3.97 (9)	2.80 (14)	2.64 (100)	2.63 (80)	2.70 (5)	1.86 (8)
3.83 (10)	2.63 (100)	2.57 (5)	2.14 (8)	2.63 (100)	1.52 (22)
3.71 (7)	2.57 (9)	2.15 (4)	1.86 (23)	2.14 (7)	1.43 (2)
3.51 (6)	2.15 (7)	1.86 (21)	1.52 (20)	1.86 (22)	
3.29 (8)	2.00 (5)	1.52 (18)	1.43 (5)	1.52 (31)	
3.12 (5)	1.86 (22)	1.43 (4)		1.43 (4)	
2.92 (5)	1.52 (19				
2.79 (30)	1.43 (4)				
2.71 (34)					
2.64 (37)					
2.56 (85)					
2.29 (7)					
2.25 (18)					
2.18 (6)					
2.13 (6)					
2.07 (19)					
2.00 (7)					
1.91 (32)					
1.86 (5)					
1.81 (5)					
1.53 (13)					
1.52 (8)					

high intensity. The pattern for the x=0.10 sample looks very much like that for pure γ-Na_3PO_4. The x=0.20 sample is also clearly γ-Na_3PO_4 although the peak at 4.29 Å again has an increased relative intensity compared to the literature values. The presence of the w-phase is barely detectable in this sample with the only indication being a very weak peak at 2.80 Å. This is significant because several months passed between preparation of the sample and measurement of its XRD pattern. A second x=0.20 sample was prepared under argon and the pattern was measured within a week. There are very few differences between the two x=0.20 patterns. The pattern for the second sample is also γ-Na_3PO_4 but without the extra intensity in the peak at 4.30 Å. The pattern for the x=0.30 sample looks very much like that of pure γ-Na_3PO_4.

Raman Spectroscopy

The ν_2 spectral region is shown in Figures 7.3 and 7.4. The spectra for the x=0.005 sample is very similar to that of α-Na_3PO_4 although the same effect is seen here as was seen in the $Na_{3-2x}Mg_xPO_4$ systems in which $x \leq 0.05$. The ν_2 mode in α-Na_3PO_4 consists of a band at 424 cm^{-1} with a shoulder at 436 cm^{-1}. This mode in the x=0.005 sample is more clearly defined as two peaks at 424 and 436 cm^{-1}. The x=0.01 sample is more ambiguous because the sample is inhomogenous. Two different spectra were obtained from this sample in all spectral regions, depending on which area of the sample was analyzed. The majority of the areas analyzed resulted in a spectrum that is identical to that seen in the x=0.005 sample. A few areas gave

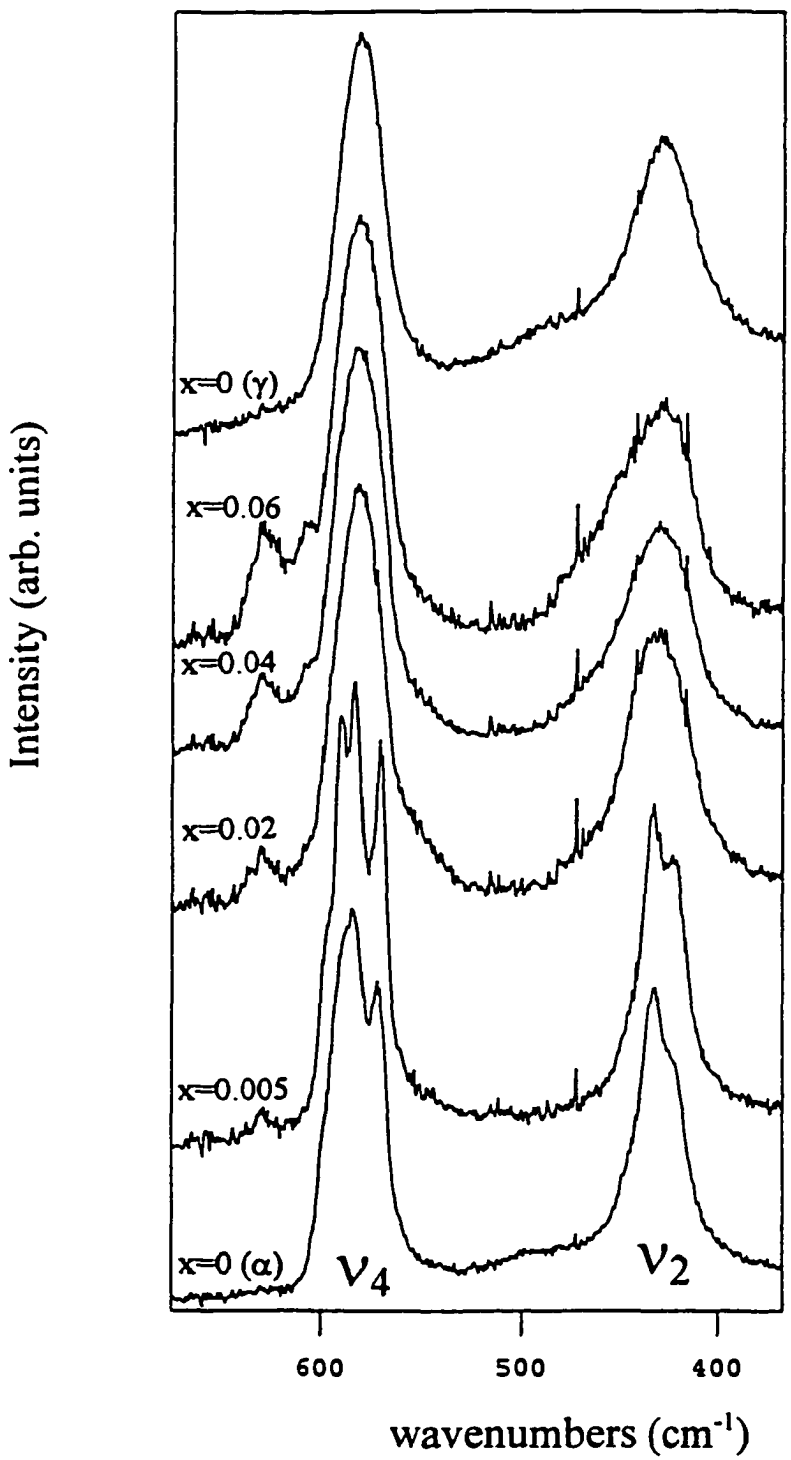

Figure 7.3. Raman spectra of $Na_{3-3x}Zn_xS_xP_{1-x}O_4$ in the ν_2 and ν_4 spectral regions for increasing values of x.

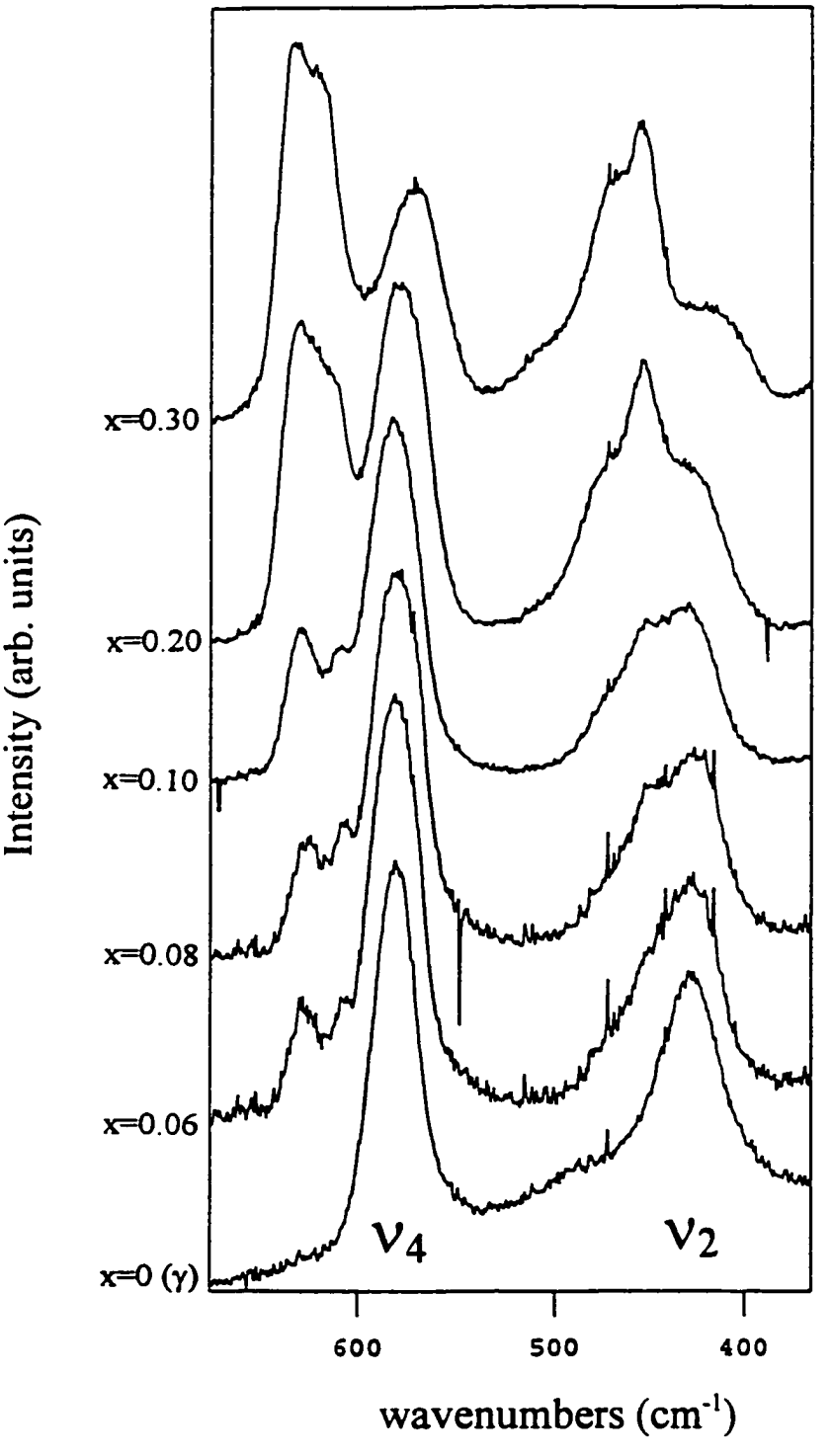

Figure 7.4. Raman spectra of $Na_{3-3x}Zn_xS_xP_{1-x}O_4$ in the ν_2 and ν_4 spectral regions for increasing values of x.

spectra that look much closer to those seen in the phase-stabilized solid solutions. The spectrum for the x=0.02 sample is the same as that of pure γ-Na_3PO_4 with a single band at 432 cm^{-1}. The spectrum does not change when x is increased to x=0.04. The peak begins to broaden and shift to lower wavenumbers for x=0.06. The band structure begins to separate into two peaks at 430 and 452 cm^{-1} in the x=0.08 sample and these peaks are clearer in the x=0.10 sample. When the concentration of $ZnSO_4$ is increased to x=0.20, the band has a dominant peak at 457 cm^{-1} with shoulders at 430 and 475 cm^{-1}. In the spectrum for the x=0.30 sample, there are peaks at 457 and 475 cm^{-1} with a broad band at 417 cm^{-1}. The band shape at higher concentrations is very similar to that observed in the SO_4^{2-}-doped system although the positions have shifted to slightly higher frequencies.

The ν_4 spectral region (seen in Figures 7.3 and 7.4) displays a series of changes with increasing x that resemble a combination of those seen in both the Zn^{2+}- and SO_4^{2-}-doped systems. The spectra for the x=0.005 and x=0.01 samples have more clearly defined band structure compared to pure α-Na_3PO_4 with peaks at 572, 585 and 591 cm^{-1}. A new band at 635 cm^{-1} also appears in the spectra. This band can be attributed to the vibrations of the SO_4^{2-} ion in the Na_3PO_4 lattice. There is an abrupt change from the α-Na_3PO_4 structure to the γ-Na_3PO_4 structure when x is increased from 0.01 to 0.02. A shoulder has appeared 612 cm^{-1} on the peak at 583 cm^{-1} and the peak at 635 cm^{-1} has increased in intensity in the spectrum for the x=0.04 sample. The spectra for the x=0.08 and 0.10 samples are very similar to that of the x=0.06 sample which has peaks at 583, 612 and 635 cm^{-1}. The peak at 612 cm^{-1} is also seen

in the Zn^{2+}-doped system. The band structure changes again when the concentration of $ZnSO_4$ is increased to x=0.20. The ν_4 mode now consists of two bands at 581 and 625 cm^{-1}, with the latter band showing some underlying structure. At a concentration of x=0.30 there are bands at 573 and 636 cm^{-1} with the latter having a shoulder at 623 cm^{-1}.

The presence of the SO_4^{2-} ions can be seen more clearly in the ν_1 spectral region (seen in Figures 7.5 and 7.6). The band at 995 can clearly be seen in the $x \geq 0.02$ samples, and is faintly present in the lower concentrations. The most interesting aspect about this region is the changes that occur in the PO_4^{3-} mode while the SO_4^{2-} mode simply increases in intensity. The ν_1 PO_4^{3-} mode narrows in bandwidth in the x=0.005 and 0.01 samples from the 10 cm^{-1} seen in pure α-Na_3PO_4 to 6 cm^{-1}. The band then broadens to 20 cm^{-1} in the x=0.02 sample, which is consistent with γ-Na_3PO_4. As x increases from 0.02 to 0.10, the bandwidth remains essentially constant but the peak position gradually shifts to 945 cm^{-1}. When the concentration increases to x=0.20, the bandwidth increases to 29 cm^{-1} and the peak shifts to 955 cm^{-1}. An additional shift in peak position is seen in the x=0.30 sample where the band appears at 962 cm^{-1}, but the bandwidth has begun to narrow and is again 20 cm^{-1}.

As was seen in the previously discussed Raman modes, the ν_3 spectral region (shown in Figures 7.7 and 7.8) has a structure like that of pure α-Na_3PO_4 but with the

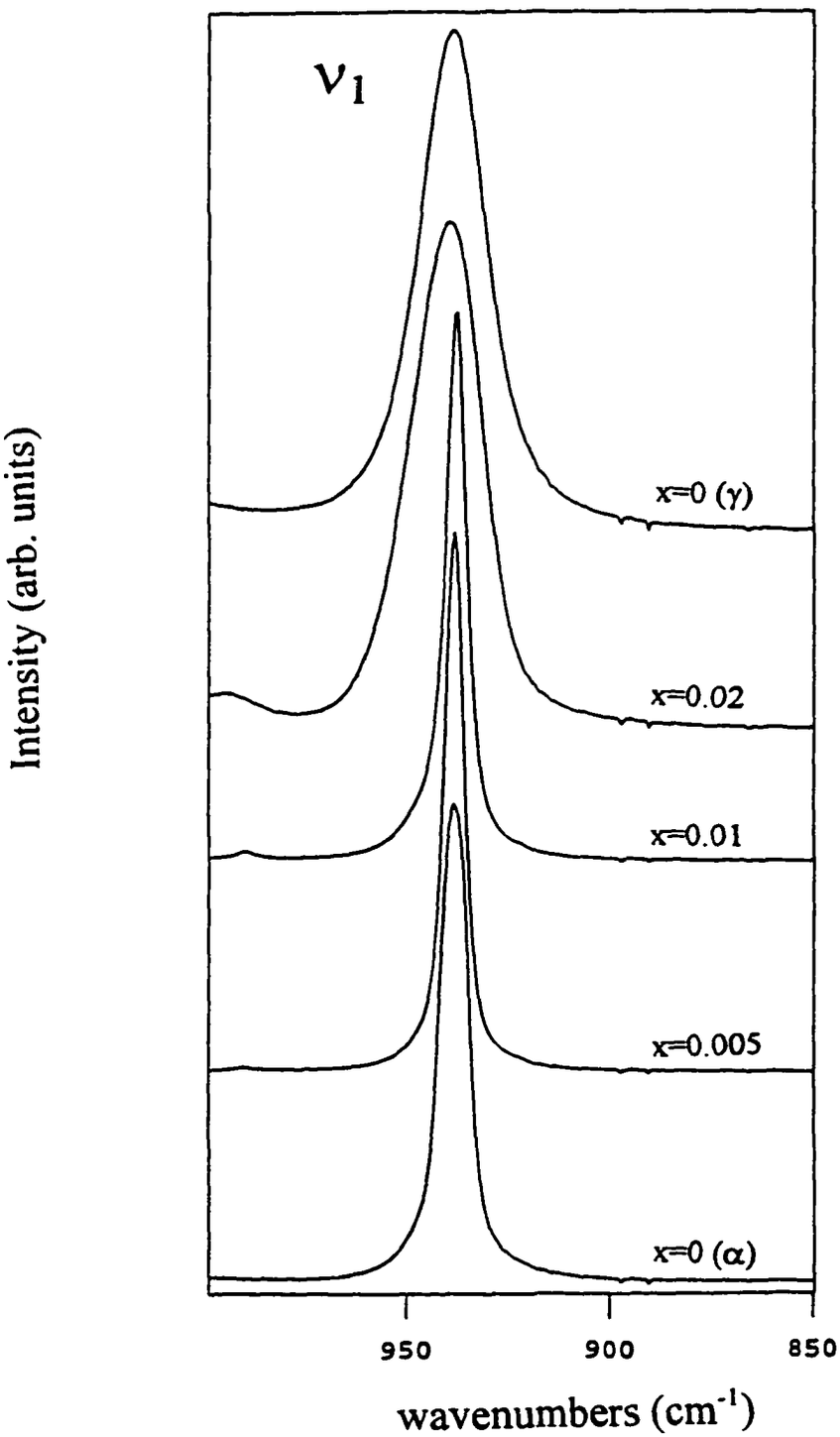

Figure 7.5. Raman spectra of $Na_{3-3x}Zn_xS_xP_{1-x}O_4$ in the ν_1 spectral region for increasing values of x.

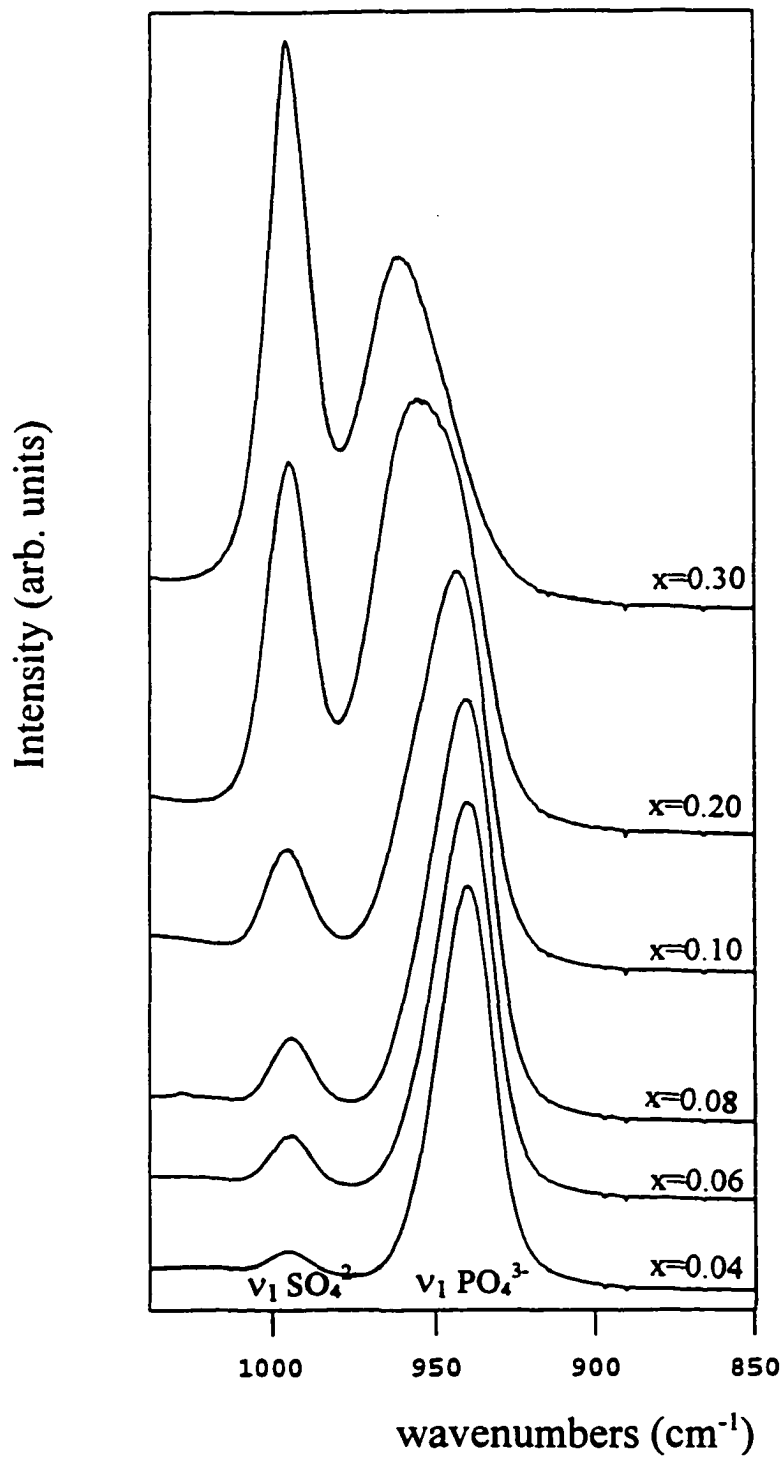

Figure 7.6. Raman spectra of $Na_{3-3x}Zn_xS_xP_{1-x}O_4$ in the ν_1 spectral region for increasing values of x.

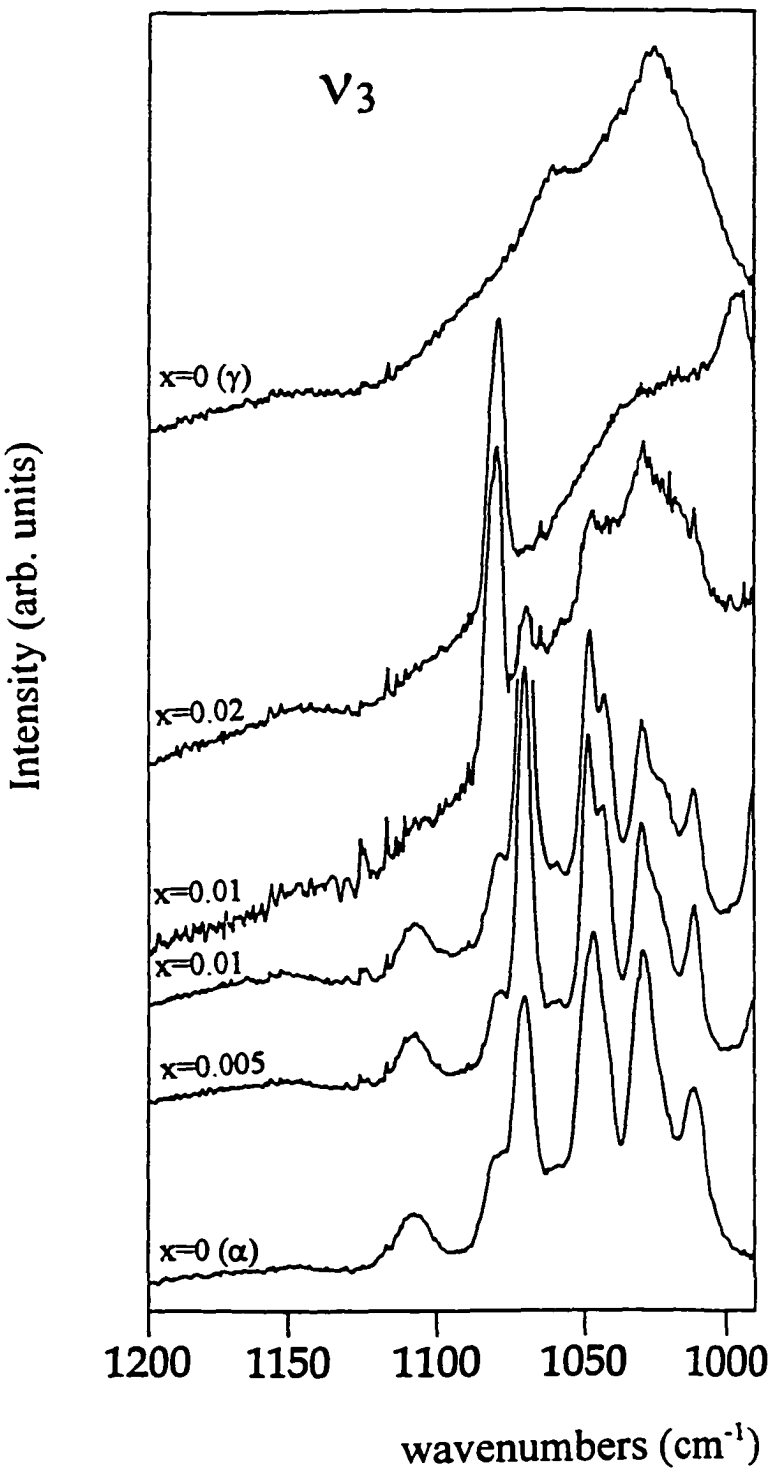

Figure 7.7. Raman spectra of $Na_{3-3x}Zn_xS_xP_{1-x}O_4$ in the ν_3 spectral region for increasing values of x.

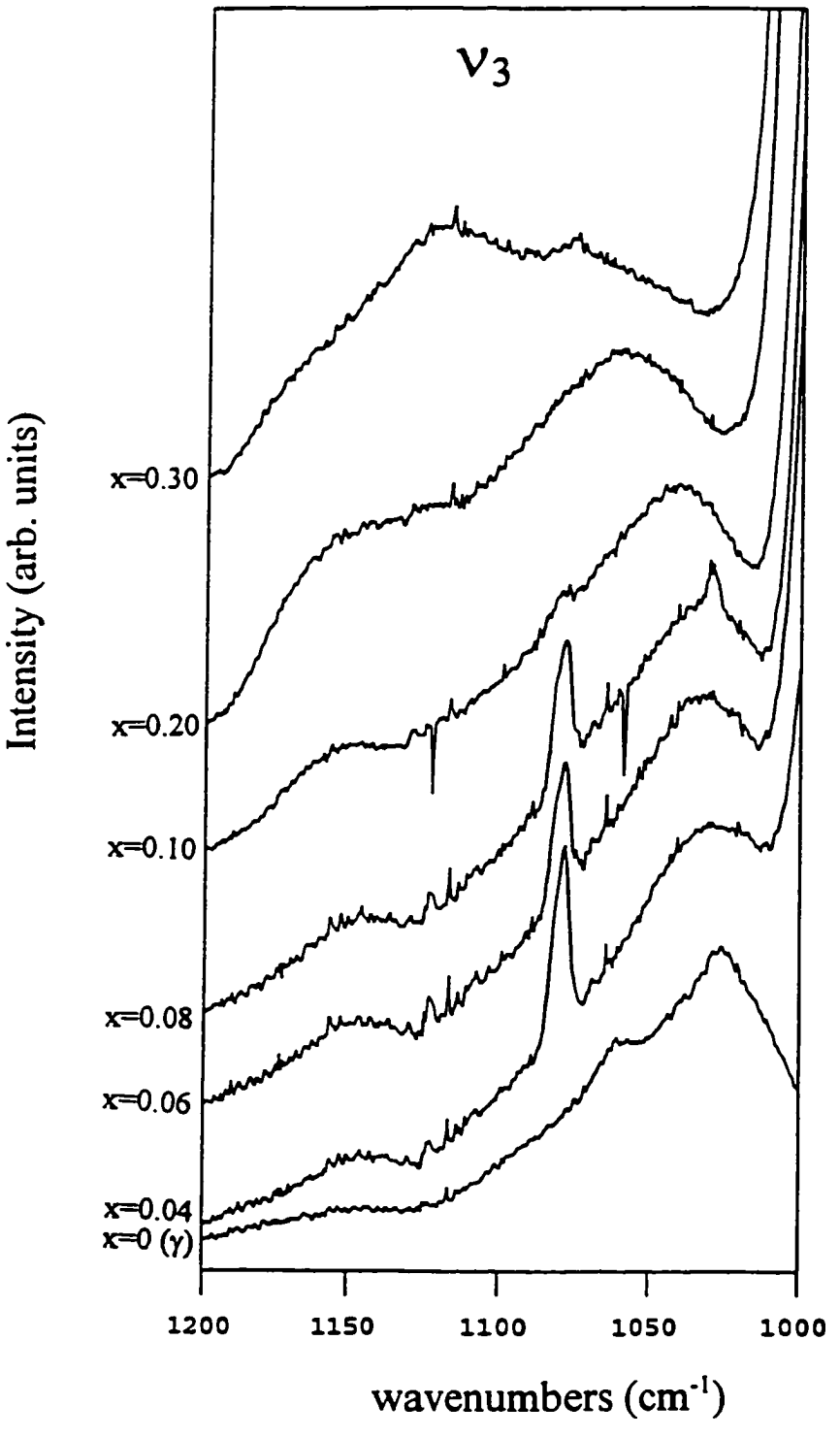

Figure 7.8. Raman spectra of $Na_{3-3x}Zn_xS_xP_{1-x}O_4$ in the ν_3 spectral region for increasing values of x.

bands in the multiplet structure more clearly defined in the x=0.005 and 0.01 samples. Where pure α-Na_3PO_4 has peaks at 1013, 1031, 1048, 1071 (with a shoulder at 1081 cm^{-1}) and 1110 cm^{-1}, the two doped samples have peaks at 1013, 1025, 1031, 1045, 1050, 1071, 1081 and 1109 cm^{-1}. The ν_3 region of the x=0.01 sample allows for further analysis of the inhomogeneity in the sample. Some areas of the sample have a band structure that is either intermediate between that of the α- and γ-Na_3PO_4 structures or is a result of the two structures superimposed. The spectrum for the x=0.02 sample is dramatically different, with a broad band centered at 1045 cm^{-1} with sharper peaks at 1086 cm^{-1} and 995 cm^{-1}. The latter peak is due to the superposition of the SO_4^{2-} ν_1 band onto the PO_4^{3-} ν_3 band structure. The band at 1086 cm^{-1} has been associated with the presence of the w-phase in previous chapters. The spectra for the x=0.04 to x=0.08 samples are very similar to that for x=0.02 although the SO_4^{2-} ν_1 band at 995 cm^{-1} is more defined in these samples and the two bands can be more easily differentiated. In these samples the PO_4^{3-} band structure, which has a single broad band centered at 1033 cm^{-1}, is consistent with that seen in pure γ-Na_3PO_4, although the peak is shifted to slightly higher frequencies. The PO_4^{3-} band has shifted to higher frequency (1044 cm^{-1}) in the x=0.10 sample and has shifted again to 1062 cm^{-1} in the x=0.20 sample. The x=0.04 to 0.08 spectra also have a broad band centered at 1155 cm^{-1} that increases in intensity with increasing x. A similar band at 1160 cm^{-1} is also seen in the SO_4^{2-}-doped system, and therefore the band at 1155 cm^{-1} in the $ZnSO_4$-doped system can be attributed to the vibrational motion of the SO_4^{2-} ion in the γ-Na_3PO_4 lattice. The SO_4^{2-} has also continued to increase in intensity and has

shifted to 1150 cm^{-1} in the x=0.20 sample. The ν_3 SO_4^{2-} and ν_3 PO_4^{3-} bands have merged into a single broad band centered at 1123 cm^{-1} in the x=0.30 sample. The band also some degree of underlying structure.

DISCUSSION

The $ZnSO_4$-doped Na_3PO_4 system has characteristics that are unique to this system in addition to having many seen in the systems doped with only cations or anions. The cation seems to dominate the stabilizing effect on the solid solution at low dopant concentrations while the presence of the anion is more dominant at high dopant concentrations. In order to compare the $ZnSO_4$-doped system to other doped systems, it is necessary to refer to them in terms of mole percents of dopants. It is not possible to simply use the x values that appear in the nominal compositional formula since these do not correspond to the mole percent of dopant in the cation doped systems. For clarity and ease of reference, however, the x value will be included in parentheses.

The Zn^{2+}- and Mg^{2+}-doped systems achieve phase stabilization at a dopant concentration of approximately 2 mole percent (x=0.06) $Zn_3(PO_4)_2$ or $Mg_3(PO_4)_2$, while the SO_4^{2-}-doped system is not phase stabilized until a dopant concentration of approximately 20 mole percent (x=0.20) Na_2SO_4 is attained. The $ZnSO_4$-doped Na_3PO_4 is also stabilized by 2 mole percent (x=0.02) dopant. However, it should be noted that at a concentration of 2 mole percent the $Zn_3(PO_4)_2$-doped system has a greater number of Zn^{2+} ions present in the host lattice than in the $ZnSO_4$-doped

system. Therefore, fewer dopant ion are necessary for phase stabilization in the $ZnSO_4$ system.

The solid solution limit for the $ZnSO_4$ system occurs at a concentration intermediate to those seen in the individually doped systems. The Mg^{2+}- and Zn^{2+}-doped systems have solid solution limits of approximately 11 mole percent (x=0.30), while the γ-Na_3PO_4 lattice can accommodate an amazing 60 mole percent (x=0.60) of Na_2SO_4. In comparison, the γ-Na_3PO_4 lattice can accommodate slightly more than 30 mole percent of $ZnSO_4$ before phase separation occurs. Obviously the lattice can accommodate significantly more anion dopant than cation dopant. It seems reasonable to assume that it is the presence of the cation that limits the extent of solid solution in the case of $ZnSO_4$, although it should be noted that more Zn^{2+} ions can be doped in the mixed system than when doping with Zn^{2+} ions alone.

The difference in the effects of the two different dopant ions is seen most clearly in the Raman spectra. At very low concentrations of $ZnSO_4$, 0.5 and 1 mole percent, the band structure is more clearly defined than in that observed in pure α-Na_3PO_4. This effect is rather interesting since it was also observed in the Mg^{2+}-doped system (in samples with dopant concentrations between 0.4 and 1.7 mole percent) but not in the Zn^{2+}-doped system. The appearance of the new peak at 611 cm^{-1} in the ν_4 region that was observed in the Zn^{2+}-doped system is also present in the $ZnSO_4$-doped system. It first appears as a shoulder in the 4 mole percent (x=0.04) sample and becomes a more distinct peak in the 10 mole percent (x=0.10) sample before disappearing in the 20 mole percent (x=0.20) sample. In the samples doped with just

Zn^{2+}, the band appears as a shoulder at 2 mole percent (x=0.06) and increases to a distinct band with increasing dopant concentrations. It is likely that the band at 611 cm^{-1} disappears in the $ZnSO_4$-doped system at higher concentrations because it is hidden by the SO_4^{2-} ν_4 band at 635 cm^{-1}. The band at 635 cm^{-1} follows much the same progression of band shape in the $ZnSO_4$ system as in the Na_2SO_4 system, but the concentrations at which certain features are seen have changed. The band first appears in the Na_2SO_4 system at about 10 mole percent (x=0.10) dopant, but does not develop the asymmetric peak profile until a concentration of 50 to 60 mole percent (x=0.50 to 0.60). In the $ZnSO_4$ system, the band shifts from a well-defined peak at concentrations ranging from 2 to 10 mole percent (x=0.02 to 0.10) to a much broader, asymmetric band at a concentration of 20 mole percent (x=0.20). The ν_3 mode displays the shift in band position that was also observed in the Zn^{2+}-doped system, but the shift is more pronounced in the $ZnSO_4$-doped system, particularly at higher dopant concentrations. The SO_4^{2-} ν_3 band at 1160 cm^{-1} that is seen in the Na_2SO_4-doped system at concentrations ranging from 20 mole percent to 60 mole percent (x=0.20 to 0.60) is also seen in the $ZnSO_4$ system at concentrations ranging from 4 mole percent to 20 mole percent (x=0.04 to 0.20). However at a $ZnSO_4$ concentration of 20 mole percent (x= 0.20), the band structure begins to merge with the PO_4^{3-} band at 1062 cm^{-1}, and a single band at 1123 cm^{-1} is present at a concentration of 30 mole percent (x=0.30).

The fact that the SO_4^{2-} bands appear at the same frequencies and with the same general bandshapes in both the Na_2SO_4- and $ZnSO_4$-doped systems provides further

evidence that these bands are due to the vibrations of the SO_4^{2-} ions in the γ-Na_3PO_4 lattice. This conclusion is further supported by the observation that these bands appear in the $ZnSO_4$-doped system at significantly lower SO_4^{2-} concentrations than in the Na_2SO_4-doped system, but the bands are observed in both systems as soon as the structure is stabilized in the γ-phase. A similar situation is observed for the new bands that appear in the Zn^{2+}-doped system. Both the band at 611 cm^{-1} and the low frequency band at 289 cm^{-1} are present in the $ZnSO_4$-doped system. However, it is obvious that the local structure observed in the $ZnSO_4$-doped system is not simply the sum of the structural distortions seen in the individually doped systems. This is seen most clearly in the ν_1 and ν_3 Raman modes where the band structure at high concentrations has features not seen in either the Zn^{2+}- or SO_4^{2-}-doped systems.

CONCLUSIONS

The analysis of the $Na_{3-3x}Zn_xS_xP_{1-x}O_4$ system results in an overall description that is similar to those seen for the $Na_{3-2x}Zn_xPO_4$ and the $Na_{3-x}S_xP_{1-x}O_4$ systems. The XRD patterns indicate a complete transition from α- to γ-Na_3PO_4 with no real intermediate structures present. The DSC results reveal the presence of a disordered α-Na_3PO_4 phase at very low concentrations of x and indicate the presence of small degrees of local ordering for higher concentrations of x. It is in the analysis of the Raman spectra that a richer description of the local structural changes is provided.

REFERENCES

1. Oyama, Y. & Kamigaito, O. *Japanese Journal of Applied Physics* **10**, 1637 (1971).

2. Jack, K.H. *Journal of Materials Science Letters* **11**, 1135-1158 (1976).

CHAPTER 8

SUMMARY OF CONCLUSIONS

The results of this study have provided a detailed and systematic analysis of the individual and combined effects of cation and anion dopants on the structure of γ-Na_3PO_4 solid solutions. In particular, the addition of Raman spectroscopy to the use of X-ray and DSC analysis allows a more complete description of the structural changes taking place in the solid solutions. This study has also emphasized the need to use a variety of techniques for structural analysis and phase characterization since very different trends were observed for each of the three techniques used. The XRD results indicate a complete transition from α- to γ-Na_3PO_4 with no intermediate structures present. The presence of a perturbed α- and/or γ-phase is observed in the DSC thermograms, but the results generally agree with the phases identified by the XRD patterns. Vibrational spectroscopy provides a richer description of the structural changes, particularly local structural changes occurring as the compositions of the doped systems are varied.

γ-Na_3PO_4 is stabilized in all four dopant systems studied. However, the dopant concentration at which stabilization occurs and the extent of solid solution formation varies dramatically. This is shown in Figure 8.1. The percentage of Na_2SO_4 necessary for complete stabilization is ten times that for the two cation dopants, with 20 mole percent of Na_2SO_4 needed compared to 2 mole percent of $Mg_3(PO_4)_2$ or $Zn_3(PO_4)_2$. The $ZnSO_4$-doped Na_3PO_4 also requires 2 mole percent of

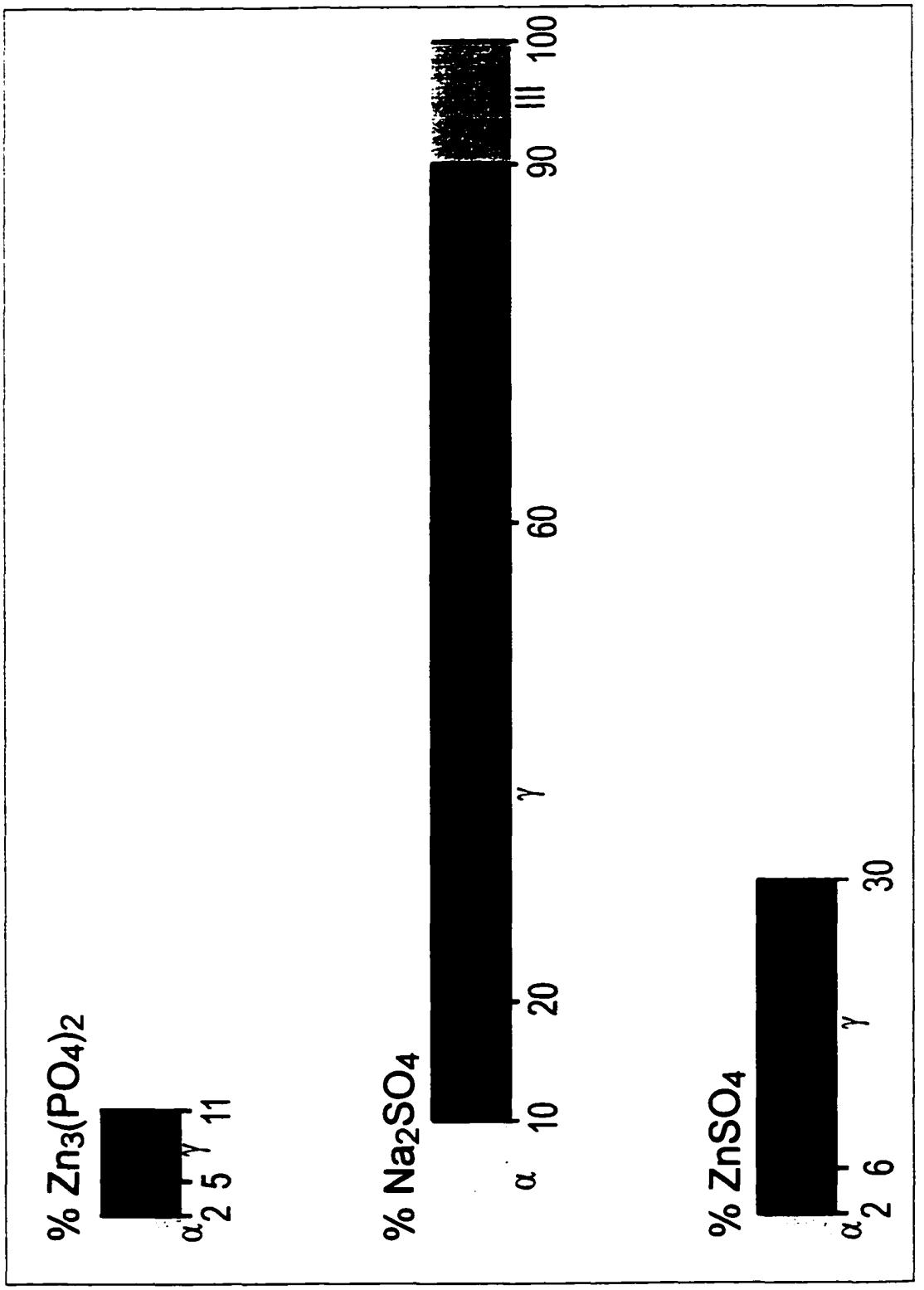

Figure 8.1. The solid solution limits of different dopants vary dramatically.

dopant for phase stabilization, but this actually corresponds to a smaller concentration of substituent ions incorporated into the lattice. Although it may require considerably more anionic dopant than cationic dopant to achieve phase stabilization, the lattice can also accommodate considerably more dopant anions than cations. Compound formation and phase separation are observed at approximately 11 mole percent of the respective phosphates in the Mg^{2+}- and Zn^{2+}-doped systems. This is in dramatic contrast to the Na_3PO_4/Na_2SO_4 system where the γ-phase is the only phase present from 20 to 60 mole percent Na_2SO_4 and is the dominant phase present from 60 to 80 mole percent Na_2SO_4. The $ZnSO_4$-doped Na_3PO_4 is intermediate between the two with phase separation occurring at slightly more than 30 mole percent dopant.

The additional structural information provided by the Raman spectroscopic data allowed for some insight into the interactions between the host lattice and the dopant ions. A comparison of the temperature-dependent Raman spectra and those of the Na_3PO_4 with incremental dopant concentrations reveals a difference in the structural changes that take place. A gradual broadening and collapse of the band structure is observed in the temperature-dependent spectra of pure Na_3PO_4 indicating the gradual increase of disorder in the structure with increasing temperature. In contrast, the doped systems display an abrupt change from the α-phase to the γ-phase with a variation of concentration of less than 0.5 mole percent. This suggests that whatever the mechanism for phase stabilization may be, there is a critical point that must be attained in order to stabilize the high-temperature phase. A comparison of the Raman spectra of the Mg^{2+}- and Zn^{2+}-doped Na_3PO_4 indicates that Zn^{2+} has a

stronger interaction than Mg^{2+} with the PO_4^{3-} ion, although they are equally effective at phase stabilization. This strong interaction is also seen in the $ZnSO_4$-doped Na_3PO_4. Raman spectroscopy provides a description of the environment of the SO_4^{2-} ions in a γ-Na_3PO_4 lattice and of how that environment changes as the percentage of SO_4^{2-} ions in the lattice increases.

FUTURE STUDIES

There is more work remaining to further characterize the structural distortions occurring in the γ-Na_3PO_4 solid solutions. The local structure of the solid solutions containing zinc ions could be determined using extended x-ray fine structure (EXAFS) analysis. This is the primary reason that much of the work focused on the Zn^{2+}- and $ZnSO_4$-doped systems. Conductivity studies also remain to be performed on the $ZnSO_4$- and Li_2SO_4-doped systems. The data were not presented here, but a sample of Na_3PO_4 doped with 10 mole percent of Li_2SO_4 was also prepared. The use of Li_2SO_4 as a dopant is significant because of the high ionic conductivity observed in the high temperature phase of this compound. The Li_2SO_4-doped Na_3PO_4 resulted in a solid solution that seems to be identical to that seen for the 10 mole percent $ZnSO_4$ solid solution. The DSC traces, XRD patterns, and Raman spectra were virtually identical for the two solid solutions. This system also needs to be studied in more detail.

IMAGE EVALUATION
TEST TARGET (QA-3)

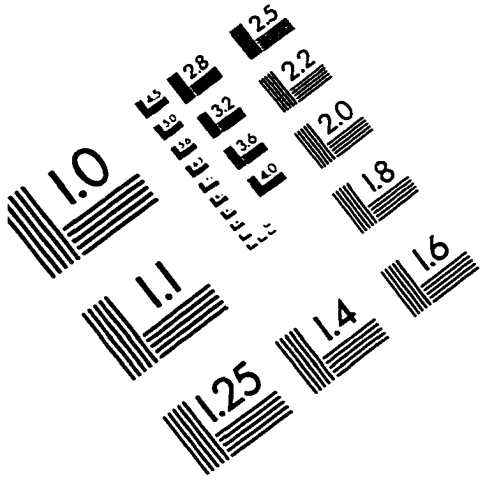

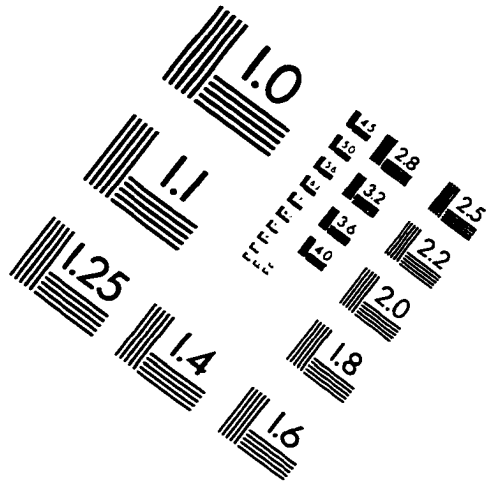

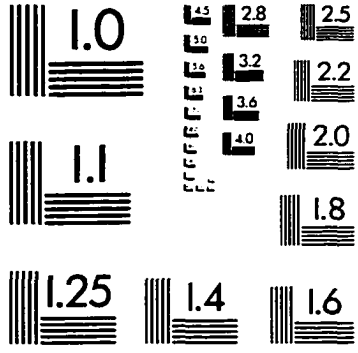

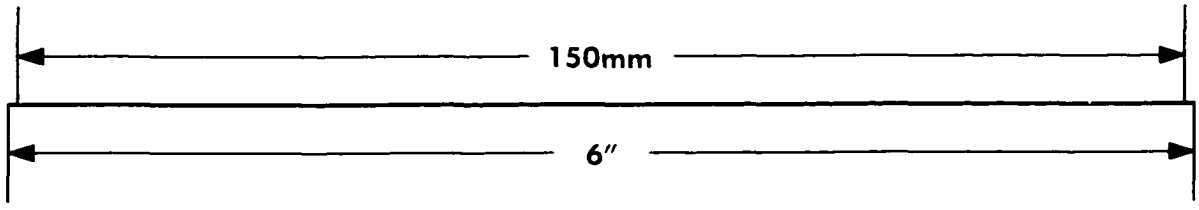

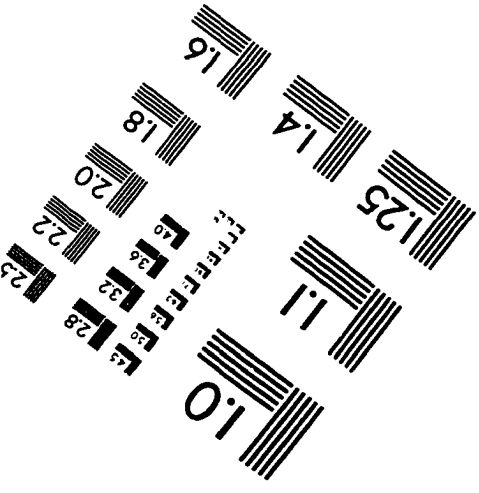

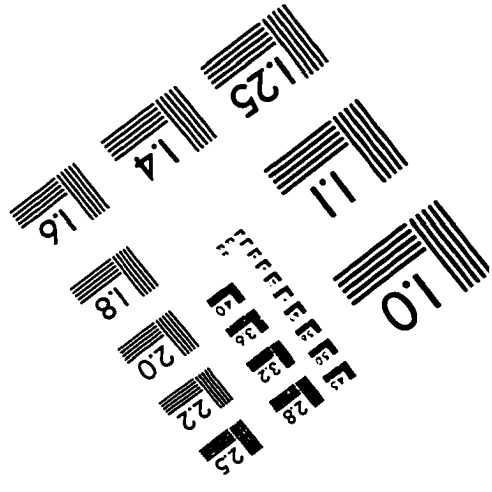

APPLIED IMAGE, Inc
1653 East Main Street
Rochester, NY 14609 USA
Phone: 716/482-0300
Fax: 716/288-5989

© 1993, Applied Image, Inc., All Rights Reserved